



THE HONG KONG
POLYTECHNIC UNIVERSITY

香港理工大學

Pao Yue-kong Library

包玉剛圖書館

Copyright Undertaking

This thesis is protected by copyright, with all rights reserved.

By reading and using the thesis, the reader understands and agrees to the following terms:

1. The reader will abide by the rules and legal ordinances governing copyright regarding the use of the thesis.
2. The reader will use the thesis for the purpose of research or private study only and not for distribution or further reproduction or any other purpose.
3. The reader agrees to indemnify and hold the University harmless from and against any loss, damage, cost, liability or expenses arising from copyright infringement or unauthorized usage.

IMPORTANT

If you have reasons to believe that any materials in this thesis are deemed not suitable to be distributed in this form, or a copyright owner having difficulty with the material being included in our database, please contact lbsys@polyu.edu.hk providing details. The Library will look into your claim and consider taking remedial action upon receipt of the written requests.

The Hong Kong Polytechnic University

Department of Applied Biology and Chemical Technology

**Synthesis of Pt and Pt-based
Electrocatalysts for Direct Liquid Fuel
Cells**

Zheng Fulin

A thesis submitted in partial fulfilment of the requirements for the degree of
Doctor of Philosophy

October 2012

Declaration

I hereby declare that this thesis entitled “**Synthesis of Pt and Pt-based Electrocatalysts for Direct Liquid Fuel Cells**” is my own work and that, to the best of my knowledge and belief, it reproduces no material previously published or written, nor material that has been accepted for the award of any other degree or diploma, except where due acknowledgement has been made in the text.

Zheng Fulin

October 2012

Abstract of thesis entitled

**Synthesis of Pt and Pt-based Electrocatalysts for Direct
Liquid Fuel Cells**

Submitted by

Zheng Fulin

for the degree of Doctor of Philosophy

at The Hong Kong Polytechnic University

in October 2012

The natural abundance of platinum (Pt), a commonly used precious metal in fuel cell devices, is limited and the price of Pt is rising in recent years. It poses great challenge for the commercialization of fuel cells, which can be a promising candidate for environmentally benign energy supply in the future. Intensive effort has been made to the development of highly efficient Pt containing catalysts for fuel cells with low Pt loading over the past decades. In view of this, the purpose of the research described in this thesis is to develop Pt-based catalysts with excellent electrochemical performance as well as enhanced Pt utilization. The key idea for the catalyst design is a core-shell structure construction with the Pt on the surface since only surface atoms take part in the electrocatalysis.

Au@Pt/MWCNTs composite was synthesized by ions adsorption - *in situ*

electrochemical reduction approach. Electrochemical analysis was used for the first time to prove that the Au@Pt/MWCNTs composite consisted of a submonolayer Pt structure on the surface of Au nanoparticles. The coverage of Pt can readily be tuned by changing the concentration of the Pt source or by repeating the ions adsorption process after each electrochemical reduction. The as prepared Au@Pt/MWCNTs catalyst displays facile electrochemical properties. Au@Pt/MWCNTs with low Pt coverage, namely below 40%, was inactive for methanol whereas it can electrooxidize formic acid through a direct pathway effectively. Also, it was proved to be an effective catalyst for methanol tolerant oxygen reduction reaction (ORR). On the other hand, Au@Pt/MWCNTs of high Pt coverage exhibits both direct and indirect oxidation of formic acid, in addition to gradual development of methanol oxidation ability. Its specific area activity toward methanol has seen as much as a 2 fold enhancement when compared to commercially available Pt/C catalyst.

PtAg hollow nanospheres were synthesized by an approach involving galvanic displacement. Ag nanoparticle precursors were first prepared as the template for the construction of the PtAg hollow structure. The thickness of the nanoshell can be easily controlled by changing the Pt source available in the galvanic replacement reaction. Both the XRD and XPS analysis confirmed that the hollow spheres consisted of a PtAg alloy. Electrochemical studies proved that the PtAg alloy possessed better electrochemical performance compared to the commercially available Pt black for both methanol and formic acid oxidations. The enhancement in the electrocatalytic capability can be ascribed to the better utilization of Pt as well as the electronic effect induced by the incorporation of

Ag.

Pd@PdPt/MWCNTs composite was fabricated by a two-step method. Pd/MWCNTs precursor was first prepared by the hydrolysis of PdCl_4^{2-} in the presence of MWCNTs in an aqueous medium at 60°C prior to its reduction by hydrogen. XRD was used to confirm the identity of the as formed PdO/MWCNTs intermediate. The surfactant free Pd/MWCNTs composite shows even size distribution of Pd nanoparticles without the formation of aggregates. The coating of Pd nanoparticles by PdPt alloy was realized through galvanic replacement between Pd and PtCl_4^{2-} at 90°C . Electrochemical investigations revealed that the resulting Pd@PdPt/MWCNTs display improved activity toward methanol and ethanol oxidations as well as better durability.

Publications arising from the thesis

1. Fulin Zheng, Wing-Tak Wong*, Ka-Fu Yung* Facile Design of Au@Pt Core-shell Nanostructures: Formation of Pt Submonolayer with Tunable Coverage and Their Applications in Electrocatalysis (Chapter 2; under submission process to *Nano Research*)
2. Fulin Zheng, Wing-Tak Wong*, Ka-Fu Yung* Synthesis of Pd@PdPt/CNTs with Excellent Electrochemical Performance for Ethanol Oxidation (Chapter 4; under submission process to *Journal of Power Sources*)

Acknowledgements

I found it fortunate to have lived and studied in Hong Kong, the city of oriental pearl, th have experienced the distinctive blend of east and west in this dynamic city. Many beautiful memories were created, especially during the time spent with Prof. Wong's group members. A number of wonderful persons, who have given me continuous support and shared my joys and tears, deserve special recognition.

First of all, I would like to express my deepest gratitude to my supervisor, Prof. Wing-Tak Wong for providing me such a precious opportunity and for his outstanding guidance and support throughout my research. His devoted research attitude inspired me not only during the past three years but will also have a great influence in my future career.

It's really difficult to list all the amazing colleagues whom I work with during my graduate work. Nevertheless, I would still like to express my appreciation by briefly naming Dr Joseph K. F. Yung, Dr Sonoe G. L Law, Dr Gary K. L. Wong, Dr C. T. Yeung, Dr Karen Y. J. Gu, Dr X. J. Zheng, Dr J. F. Jun, Dr Arthur H. H. Leung, Mr K. K. Ho, Mr Summy W. S. Lo, Mr Y. Y. Wang, Mr Ming Hao, Miss Dorothy Y. O. Fung, Miss Christine Ng.

Many thanks also go to Dr Lu Wei and Dr. Frankie Y. F. Chan for their kind support in the microscopic studies.

I would like to acknowledge the receipt of a postgraduate studentship (2009-2012) administrated by The Hong Kong Polytechnic University. The award of a conference grant from the CRGC to attend the Summer School on Fuel Cells in Helsinki, Finland, is also

gratefully acknowledged.

Finally, I am deeply thankful to my family, especially my wife Mrs S. L. Yu, who has always been there for me, their constant love and care provides the backbone for me to overcome any difficulties I encountered.

Table of Contents

Chapter 1	1
Introduction to Direct Liquid Fuel cells and Pt-based Nanostructures Electrocatalysts	1
1.1 Introduction to direct liquid fuel cells	1
1.1.1 An overview of fuel cells	1
1.1.2 A brief overview of fuel cell history.....	4
1.1.3 Introduction to several types of fuel cell.....	6
1.2 Pt-based nanostructures electrocatalysts for fuel cells	12
1.2.1 A brief introduction to nanoscience.....	12
1.2.2 Nano-materials as electrocatalysts.....	13
1.2.3 Synthetic methods of Pt-based nano-materials	14
1.2.4 Characterization techniques of Pt-based electrocatalysts	19
1.2.5 Anodic electrochemical reactions in direct liquid fuel cells.....	21
1.2.6 Improvement of catalytic performance for direct liquid fuel cells.....	27
1.3 Scope of this thesis.....	32
References.....	33
Chapter 2.....	45
Synthesis of Ultralow Pt Loading Au@Pt/MWCNTs for Formic Acid Electrooxidation and Methanol-Tolerant Oxygen Reduction Reaction.....	45
2.1 Background.....	45
2.1.1 A brief overview of carbon nanotubes.....	45
2.1.2 Recent development of electrocatalysts for formic acid	50

2.1.3	Recent development of Pt-based ORR catalyst.....	51
2.1.4	Synthesis of ultralow Pt loading catalysts.....	52
2.2	Synthesis of ultralow loading Pt catalysts for formic acid oxidation and methanol tolerant oxygen reduction reaction.....	54
2.2.1	Functionalization of multiwall carbon nanotubes (MWCNTs).....	55
2.2.2	Synthesis of Au/MWCNTs composite.....	56
2.2.3	Synthesis of ultralow Pt loading Au@Pt/MWCNTs composite.....	56
2.2.4	Morphology and phase characterization.....	57
2.2.5	Metal loading analysis.....	57
2.2.6	Electrochemical studies.....	58
2.3	Results and discussion.....	58
2.3.1	MWCNTs functionalization.....	58
2.3.2	Au/MWCNTs composite.....	60
2.3.3	Au@Pt/MWCNTs composite.....	63
2.3.4	Electrochemical oxidation of formic acid.....	76
2.3.5	Methanol tolerant ORR catalysis.....	84
2.4	Summary.....	91
	References.....	93
Chapter 3	100
	Synthesis of Hollow PtAg Nanostructures with Excellent Electrocatalytic Performances	100
3.1	Background.....	100
3.1.1	An overview of hollow nanostructures.....	100

3.1.2 Synthesis of hollow nanostructures.....	101
3.1.3 Mechanism of the formation of hollow structure through galvanic displacement.....	106
3.2 Synthesis of PtAg hollow spheres.....	108
3.2.1 Preparation of Ag nanoparticles template	108
3.2.2 Synthesis of the PtAg hollow spheres	108
3.2.3 UV-visible spectroscopic measurement.....	109
3.3.4 Physical characterizations	109
3.3.5 Electrochemical analysis	110
3.4 Results and discussion	111
3.4.1 UV-visible spectroscopic analyses	111
3.4.2 Morphology characterization	112
3.4.3 Structural analyses	119
3.4.4 Composition analyses.....	123
3.4.5 Electrochemical characterizations.....	125
3.5 Summary	129
References.....	131
Chapter 4.....	137
Synthesis and Characterization of Pd@PdPt/MWCNTs Core-Shell Structure for Electro-catalysis	137
4.1 Introduction.....	137
4.1.1 A brief overview of core-shell structure in electrocatalysis	137

4.1.2 Synthesis of M@Pt core-shell materials	138
4.1.3 Recent development of Pt-Pd materials for electrocatalysis	142
4.2 Preparation of Pd@PdPt/MWCNTs composite.....	144
4.2.1 Catalyst preparation	144
4.2.2 Electrochemical measurements	145
4.3 Results and discussion	146
4.3.1 Scheme of preparation of Pd@PdPt/MWCNTs	146
4.3.2 Verification of the hydrolysis of PdCl ₄ ²⁻	147
4.3.3 EDS, XRD and XPS characterizations.....	150
4.3.4 TEM characterization.....	153
4.3.5 Electrochemical characterization	156
4.4 Summary	161
References.....	163
Chapter 5.....	168
Conclustions.....	168
Chapter 6.....	171
Experimental Details.....	171
6.1 Materials	171
6.2 Sample preparations	171
6.2.1 Au/MWCNTs composite	171
6.2.2 Au@Pt/MWCNTs composite	172
6.2.3 PtAg hollow nanospheres composite	172

6.2.4 Pd@PdPt/MWCNTs composite	172
6.3 Instrumentation	172
6.3.1 Transmission Electron Microscope (TEM)	172
6.3.2 Powder X-ray Diffraction (XRD).....	173
6.3.3 UV-visible spectroscopy (UV-vis)	173
6.3.4 X-ray Photoelectron Spectroscopy (XPS).....	173
6.4 Electrochemical Measurements	174

Abbreviations and Symbols

DLFC	direct liquid fuel cell
DMFC	direct methanol fuel cell
PEMFC	proton exchange membrane fuel cell
MCFC	molten oxide fuel cell
PAFC	phosphoric acid fuel cell
SOFC	solid oxide fuel cell
AFC	alkaline fuel cell
MWCNT	multiwall carbon Nanotube
CA	chronoamperometry
CV	cyclic voltammetry
LSV	linear sweep voltammetry
ADT	accelerated durability test
rpm	rotation per minute
GCE	glass carbon electrode
SCE	saturated calomel electrode
RDE	rotating disk electrode
ORR	oxygen reduction reaction
EDS	energy dispersive X-ray spectroscopy
fcc	face-centered cubic
HRTEM	high resolution transmission electron microscope

TEM	transmission electron microscope
min	minute
SAED	selected area electron diffraction
SEM	scanning electron microscope
XRD	X-Ray diffraction
XPS	X-Ray photoelectron spectroscopy
UV	ultra violet
ICP-MS	inductively coupled plasma-mass spectroscopy

Chapter 1

Introduction to Direct Liquid Fuel cells and Pt-based Nanostructures Electrocatalysts

1.1 Introduction to direct liquid fuel cells

1.1.1 An overview of fuel cells

Fuel cell is a device that can convert chemical energy directly to electrical energy. Direct liquid fuel cells represent a class of fuel cells which uses aqueous solutions of, for example, methanol, ethanol, and formic acid as fuels in the anode. In contrast to traditional combustion process, the energy conversion process takes place in fuel cells through electrochemical reactions. Therefore, it is not subject to the Carrot Limit ($\eta=1-T_L/T_H$, where T_L and T_H represent the low and high temperature source, respectively) which is a theoretical limit for energy conversion efficiency for a combustion process. The comparison of traditional combustion and electrochemical energy conversion of fuels is illustrated in Figure 1.1. Fuel cells can extract energy from fuels with higher efficiency (40-70%), while the value for internal combustion engines is around 30%. Moreover, fuel cell devices can operate with less atmospheric emissions as compared to traditional fossil fuels. NO_x , CO_2 , CO , SO_2 and other volatile organic compounds commonly emitted from fossil fuels, which can potentially cause serious environmental damages, whereas an operating direct liquid fuel cell device emits only CO_2 that may lead to global warming

effect. However, a fuel cell with an energy efficiency of 60% would emit 35-60% less CO₂ than fossil fuels. [1]

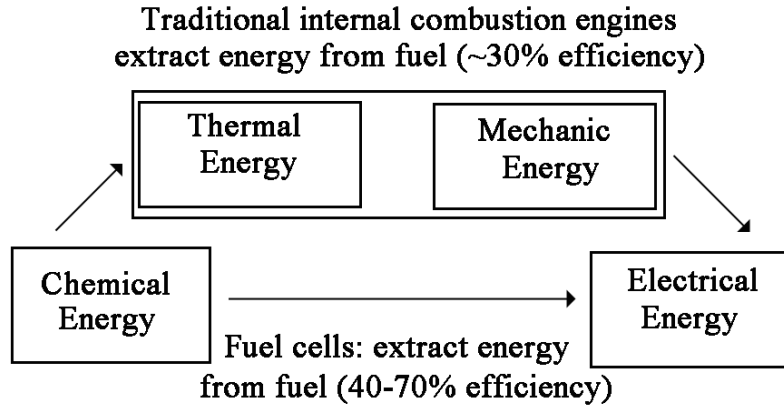


Figure 1.1 Energy conversions of fuels. [1]

As illustrated in Figure 1.2, similar to a battery, a fuel cell device has three major components: anode, cathode and the membrane. Fuels are oxidized in the anode generating electrons and relevant products (such as carbon dioxide or water). Electrons flow from the outside circuit to the cathode thus resulting in electricity. In the cathode, oxygen is reduced. To complete the cycle, ions formed in the anode or cathode travel through the membrane, which is filled with electrolytes, by diffusion. For example, the reaction for a hydrogen fuel cell device can be represented as follows,



Theoretically, at a constant pressure of one atmosphere, the available voltage for a fuel cell can be calculated from the change of Gibbs free energy (ΔG) between the initial state of the reactants and the final state of the products by the equation:

$$E = \Delta G/nF \quad (1.4)$$

where: n is the number of electron transfer in the electrochemical reaction; and F is Faraday constant;

Catalysts in the cathode and the anode are critical parts for a fuel cell which have a significant effect on the performance of a fuel cell. Presently, state-of-the-art of catalysts for both cathode and anode are either Pt or Pt-based materials, although some substitutes have also been applied as electrodes. For the membrane, which is used as electrolyte, mainly consists of polymers for low temperature fuel cells or ceramic for high temperature fuel cells.

Both batteries and fuel cells convert chemical energy into electrical energy. When batteries are depleted, they must be discarded or recharged by external current for a long period of time. However, a fuel cell can run infinitely as long as fuel is supplied.

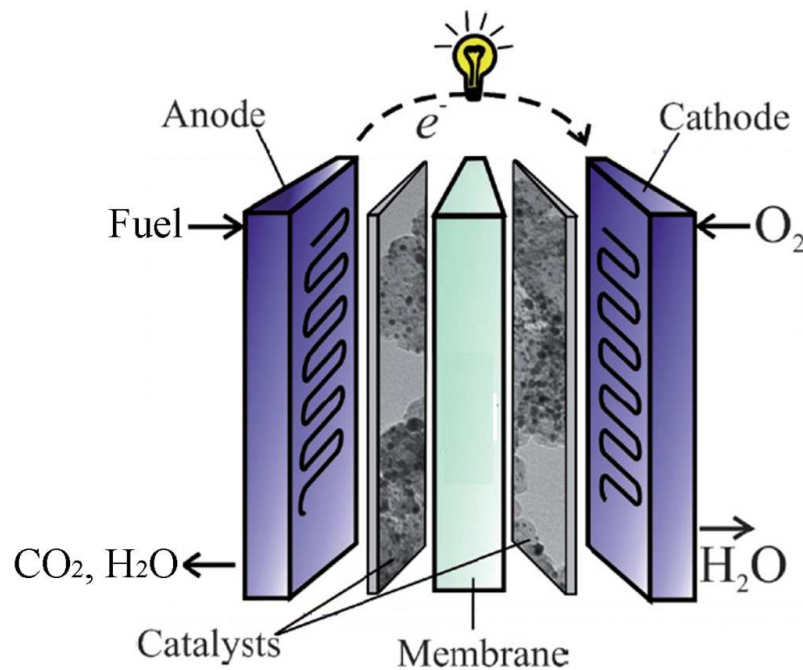


Figure 1.2 A simplified illustration of fuel cell devices.

1.1.2 A brief overview of fuel cell history

Table 1.1 presents a brief summary of fuel cell history containing some milestone events. The concept of fuel cell can be dated back to the nineteenth century when Humphry Davy demonstrated a fully effective fuel cell. Afterwards, the development and advancement of fuel cell technology was achieved by many scientists. However, it was not until 1959, around 150 year after the invention of the fuel cell concept, that a real fuel cell system came to practice, demonstrated by Bacon. Afterwards, space programs had induced great motivation for the development of fuel cell technology for which many pioneering fuel cell systems were designed for manned space missions. Organizations such as NASA, and some industrial companies like General Electric played a critical role in the advancement of fuel cell technology. The oil crisis and the increasing awareness on environmental protection in the 1970s stimulated great efforts in the research of fuel cells. For example, many nations and large companies have initiated fuel cell related projects, aiming to develop efficient form of energy generation. In the 1980s and the 1990s, substantial technical and commercial development continued, especially for areas in stationary and transportation sectors. In the mid-2000s, tens of fuel cell buses were deployed in Europe, China and Australia. Fuel cell devices for end-users with written warranties and service capability had come into market in 2007.

Table1.1 A brief summary of fuel cell development [2]

Year	Events
1801	Fuel cells demonstration by Humphry Davy
1839	The first fuel cell invention (gas battery) made by William Grove
1889	Further development of Grove's invention by Charles Langer and Ludwig Mond and firstly named fuel cell
1950s	Proton exchange membrane fuel cell invention by General Electric
1959	Demonstration of a 5kW alkaline fuel cell by Francis Bacon
1960s	Fuel cell applications in space missions by NASA
1970s	Further development of fuel cell technology prompted by the oil crisis
1980s	Fuel cell applications in submarines by the US Navy
1990s	Development of large stationary fuel cells for industrial and commercial locations
2007	Commercialization of fuel cells as auxiliary power unit (APU) and stationary backup power
2008	First publically release of fuel cell vehicle (FCX Clarity) by Honda Inc.
2009	Commercial available of fuel cell chargers and fuel cell mirco-combined heat and power units in Japan

1.1.3 Introduction to several types of fuel cell

1.1.3.1 Proton exchange membrane fuel cell (PEMFC)

Figure 1.3 shows an illustration of PEMFC. Hydrogen is pumped into the anode and separated into electrons and protons by the catalysts. Electrons travel to the cathode through the external circuit generating electricity while protons pass through the membrane to the cathode. In the cathodic side, oxygen will combine with the protons under the catalysis of a precious metal to form water. Catalysts used for PEMFC are normally Pt-based materials, and the electrolyte is water base or acidic polymer membranes. Currently, PEMFCs are the leading technology for light duty vehicles and material handling vehicles. They are also applied in some stationary power supplies.

1.1.3.2 Direct methanol fuel cell (DMFC)

DMFCs share the similar major parts with that of PEMFCs including the membrane and the cathodic catalyst, however the catalysts for the anode are normally Pt-Ru material which are able to draw hydrogen from methanol and resist CO poisoning. Figure 1.4 presents a simplified illustration of DMFC. It is essentially identical to PEMFC except that the fuel used in DMFC is pure methanol instead of hydrogen. Methanol offers several advantages as a fuel compared to hydrogen including the ease of transportation and storage. Moreover, the energy density of DMFC is higher than that of PEMFC. DMFCs tend to be used in applications with modest power requirements. Therefore, it is a promising power supply for mobile electronic devices or chargers and portable power packs.

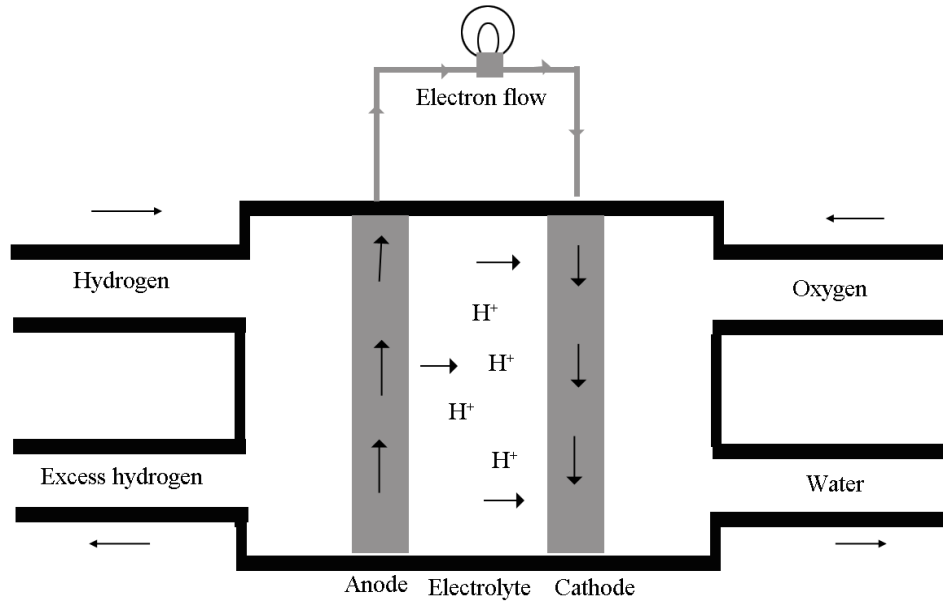


Figure 1.3 Simplified illustration of a proton exchange membrane fuel cell.

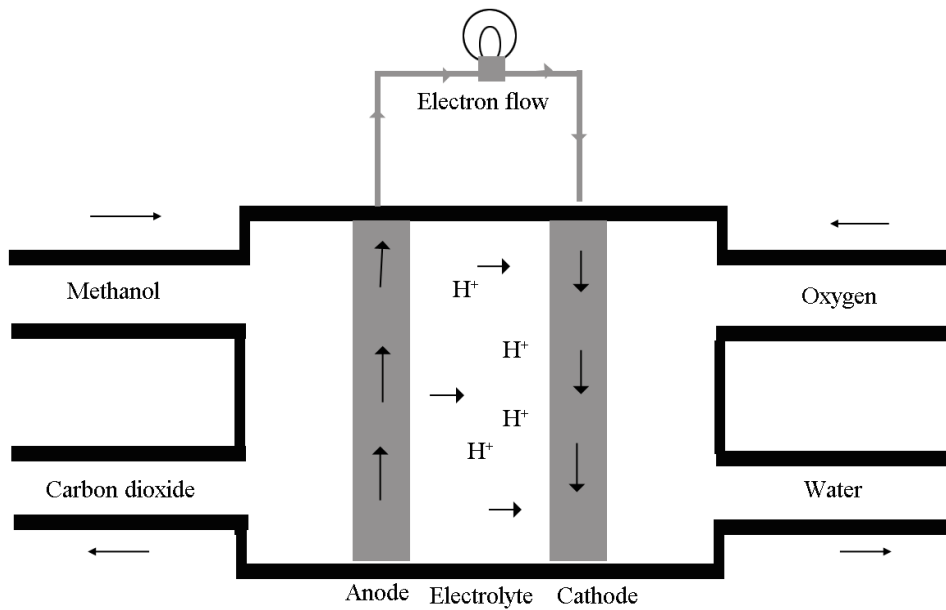


Figure 1.4 Simplified illustration of a direct methanol fuel cell.

1.1.3.3 Solid oxide fuel cell (SOFC)

Solid oxide fuel cells are high-temperature fuel cells which normally operate at 800 to 1000°C. As shown in Figure 1.5, it uses syngas (carbon monoxide and hydrogen) as the fuel. The membrane of SOFC is normally a solid ceramic electrolyte such as yttria-stabilized zirconia. Oxygen ions formed in the cathode travel through the solid ceramic to the anodic side and combine with protons to form water. The high temperature operation provides several advantages. It eliminates the need of metal catalysts and also improved the reaction kinetics. Furthermore, fuel reforming can be completed within the cell itself, which means that a variety of hydrocarbons can be used as fuels. However, there are still some disadvantages such as a time consuming start up and the need of robust, heat-resistant materials for the cell construction. SOFC is generally used in stationary power generation such as off-grid power supplies. It has also found applications in combined heat and power (CHP) for household installations.

1.1.3.4 Alkaline fuel cell (AFC)

Similar to PEMFC, alkaline fuel cell also use pure hydrogen as fuel. On the other hand, the electrolyte in AFCs is an alkaline solution such as aqueous potassium hydroxide. As shown in Figure 1.6, hydroxide ions pass through the membrane from the cathode to the anode. Though Pt is the most commonly used catalysts for AFCs, other non-precious metals can be a substitute for Pt, with nickel being one of the most promising candidate for an effective catalyst in AFC. Currently, AFCs have limited commercial applications but have instead found a niche in the use in space programs by NASA for the supply of energy as

well as water.

1.1.3.5 Other fuel cell systems

Apart from the above mentioned fuel cells, there are other types of fuel cell including the molten carbonate fuel cell (MCFC) and the phosphoric acid fuel cell (PAFC). MCFCs are another kind of high-temperature fuel cell which usually operate at around 650°C. A molten carbonate salt such as potassium carbonate, sodium carbonate or lithium carbonate suspended in a porous ceramic is used as the electrolyte for MCFC. It finds application for stationary power supplies with large energy capacity (in case of megawatt) and large CHP devices. Alternatively, PAFCs are a kind of moderate temperature fuel cell system which runs at around 180°C with phosphoric acid being used as electrolyte for PAFC. They are usually used in stationary power generation at range of between 100 to 400kW. A summary of the fuel cells mentioned is presented in Table 1.2.

Table 1.2 Categorization of fuel cells

Systems	PEMFC	DMFC	MCFC	PAFC	SOFC	AFC
Electrolyte	Ion exchange membrane	Polymer membrane	Immobilized liquid molten carbonate	Immobilized liquid phosphoric acid	Ceramic	Potassium hydroxide
Operating temperature/°C	80-200	60-130	650	200	1000	60-90
Electrical efficiency/%	40-60	40	45-60	35-40	50-65	45-60
Typical electrical power/kW	<250	<1	>200	>50	<200	>20
Applications	Vehicles, small stationary	PorTable	stationary	stationary	stationary	Submarines, spacecrafts

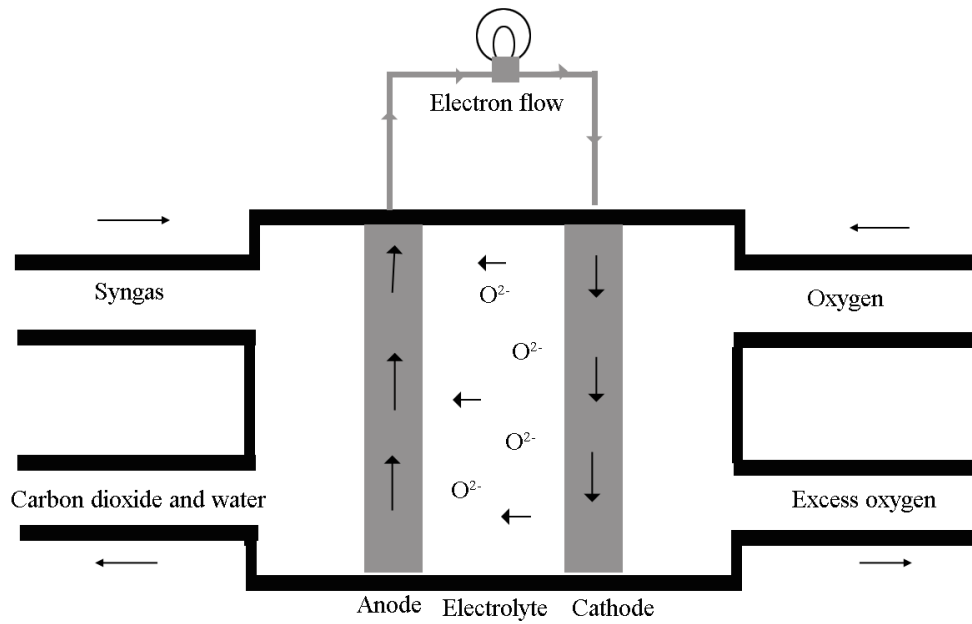


Figure 1.5 Simplified illustration of a solid oxide fuel cell.

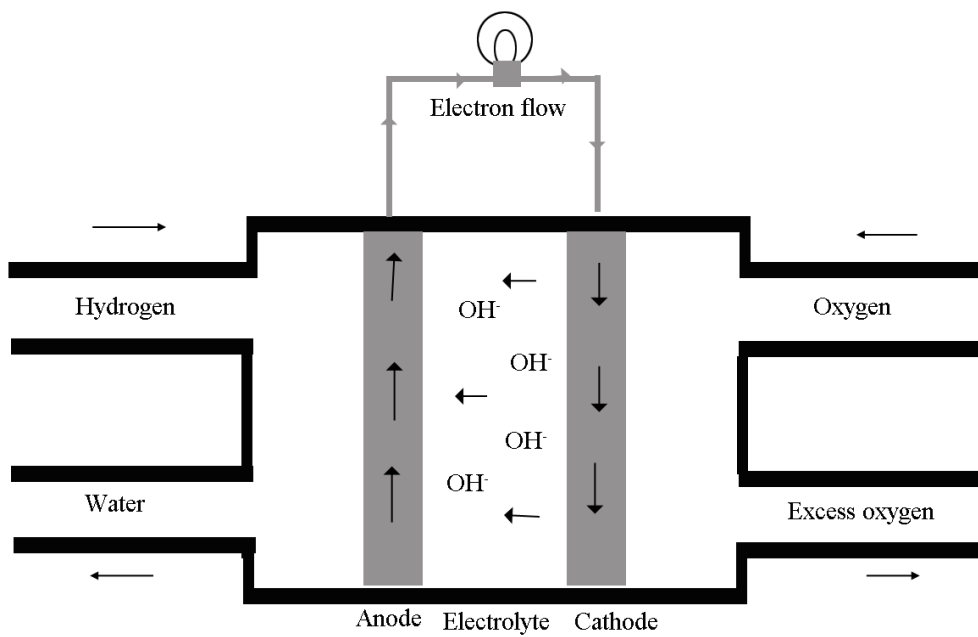


Figure 1.6 Simplified illustration of an alkaline fuel cell.

1.2 Pt-based nanostructures electrocatalysts for fuel cells

As mentioned in the previous section, Pt and Pt-based materials play a key role in the catalysis of the electrochemical reactions taking place in fuel cells, particularly for low-temperature fuel cells. The limited natural abundance of Pt poses a great challenge for the wide applications of fuel cell devices in a sustainable way. With this concern, nanotechnology appears to provide a better solution for breakthrough developments of fuel cell catalysts. For example, a 10 to 100 fold reduction of Pt usage can be achieved by using nanosize electrocatalyst particles. [3]

1.2.1 A brief introduction to nanoscience

The origin of nanoscience can be dated back to 1959, Feynman gave a lecture at The American Physical Society in which he laid out some theoretical phenomena of nanoscale materials. However, it was not until the invention of scanning tunneling microscope (STM) that nanoscience really sprang into the public consciousness. [4] The first scientific publication on nanoscience by Feynman was in 1992. [5] Since then, over the past two decades, nanoscience has developed into a multi-disciplinary, highly diversified area of science with which wide applications can be found in different fields of chemistry, biology, physics and geography.

Nanoscience deals with nano-materials which have at least one dimension ranging from 1 to 100nm. They mainly include nanostructures of zero (dots), one (wires) or two (layers) dimensions. Due to the nano-size effect, nano-materials exhibit unique properties different from their bulk counterparts. For instance, quantum dots are small semiconductors with

increased band gap owing to size quantization: a mesoscopic physical phenomenon where electron transport in small wires or thin films does not obey the Ohm's law. [6] The principles which govern the behaviors of nano-materials are quantum mechanics which were developed in response to the problems posed by small systems in the early twentieth century.

1.2.2 Nano-materials as electrocatalysts

Catalytic reactions are highly sensitive to the heterogeneous interface of nano-materials where catalysis takes place. [7] In practical applications, the nanoscale features are very important since they do not follow straightforwardly the macroscopic properties of materials. In the case of electrocatalysis, charge transfer reactions occur at the interface of a solid catalyst and the electrolyte. [8] Therefore, the surface properties of the nanoscale electrocatalysts including electronic and structural properties have great influence on the electrochemical reactions. Nano-materials can offer many advantages as electrocatalysts when compared to their bulk counterparts such as large surface area to volume ratio, fast kinetics as well as high turnover frequency. Mesoporous nanostructural Pt films have been demonstrated to exhibit higher activity as well as better durability than commercially available Pt/C catalysts due to their larger surface area. [9, 10] Pt nanoparticles have attracted significant interest recently, [11, 12] particularly Pt nanoparticles supported on nano-materials. [13-17] The use of supporting materials (carbon base materials in most cases) enhances the utilization of Pt while activity can be well maintained. Pt nanowires [18]

and Pt nanostars [19] were successfully fabricated for ethanol electrooxidation and oxygen reduction reaction, and displayed excellent electrochemical performance including activity and stability. The activity of the electrocatalyst is also related closely to the shape or even the exposed crystal plane of the materials. For instance, in a H_2SO_4 medium, the activity of Pt (100) for oxygen reduction reaction (ORR) is higher than that of Pt(111) due to the different adsorption ability of sulfates on the facets. [20] Pt with cubic shape shows vastly improved electrocatalytic activity for methanol, ethanol and formic acid electrooxidation as compared to spherical Pt nanoparticles. [21]

1.2.3 Synthetic methods of Pt-based nano-materials

1.2.3.1 Electrochemical deposition

Electrochemical deposition is a facile method for the preparation of Pt-based nano-materials. [22-27] It involves the use of a two- or three-electrode electrochemical system, with a conductive substrate as the working electrode. The Pt or other metal sources are supplied in the form of a conducting medium (the electrolyte). When a certain potential is applied, the metal nano-materials are reduced on the working electrode. A variety of electrochemical techniques have been developed to analyze Pt or Pt-based nanomaterials including chronopotentiometry, chronoamperometry, potential step experiments, potential pulse experiments and cyclic voltammetry. By using electrochemical deposition, a variety of nano-materials including nanoparticles, [28-32] nanowires and nanorods [33-37] can be easily synthesized on conducting materials.

It is a straightforward approach to control the morphology of the electrodeposited nano-materials by simply employing substrates with different templates. Paul et al. [18] used porous alumina as the template to synthesize Pt-Cu nanowires by electrochemical deposition, and the resulting nanowires have smaller diameter than the pore size of the template. The applied deposition current density has great influence on the morphology of the Pt nanowires as higher current density results in an irregular pore size on the nanowires owing to the delloying effect of Cu. By properly designing the electrochemical deposition program, Pt nanocrystal with high index facets on glass carbon was successfully fabricated. [38] Pt nanoparticle precursors were first synthesized on the glass carbon electrode by electrodeposition. Subsequently, the as prepared precursors bearing electrode was subject to a square-wave potential treatment in the presence of ascorbic acid, which was facilitated to form Pt with high index facets. These high index facets were stable and have higher energy, thus resulting in an enhancement of electrocatalytic activity as compared to regular Pt nanoparticles. Electrochemical deposition is in fact a powerful method to synthesize Pt alloy nano-materials. PtPb alloy nanoparticles were electrodeposited on multiwall carbon nanotubes (MWCNTs) by means of step potential approach. [39] The PtPb alloy nanoparticles have a size ranging from 10 – 40 nm with a snowflake morphology. In addition, owing to the ease of alloy formation under the electrodeposited condition, by employing suitable metal sources and adjusting the deposit condition, ternary and quaternary [40] alloys can be obtained.

1.2.3.2 Electroless deposition

Another promising method for the preparation of Pt or Pt-based nano-materials is electroless deposition. It is the most straightforward and efficient approach which finds its applications in various fields such as battery technology, medical devices, corrosion resistant materials and electronics. [41] This method involves the reduction of a Pt source in a solution medium containing a reducing agent, for example, sodium, sodium borohydride, ethylene glycol, oleyamine and ascorbic acid. Electroless deposition is commonly used in the plating industry and in many situations where conventional electrical deposit is not applicable. [42, 43] By adjusting the synthetic conditions, Pt nanoparticles, [44-46] nanowires and nanorods, [47, 48] nanocrystals of different shape [49-52] were successfully prepared. Pt nanoparticles are the most common product for electroless deposition. With regards to the Pt supported nano-materials, pretreatment of the support substrates is needed when some inert supporting materials are used. For instance, carbon base supports are normally pretreated by surface oxidation by nitric acid to generate functional groups such as hydroxyl, carboxyl and carbonyl on the surface. These created functional groups can serve as the anchoring sites for the Pt ions which will enhance the interaction between the resulting Pt nanoparticles and the supports. Electroless deposition is a versatile approach for the synthesis of Pt alloy nano-materials as well. [53-57] It generally involves the co-reduction of a solution of different metal sources in the presence of some surfactants and capping agents.

1.2.3.3 Hydrothermal and solvothermal method

Hydrothermal and solvothermal methods are easily-conducted approach to generate Pt and Pt-based nano-materials. [58-62] In the case of hydrothermal method, reduction of Pt source takes place in an aqueous medium while it occurs in a non-aqueous solution in a solvothermal approach. The most common precursor for hydrothermal processes is $\text{H}_2\text{PtCl}_6 \cdot 6\text{H}_2\text{O}$, [63, 64] whereas in solvothermal processes the precursor is frequently platinum acetylacetonate, $\text{Pt}(\text{acac})_2$. [65, 66] In contrast to electroless deposition processes, these approaches involve a heterogeneous reaction that takes place under high temperature and pressure in a close system, such as a Teflon lined autoclave enclosed in a stainless steel vessel. The hydrothermal and solvothermal methods can be employed to prepare various nano-materials ranging from nanoparticles, [67, 68] nanodendrites, [69] nanowires [65, 66] and nanocrystals with distinct shapes. [70] Furthermore, it is very easy to use these approaches to synthesize Pt-based binary [71] and ternary nano-materials. [72] The morphology and composition of the Pt-based nano-materials prepared through hydrothermal or solvothermal processes can be easily controlled by varying the reaction parameters such as the pH, temperature and precursors. Additionally, it is also quite suitable for large scale production. However, disadvantages include the need for high temperature and pressure and the use of autoclaves in contrast to other preparing methods.

1.2.3.4 Sol-Gel method

Sol-Gel method is a useful way to synthesize Pt or Pt-based nano-materials with

uniform size and distribution. Similar to the hydrothermal or solvothermal methods, it can be categorized as a wet chemical approach. The major different is that the Sol-Gel method involves the process of hydrolysis and polycondensation of the precursors (mainly metal alkoxides) which are formed prior to the synthesis. $\text{H}_2\text{PtCl}_6 \cdot 6\text{H}_2\text{O}$ is the Pt source for an aqueous system [73-75] while a non-aqueous process uses organometallic precursors. [76-78] Sol-Gel method can be use to create binary Pt-based nano-materials in large quantity scale. [79, 80] Moreover, it is very convenient to prepare Pt nanoparticles on a number of supporting materials such as aluminum, [81] titanium, [82] silicates [83] and carbon [84] using this method.

1.2.3.5 Physical method

Owing to the advancement of engineering technologies, many physical methods have been developed for the preparation of Pt and Pt-based nano-materials including sputtering, [85-87] irradiation, [88-90] electron beam or ion deposition [91-93] and laser ablation. [94, 95] All these processes mentioned involve physical change of the relevant metal precursors rather than chemical modification, therefore, they are classified as physical methods. Physical methods are versatile and can be employed to fabricate materials ranging from nanosize films, nanoparticles, nanowires and nanorods. In the sputtering and laser ablation processes, high purity Pt metal is used as the Pt source while in electron beam or ion deposition Pt hydrocarbonate is used. Irradiation method involves the use of $\text{H}_2\text{PtCl}_6 \cdot 6\text{H}_2\text{O}$ and other kinds of additives which undergo physical changes upon the irradiation by a

variety of sources such as γ , UV-visible, microwave and sonication. The disadvantage of a physical methods is the need of special instruments, which is not often applicable in term of large scale preparation.

1.2.4 Characterization techniques of Pt-based electrocatalysts

1.2.4.1 Physical characterization

Physical characterizations mainly includes crystallographic, morphological and electronic analysis. X-ray diffraction (XRD) is the most common method to study the crystal structure of the as prepared samples. It is normally employed for phase identification as well as estimation of the particle size through the Scherrer equation. Scanning electronic microscope (SEM) and transmission electronic microscope (TEM) is highly useful for the morphology observation. Selected area diffraction (SAED) and high resolution transmission electronic microscope is applicable for crystalline study of smaller nano-materials (within several nanometers). In term of composition analysis, energy dispersive spectroscopy (EDS) is commonly used. Inductively coupled plasma mass spectroscope (ICP-MS) is adopted for highly accurate composition studies and catalyst loading measurement. For the binary and ternary metal systems characterization, X-ray photoelectron spectrometry (XPS) is used to verify the formation of alloys. All the techniques mentioned can give insight into the relationship between the structure and the electrocatalytic performance.

1.2.4.2 Electrochemical performance evaluation

Cyclic voltammetry (CV) in an acid medium is adopted to assess the electrochemical active area (ECA) of the Pt and Pt-based nano-materials. CVs and linear sweep voltammetry (LSV) in relevant electrolytes are commonly used to evaluate the catalytic activity of the sample catalysts. Chronoamperometry and repeating CVs can be used for durability analysis. Samples preadsorbed with CO under CO saturated electrolyte and a subsequent LSV study allow for understanding the CO tolerance properties. For reaction mechanism investigation, *in situ* infrared spectroscopy (*in situ* IR) and electrochemical impedance spectroscopy (EIS) are commonly used.

For the purpose of clarity, characterization techniques mentioned above are summarized in Table 1.3.

Table 1.3 characterization techniques for Pt and Pt-based electrocatalysts

Technique	Properties studied
XRD	Crystalline
EDS	Composition
SEM	Morphology
TEM	Morphology
SAED	Crystalline
XPS	Electronic
ICP	Metal loading
CV	ECA, activity evaluation
LSV	Activity evaluation
CO stripping	Poisoning study
Chronoampermetry	Durability analysis
EIS	Mechanism study

1.2.5 Anodic electrochemical reactions in direct liquid fuel cells

1.2.5.1 Methanol oxidation

Methanol is used as fuel in direct methanol fuel cells (DMFCs). Therefore, the electrochemical reaction occurs in the anode of DMFCs is methanol electrooxidation which can be represented by the equation below,



It is a 6-electron transfer process which can offer a theoretical energy density of 4900 Wh L⁻¹. [96] Between CH₃OH and the ideal product CO₂, there exists various intermediate species such as formaldehyde, carbon monoxide and formic acid, which are produced at different carbon oxidation stages between methanol and carbon dioxide. The reaction mechanism of methanol oxidation is rather complex process and has been extensively studied in the past decades. [97-106] It included the density function theory (DFT) calculations as well as *in situ* measurements by IR and mass spectroscopy. Though variations exist from different research groups, it is generally accepted that the electrooxidation of methanol occurs mainly through dual pathway mechanism which is presented in Figure 1.7. In an indirect oxidation, methanol first dissociates to form CO at low potential and subsequently undergoes further oxidation at a higher potential to the final product CO₂. On the other hand, HCHO, HCOOH and HCOOCH₃ are the major intermediates in the direct oxidation. These dissoluble intermediates can be further oxidized to CO₂ by convection. In an ideal condition, the CO-intermediate oxidation is the dominant pathway for methanol electrooxidation. It can be explained by the fact that the energy barrier for bonds breakage is in the order of C-O > C-H > O-H. [104] However, in real life experiments, there are many factors that are needed to be taken into consideration. For instance, methanol oxidation in sulfuric acid shows preference for direct oxidation while the indirect pathway is found to be favored in perchloric acid. [102] This is owing to the different absorption behaviors of the anions in the relevant electrolyte. Additionally, steps and terraces in the Pt catalysts are also known to play key a role in the methanol oxidation process. Electronic effect which is induced by the incorporation of a different metal into the

Pt lattice has significant influence on the oxidation process. [107]

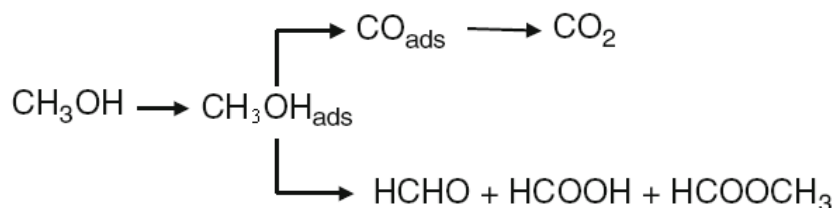


Figure 1.7 Illustration of methanol oxidation mechanism.

Owing to the well established bi-functional mechanism, [108, 109] PtRu is a state-of-the-art electrocatalyst for methanol oxidation that has come into application in commercial DMFC anodic catalysts. The presence of Ru activates water to form OH⁻ at a relevant low potential which oxidizes the as generated CO on Pt. However, some researches proposed other possible reasons for the enhanced activity of PtRu, known as the ligand effect, namely that Ru lowers the binding energy of Pt-CO of the nearby Pt atoms. [110, 111]

1.2.5.2 Ethanol oxidation

Theoretically, ethanol is a better fuel for direct liquid fuel cells since it processes many advantages as compared to methanol including low toxicity, easy production from biomass distillation as well as high energy density owing to its 12 electron transferring for a completed oxidation to carbon dioxide. [112-114] The oxidation of ethanol is presented as Equation 1.6. An energy density of 6280 WhL⁻¹ can be calculated by the equation 1.2 coupling with the oxygen reduction reaction on the cathode.



The reaction mechanism of ethanol oxidation is a complex multi-step process which involves intermediates such as adsorbed acetate, carbon monoxide, CH_x species, acetyl, acetic acid, acetaldehyde and finally carbon dioxide. [115-121] The general scheme for ethanol oxidation on a Pt electrode is showed in Figure 1.8. Other than carbon dioxide, side products formed during ethanol oxidation are not desirable since they lower the overall energy density. Nevertheless, CO_2 formation involves C-C bond cleavage which is not preferable on the Pt electrode. Moreover, CO and acetate intermediates are strongly adsorbed on the Pt surface which degrade the catalytic performance. Therefore, a second metal is usually added to the Pt catalysts to minimize the poisoning effects. Sn and Ru are found to be among the most efficient metals for the enhancement of Pt activity for ethanol oxidation. Similar to the case of methanol, several possible effects including the bifunctional mechanism and ligand effect have been proposed for the improvement of the catalytic activity.

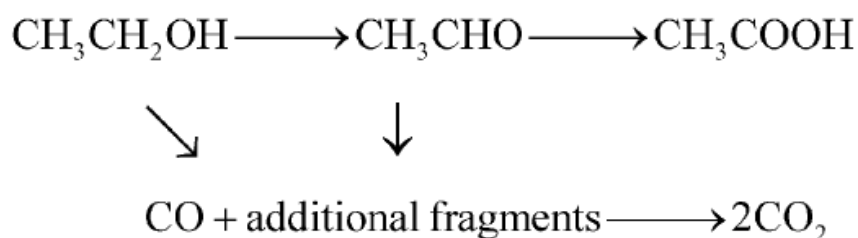


Figure 1.8 Illustration of the ethanol oxidation mechanism.

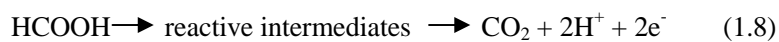
1.2.5.3 Formic acid oxidation

Theoretically, the final product for formic acid oxidation is CO₂ and it is a two electron transfer process. The reaction equation can be presented as follows:



The reversible potential for reaction (1.7) can be thermodynamically calculated approximately based on the Gibbs energy change, ΔG. A -0.25V was obtained for the above reaction, which means that formic acid is more easily electrooxidized when compares to methanol and hydrogen. [122] It results in a 1480mV of theoretical electromotive force (EMF) for direct formic acid fuel cells in relation to the theoretical oxygen reduction potential in the same electrolyte.

In the past decade intensive investigations have been aimed to understand the mechanism of HCOOH electrooxidation. [123-125] It is widely believed that formic acid oxidation on platinum surface undergoes a dual-pathway mechanism. [126-128] In the direct pathway, formic acid, most likely an adsorbed, molecular HCOOH_(ad) species, is oxidized “directly” via one or several reactive intermediates to CO₂, without the formation of CO_(ad) as shown in reaction (1.8). While in the indirect pathway, dehydration occurs to form adsorbed CO_{ad}, which is then oxidized to CO₂ as presented in reaction (1.9).



In addition to the above dual-pathway mechanism, Osawa [129] and Behm [130] recently proposed a third pathway for formic acid oxidation base on *in situ* IR studies. The so-called “triple pathway” involved bridge-bonded formate formation and subsequent

oxidation to CO₂. Therefore, the oxidation of formic acid can be summarized by the following diagram: [131]

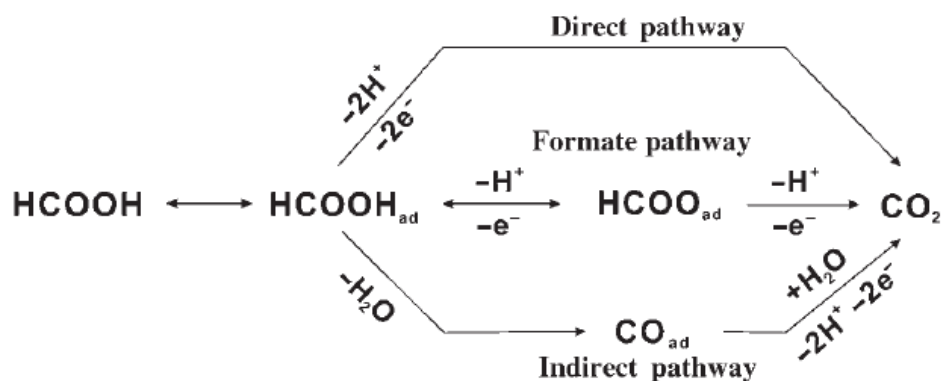


Figure 1.9 Scheme of formic acid oxidation.

1.2.5.4 Oxygen reduction

Oxygen reduction reaction is a four electron transfer process which is presented in reaction (1.10).



This is the cathodic reaction occurring in most direct liquid fuel cells (DLFCs). Similar to the anodic catalyst, Pt or Pt containing materials are commonly used at the cathode for DLFCs as the oxygen reduction catalysts. [132] The high cost of Pt limits the commercialization of fuel cells devices as both anode and cathode require Pt. Moreover, the slow kinetic dynamics of ORR on Pt also pose great challenge to fuel cells applications. The electrochemical ORR on Pt electrodes proceeds via a complex multi-step mechanism. [133-139] The mechanism depends on the experimental conditions, such as solvent, pH of

the electrolyte, as well as the electrode materials. Oxygen is reduced to superoxide (reaction (1.11)) in aprotic solvents while 2-electron or 4-electron reductions are the predominant pathways in aqueous and organic solvents, as shown in reaction (1.12) (1.10).



Recently, Sovinova [140] proposed a dual-path mechanism for ORR based on experimental and simulation studies: under a potential of 0.8V (vs NHE), the ORR proceeded predominantly via a 2-electron pathway with H_2O_2 as the main product (1.12); while at potential between 0.8V and the onset of the ORR a 4-electron path is dominant.

1.2.6 Improvement of catalytic performance for direct liquid fuel cells

1.2.6.1 Size control

Since the electrochemical reaction is a heterogeneous process which takes place on the catalyst surface, therefore, it is pivotal to increase the surface to volume ratio of the catalyst material in order to enhance the catalytic activity. One straightforward approach for substantial surface area increment is to reduce the size of the materials. Moreover, fabrication of materials with larger surface to volume ratio can also lower the usage of the precious metal, which is important for the commercialization of fuel cells. In general, platinum nanoparticles can be easily obtained by reducing platinum salt with hydrogen, [141, 142] hydrazine, [143] alcohol, [144-146] or sodium borohydride. [147] Antoine et al.

[15] investigate the activity of hydrogen oxidation on platinum particle size ranging from 2.5 nm to 28 nm by a model simulation. They concluded that decreasing the particle size can enhance the overall activity. Monodispersed Pt nanoparticles with an average particle size of 1.8, 2.3, 3.4, 3.8, 4.7, and 5.8 nm were synthesized by reducing platinum(II) acetylacetonate with 1,2-hexadecanediol in the presence of a long-chain carboxylic acid and alkylamine stabilizing agents. [149] The particle size can be well tuned by varying the refluxing time and a combination of either oleic acid and oleylamine or nonanoic acid and nonylamine protecting agents. The catalyst with an average diameter of 1.8 nm was found to possess the highest activity toward hydrogen oxidation. With regards to ORR, Pt nanoparticles with an average diameter of 2.2nm was proved to possess the best activity, [150] which is in good agreement with the fact that commercially available Pt/C with 2.5nm exhibiting the highest activity. Preparation of Pt nanoparticles with size ranging from 1-5nm was conducted by layer-by-layer construction through the displacement of under potential depositing Cu by Pt. The maximal activity at 2.2nm is owing to the weakest oxygen binding for all surface sites of the 2.2nm particles, which was confirmed by DFT calculations. Wan et al. [151] first prepared Pt nanoparticles and modified them with triphenylphosphine. The modified Pt nanoparticles were deposit onto carbon nanotubes. The organic molecules on the surface of the particle prevented the aggregation while acting as cross-linkers. The prepared Pt-CNT composite exhibited better catalytic performance in methanol oxidation in comparison to the commercial E-TEK catalyst. Recently, a peptide-mediated method was adapted to synthesized Pt particle ranging from sub-2 nm seed crystals to monodispersed 4 nm Pt polyhedra and 7 to 8 nm Pt cubes. [152] The merit

of this method is that it was conducted under ambient condition and the peptide could be removed from the metal surfaces at mild pH or in the present of enzymes.

Though materials with smaller size display higher activity, their stability is a key issue for fuel cell applications. As the size of the materials becomes smaller, a higher surface energy will be resulted thus leading to higher possibility for the aggregation and dissolution during the operation. Therefore, further efforts are still needed in respect to durability improvement.

1.2.6.2 Shape control

Shape control is another way to enhance the catalytic activity of platinum. It is reported that the catalysis by metal nanocrystals is often surface structure dependent. [153-157] For instance, Pt nanocubes with {100} terminated exhibited significantly enhanced electrocatalytic activity for oxygen reduction reaction. [158, 159] In general, metal nanocrystals tend to form facets which process minimum surface energy in order to minimize the total excess free energy. For example, platinum is usually bounded by three low-index planes, namely {100}, {110} and {111} with a face-centered cubic (fcc) symmetry. Normally, the shape of the nanocrystals is governed by thermodynamic and kinetic factors, which are controlled by both the intrinsic structural properties of the metal and reaction conditions such as solvents, capping agents or reducing agents. Therefore, it offers great potential to synthesize nanocrystals of different shapes by simply varying the synthetic conditions. Pt nanocrystals can be synthesized in a non-aqueous or aqueous

system. The platinum precursors can be hexachloroplatinic acid (H_2PtCl_6), potassium tetrachloroplatinate (K_2PtCl_4), potassium hexachloroplatinate (K_2PtCl_6), or platinum acetylacetonate ($\text{Pt}(\text{acac})_2$) depending on the choice of solvents. [160] Borohydride, hydrazine, hydrogen, citrate, and ascorbic acid can be used as reducing agents in an aqueous solution and diols, polyols and amines are commonly used in organic systems. Polycrystalline Pt nanoparticles (NPs) and length-controlled Pt nanorods (NRs) with exposed high index facets were prepared through a catalytic growth approach from Mn_3O_4 NPs. [161] Mn_3O_4 played a critical role in this preparation. Pt nanocrystals with high-index contain a high density of steps and kinks that consist of a large number of low-coordinated atoms, which will result in the improvement of catalytic activity. The Pt NRs exhibit higher catalytic activity and stability for the oxidization of methanol than commercially available Pt/C catalysts, indicating potential applications in direct methanol fuel cells. Platinum nanocubes can be obtained by a non-aqueous synthesis in the presence of $\text{Fe}(\text{CO})_5$, [162] $\text{Co}_2(\text{CO})_8$, [163] $\text{W}(\text{CO})_6$. [164] It is demonstrated that the favorable growth of Pt nanocube is mainly due to the co-adsorption of CO and amine on the Pt {100} surface. Pt nanocube was found to display higher activity toward methanol, ethanol and formic acid oxidation owing to the dominantly exposed (100) facets as compared to Pt nanospheres. [21] Moreover, Pt concave nanocrystals were prepared by the reduction of Pt pyrophosphato complex in presence of Br^- ions as the capping agent. [165] The concave Pt nanocrystals were enclosed by high index facets including (520), (720) and (830), and thus exhibited substantially enhanced electrocatalytic activity compared to Pt cubes and the commercial Pt/C. Recently, *in situ* shaping of Pt nanoparticles on carbon support was achieved by a one

pot synthesis in the presence of both an anchoring agent and the carbon support. [166] Cysteamine was used as the anchoring agent as well as the shape-controlled agent which induces Pt nanocubes overgrown on the carbon supports. The *in situ* cubic Pt/C possesses superior performance for ORR catalysis.

1.2.6.3 Incorporation of other metals

It is generally accepted that M-Pt nanocrystals exhibit better electrocatalytic activity attributed to a so called bifunctional mechanism. [167] One commonly studied example is PtRu which shows excellent activity towards methanol oxidation compared to pure Pt-based nano-materials going through the bifunctional mechanism. [168-173] Other metals such as Ni, [174] Mn, [175] Co, [176] Cu [177] and Zn [178] were also proven to be the promoter for electrocatalytic activity in form of PtM electrocatalysts. Other than bifunctional mechanism, similar to the case of Ru, another possibility for the enhancement of catalytic performance is the electronic effect induced by the foreign metal. It is considered that the incorporation of another metal into the lattice would shift the d-orbitals of Pt and in turn weakening the binding to the reaction intermediates. However, further investigations are needed for direct evidences for this theory even though there are some computational simulations shedding light on the electronic effect. Recently, Pt containing ternary alloys were demonstrated to exhibit improved catalytic activity including PtRuNi, [179] PtRuOs, [180] PtRuIr, [181] PtRuW, [182] PtRuSn [183] and PtRuRh. [184] Some models have been proposed to account for the excellent activity. For instance, in case of

PtRuNi, the enhancement is ascribed to hydrogen spillover on Ni which liberates the Pt active sites. For PtRuSn, Sn behaves as the electronic modifier while the Ru acts as a water activator. As for PtRuW, hydrogen ions transferring to the tungsten oxide was suggested, which resulted in the catalytic improvement.

1.3 Scope of this thesis

As mentioned above that the high cost of Pt electrocatalysts hinders the widespread applications of fuel cells on a commercialized level. Therefore, the aim of the thesis is to develop Pt containing electrocatalysts with enhanced Pt utilization as well as improved activity for direct liquid fuel cells.

In Chapter 2, atomic design of Pt on the surface of Au nanoparticles was achieved by ion-adsorption and *in situ* electrochemical reduction. The submonolayer Pt structure was illustrated by CVs accompanied with ICP-MS analysis. The electrochemical properties of the resulting catalysts were fully studied. In Chapter 3, PtAg hollow nano-sphere was prepared through galvanic displacement. Physical characterizations including XRD, XPS and HRTEM were employed to verify the PtAg alloy formation. A detailed investigation of the as synthesized PtAg catalyst for formic acid and methanol oxidation were carried out and compared to commercially available Pt catalysts. In Chapter 4, Pd@PdPt/MWCNTs composite was fabricated via a two-step process which involved the preparation of Pd/MWCNTs precursor and the galvanic replacement between Pd and PtCl_4^{2-} . The electrochemical performance of Pd@PdPt/MWCNTs electrocatalyst for methanol and ethanol oxidation was thoroughly studied.

References

- [1] C. J. Zhong, J. Luo, P. N. Njoki, D. Mott, B. Wanjala, R. Loukrakpam, S. Lim, L. Wang, B. Fang, Z. Xu, *Energy Environ. Sci.* **2008**, 1, 454.
- [2] Website: fuelcelltoday (www.fuelcelltoday.com).
- [3] P. Costamagna, S. Srinivasan, *Quantum jumps in the PEMFC science and technology from the 1960s to the year 2000: part I. Fundamental scientific aspects. J. Power Sources* **2001**, pp 242.
- [4] G. Binnig, H. Rohrer, Ch. Gerber, E. Weibel, *Phys. Rev. Lett.* **1982**, 49, 57.
- [5] R. P. Feynman, *J. MEMS* **1992**, 1, 60.
- [6] S. M. Lindsay, *Introduction to Nanoscience*, Oxford University Press, New York, **2010**, Chapter 1, 11.
- [7] G. A. Somorjai, Y. Li, *Introduction to Surface Chemistry and Catalysis*, Wiley & Sons, Hoboken, **2010**, Chapter 1, 15.
- [8] W. Schmickler, *Interfacial Electrochemistry*, Oxford University Press, New York, 1996, Chapter 1, 24.
- [9] H. Wang, L. Wang, T. Sato, Y. Sakamoto, S. Tominaka, K. Miyasaka, N. Miyamoto, Y. Nemoto, O. Terasaki, Y. Yamauchi, *Chem. Mater.* **2012**, 24 (9), 1591.
- [10] J. Kibsgaard, Y. Gorlin, Z. Chen, and F. T. Aramillo, *J. Am. Chem. Soc.* **2012**, 134 (18), 7758.
- [11] J. Wang, X. B. Zhang, Z. L. Wang, L. M. Wang, W. Xing, X. Liu, *Nanoscale* **2012**, 4, 1549.
- [12] H. H. Wang, Z. Y. Zhou, Q. Yuan, N. Tian, S. G. Sun, *Chem. Commun.* **2011**, 47,

3407.

- [13] C.. Venkateswara Rao, B. Viswanathan, *J. Phys. Chem. C* **2010**, 114 (18), 8661.
- [14] B. Fang, M. S. Kim, J. H. Kim, M. Y. Song, Y. J. Wang, H. Wang, D. P. Wilkinson J. S. Yu, *J. Mater. Chem.* **2011**, 21, 8066.
- [15] H. Huang, D. Sun, X. Wang, *J. Phys. Chem. C* **2011**, 115, 19405.
- [16] L. Gana, R. Lv, H. Du, B. Li, F. Kang, *Carbon* **2009**, 47,1833.
- [17] M. S. Saha, R. Li, X. Sun, *J. Power Source* **2008**, 177, 314.
- [18] X. Zhang, W. Lu, J. Da, H. Wang, D. Zhao, P. A. Webley, *Chem. Commun.* **2009**, 45, 195.
- [19] S. Sun, G. Zhang, D. Geng, Y. Chen, R. Li, M. Cai, X. Sun, *Angew. Chem.* **2011**, 50, 422.
- [20] C. Wang, H. Daimon, T. Onodera, T. Koda, S. Sun, *Angew. Chem.* **2008**, 120, 3644.
- [21] Y. W. Lee, S. B. Han, D. Y. Kim, K. W. Park, *Chem. Commun.* **2011**, 47, 6296.
- [22] S. D. Thompson, L.R. Jordan, M. Forsyth, *Electrochim. Acta* **2001**, 46, 1657.
- [23] S. D. Thompson, L. R. Jordan, A. K. Shukla, M. Forsyth, *J. Electroanal. Chem.* **2001**, 515, 61.
- [24] H. Kim, N. P. Subramanian, B. N. Popov, *J. Power Sources* **2004**, 138,14.
- [25] O. Antoine, R. Durand, *J. Electroche. Solid State Lett.* **2001**, 4, A55.
- [26] E. J. Taylor, E. B. Anderson, N. R. K. Vilambi, *J. Electrochem. Soc.* **1992**, 139, L45.
- [27] N. R. K. Vilambi, E. B. Anderson, E. Taylor, *J. US Patent* **1992**, 5, 84.
- [28] M. C. Tsai, T. K. Yeh, C. H. Tsai, *Electrochem. Commun.* **2006**, 8, 1445.
- [29] A. Bauer, E. L. Gyenge, C. W. Oloman, *Electrochim. Acta* **2006**, 51, 5356.

- [30] F. Gloaguen, J. M. Leager, C. Lamy, A. Marmann, U. Stimming, R. Vogela, *Electrochim. Acta* **1999**, 44, 1805.
- [31] G. Siné, I. Duo, B. Elroustom, G. Fóti, Ch. Comminellis, *J. Appl. Electrochem.* **2006**, 36, 847.
- [32] L. M. Plyasova, I. Y. Molina, A. N. Gavrilov, S. V. Cherepanova, O. V. Cherstiouk, N. A. Rudin, E. R. Savinova, G. A. Tsirlina, *Electrochim. Acta* **2006**, 51, 4477.
- [33] G. Y. Zhao, C. L. Xu, D. J. Guo, H. Li, H. L. Li, *Appl. Surf. Sci.* **2007**, 253, 3242.
- [34] U. H. Lee, J. H. Lee, D. Y. Jung, Y. U. Kwon, *Adv. Mater.* **2006**, 18, 2825.
- [35] G. Y. Zhao, C. L. Xu, D. J. Guo, H. Li, H. L. Li, *J. Power Sources* **2006**, 162, 492.
- [36] M. Yang, F. Qu, Y. Lu, Y. He, G. Shen, R. Yu, *Biomaterials* **2006**, 27, 5944.
- [37] F. Liu, J. L. Yang, W. Zhou, *Adv. Funct. Mater.* **2005**, 15, 1459.
- [38] Tian, N.; Zhou, Z.-Y.; Sun, S.-G.; Ding, Y.; Wang, Z. L. *Science* **2007**, 316, 732.
- [39] J. L. Lu, S. F. Lu, D. Wang, M. Yang, Z. Liu, Ch. W. Xu., S. P. Jiang, *Electrochim. Acta* **2009**, 54, 5486.
- [40] J. H. Jiang, A. Kucernak, *Electrochem. Commun.* **2009**, 11, 1005.
- [41] S.S. Djokic, B. E. Conway, R. E. White, *Modern aspects of electrochemistry*, Kluwer Academic/Plenum Publishers **2002**, 35.
- [42] C. Kerr, D. Barker, F. Walsh, *Electroless deposition of metals Trans IMF* **2001**, 79(1), 41e6.
- [43] P. Steinmetz, S. Alperine, A. Friant-Costantini, P. Josso, *Surf. Coat. Technol.* **1990**, 43(44), 500.
- [44] J. J. Wang, G. P. Yin, J. Zhang, Z. B. Wang, Y. Z. Gao, *Electrochim. Acta* **2007**, 52,

7042.

- [45] J. Wang, G. Yin, Y. Shao, Z. Wang, Y. Gao, *J. Electrochem. Soc.* **2007**, 154, B687.
- [46] W. Yao, J. Yang, J. Wang, Y. Nuli, *Electrochem. Commun.* **2007**, 9, 1029.
- [47] Y. Song, R. M. Garcia, R. M. Dorin, H. Wang, Y. Qiu, E. N. Coker, W. A. Steen, J. E. Miller, J. A. Shelnutt, *Nano Lett.* **2007**, 7, 3650.
- [48] S. Z. Chu, H. Kawamura, M. Mori, *J. Electrochem. Soc.* **2008**, 155, D414.
- [49] L. Qu, L. Dai, E. Osawa, *J. Am. Chem. Soc.* **2006**, 128, 5523.
- [50] J. Chen, B. Lim, E. P. Lee, Y. Xia, *Nano Today* **2009**, 4, 81.
- [51] C. Susut, T. D. Nguyen, G. B. Chapman, Y. Tong, *Electrochim. Acta* **2008**, 53, 6135.
- [52] R. M. Rioux, H. Song, M. Grass, S. Habas, K. Niesz, J. D. Hoefelmeyer, P. Yang, G. A. Somorjai, *Top. Catal.* **2006**, 39, 167.
- [53] M. Harada, H. J. Einaga, *Colloid Interface Sci.* **2007**, 308, 568.
- [54] J. Prabhuram, T. S. Zhao, Z. X. Liang, R. Chen, *Electrochim. Acta* **2007**, 52, 2649.
- [55] C. Roychowdhury, F. Matsumoto, V. B. Zeldovich, S. C. Warren, P. F. Mutolo, M. J. Ballesteros, U. Wiesner, H. D. Abrua, F. J. DiSalvo, *Chem. Mater.* **2006**, 18, 3365.
- [56] D. Nagao, Y. Shimazaki, Y. Kobayashi, M. Konno, *Colloids Surf.* **2006**, 273, 97.
- [57] J. W. Guo, T. S. Zhao, J. Prabhuram, R. Chen, C. W. Wong, *Electrochim. Acta* **2005**, 51, 754.
- [58] O. Masala, R. Seshadri, *Annu. Rev. Mater. Res.* **2004**, 34, 41.
- [59] G. J. Demazeau, *Mater. Sci.* **2008**, 43, 2104.
- [60] K. Byrappa, T. Adschiri, *Prog. Cryst. Growth Charact. Mater.* **2007**, 53, 117.
- [61] Q. Yi, J. Zhang, A. Chen, X. Liu, G. Xu, Z. Zhou, *J. Appl. Electrochem.* **2008**, 38, 695.

- [62] P. Holt-Hindle, Q. Yi, G. Wu, K. Koczkur, A. Chen, *J. Electrochem. Soc.* **2008**, 155, K5.
- [63] Q. Yi, W. Huang, X. Liu, G. Xu, Z. Zhou, A. Chen, *J. Electroanal. Chem.* **2008**, 197, 619.
- [64] J. Wang, P. Holt-Hindle, D. MacDonald, D. F. Thomas, A. Chen, *Electrochim. Acta* **2008**, 53, 6944.
- [65] Z. Zhang, D. A. Blom, Z. Gai, J. R. Thompson, J. Shen, S. Dai, *J. Am. Chem. Soc.* **2003**, 125, 7528.
- [66] Y. Hou, H. Kondoh, R. Che, M. Takeguchi, T. Ohta, *Small* **2006**, 2, 235.
- [67] D. U. Hong, C. H. Han, S. H. Park, I. J. Kim, J. Gwak, S.-D. Han, H. J. Kim, *Curr. Appl. Phys.* **2009**, 9, 172.
- [68] X. Peng, K. Koczkur, S. Nigro, A. Chen, *Chem. Commun.* **2004**, 2872.
- [69] J. Wang, D. F. Thomas, A. Chen, *Chem. Commun.* **2008**, 5010.
- [70] H. Chen, Y. Wang, S. Dong, *Inorg. Chem.* **2007**, 46, 10587.
- [71] P. Holt-Hindle, S. Nigro, M. Asmussen, A. Chen, *Electrochem. Commun.* **2008**, 10, 1438.
- [72] Q. Yi, L. Li, W. Yu, Z. Zhou, X. Liu, G. Xu, *J. Alloys Compd.* **2008**, 466, 52.
- [73] H. Shiga, T. Okubo, M. Sadakata, *Ind. Eng. Chem. Res.* **1996**, 35, 4479.
- [74] D. Bae, K. Han, J. H. Adair, *J. Am. Ceram. Soc.* **2002**, 85, 1321.
- [75] M. Yang, Y. Yang, Y. Liu, G. Shen, R. Yu, *Biosens. Bioelectron.* **2006**, 21, 1125.
- [76] B. Breitscheidel, J. Zieder, U. Schubert, *Chem. Mater.* **1991**, 3, 559.
- [77] L. Hu, K. A. Boateng, J. M. Hill, *J. Mol. Catal. A: Chem.* **2006**, 259, 51.

- [78] B. K. Jena, C. R. Raj, *J. Phys. Chem. C* **2008**, 112, 3496.
- [79] K. Balakrishnan, R. D. Gonzalez, *Langmuir* **1994**, 10, 2487.
- [80] M. Yang, Y. Yang, Y. Liu, G. Shen, R. Yu, *Biosens. Bioelectron.* **2006**, 21, 1125.
- [81] R. J. Bass, T. M. Dunn, Y. Lin, K. L. Hohn, *Ind. Eng. Chem. Res.* **2008**, 47, 7184.
- [82] G. Facchin, G. Caruran, R. Campostrini, S. Gialanella, L. Lutterotti, L. Armelao, G. Marci, L. Palmisano, A. Sclafani, *J. Sol-Gel Sci. Technol.* **2000**, 18, 29.
- [83] L. W. Beakley, S. E. Yost, R. Cheng, B. D. Chandler, *Appl. Catal., A* **2005**, 292, 124.
- [84] X. Kang, Z. Mai, X. Zou, P. Cai, J. Mo, *Talanta* **2008**, 74, 879.
- [85] H. Rabat, C. Andrezza, P. Brault, A. Caillard, F. Beguin, C. Charles, R. Boswell, *Carbon* **2009**, 47, 209.
- [86] M. Miyauchi, *Phys. Chem. Chem. Phys.* **2008**, 10, 6258.
- [87] W. Lee, M. Alhosan, S. L. Yohe, N. L. Macy, W. H. Smyrl, *J. Electrochem. Soc.* **2009**, 155, B915.
- [88] N. Perkas, D. P. Minh, P. Gallezot, A. Gedanken, M. Besson, *Appl. Catal. B* **2005**, 59, 121.
- [89] Y. H. Ng, S. Ikeda, T. Harada, S. Park, T. Sakata, H. Mori, M. Matsumura, *Chem. Mater.* **2008**, 20, 1154.
- [90] H. Wang, X. Sun, Y. Ye, S. Qiu, *J. Power Sources* **2006**, 161, 839.
- [91] H. Plank, C. Gspan, M. Dienstleder, G. Kothleitner, F. Hofer, *Nanotechnology* **2008**, 19, 485302.
- [92] L. Penate-Quesada, J. Mitra, P. Dawson, *Nanotechnology* **2007**, 18, 215203.
- [93] S. Frabboni, G. C. Gazzadi, L. Felisari, A. Spessot, *Appl. Phys. Lett.* **2006**, 88, 213116.

- [94] P. Bommersbach, M. Chaker, M. Mohamedi, D. Guay, *J. Phys. Chem. C* **2008**, 112, 14672.
- [95] W. T. Nichols, T. Sasaki, N. Koshizakia, *J. Appl. Phys.* **2006**, 100, 114913.
- [96] S. Uhm, H. J. Lee, J. Lee, *Phys. Chem. Chem. Phys.* **2009**, 11, 9326.
- [97] L. W. Liao, S. X. Liu, Q. Tao, B. Geng, P. Zhang, C. M. Wang, Y. X. Chen, S. Ye, *J. Electroanal. Chem.* **2011**, 650, 233.
- [98] S. K. Desai, M. Neurock, K. Kourtakis, *J. Phys. Chem. B* **2002**, 106, 2559.
- [99] Y. P. Sun, L. Xing, K. Scott, *J. Power Sources* **2010**, 195, 1.
- [100] Q. S. Chen, S. G. Sun, Z. Y. Zhou, Y. X. Chen, S. B. Deng, *Phys. Chem. Chem. Phys.* **2008**, 10, 3645.
- [101] H. Wang, H. D. Abrun, *Struct. Bond* **2011**, 141, 33.
- [102] T. H. M. Housmans, A. H. Wonders, M. T. M. Koper, *J. Phys. Chem. B* **2006**, 110, 10021.
- [103] W. Gao, M. Zhao, Q. Jiang, *Chem. Phys. Chem.* **2008**, 9, 2092.
- [104] C. Y. Niu, J. Jiao, B. Xing, G. C. Wang, X. H. Bu *J. Comput. Chem.* **2010**, 31, 10 .
- [105] K. Kunimatsu, H. Hanawa, H. Uchida, M. Watanabe, *J. Electroanal. Chem.* **2009**, 632, 109.
- [106] S. X. Liu, L. W. Liao, Q. Tao, Y. X. Chen, S. Ye, *Chem. Chem. Phys.* **2011**, 13, 9725.
- [107] G. A. Tritsarlis, J. Rossmeisl, *J. Phys. Chem. C* **2012**, 116 (22), 11980.
- [108] M. Watanabe, S. Motoo, *J. Electroanal. Chem.* **1975**, 60, 267.
- [109] H. A. Gasteiger, N. Markovic, P. N. Ross, E. J. Cairns, *J. Phys. Chem.* **1994**, 98, 617.

- [110] T. Iwasita, F. C. Nart, W. Vielstich, *Ber. Bunsen. Phys. Chem.* **1990**, *94*, 1030–1034.
- [111] T. Frelink, W. Visscher, J. A. R. Van Veen, *Langmuir* **1996**, *12*, 3702.
- [112] C. Lamy, A. Lima, V. LeRhun, F. Delime, C. Coutanceau, J. M. Léger, *J. Power Sources* **2002**, *105*, 283.
- [113] J. Wang, S. Wasmus, R. F. Savinell, *J. Electrochem. Soc.* **1995**, *142*, 4218.
- [114] R. Parsons, T. Vandernoot, *J. Electroanal. Chem.* **1988**, *257*, 9.
- [115] H. Hitmi, E. M. Belgsir, J. M. Léger, C. Lamy, R. O. Lezna, *Electrochim. Acta* **1994**, *39*, 407.
- [116] F. Vigier, S. Rousseau, C. Coutanceau, J. M. Leger, C. Lamy, C. Lamy, *Top. Catal.* **2006**, *40*, 111.
- [117] B. Bittins-Cattaneo, S. Wilhelm, E. Cattaneo, H. Buschmann, W. Vielstich, *Ber. Bunsen. Phys. Chem.* **1988**, *92*, 1210.
- [118] M. Shao, R. Adzic, *Electrochim. Acta* **2005**, *50*, 2415.
- [119] M. Heinen, Z. Jusys, R. J. Behm, *J. Phys. Chem. C* **2010**, *114*, 9850.
- [120] S. C. S. Lai, S. E. F. Kleyn, V. Rosca, M. T. M. Koper, *J. Phys. Chem. C* **2008**, *112*, 19080.
- [121] S. Rousseau, C. Coutanceau, C. Lamy, J. M. Leger, *J. Power Sources* **2006**, *158*, 18.
- [122] S. Uhm, H. J. Lee, J. Lee, *Phys. Chem. Chem. Phys.* **2009**, *11*, 9326.
- [123] N. M. Markovic, H. A. Gasteiger, P. N. Ross, X. D. Jiang, I. Villegas, M. J. Weaver, *Electrochim. Acta* **1995**, *40*, 91.
- [124] R. Parsons, T. VanderNoot, *J. Electroanal. Chem.* **1988**, *257*, 9.
- [125] N. Kizhakevariam, M. J. Weaver, *Surf. Sci.* **1994**, *310*, 183.

- [126] A.Capon, R.Parsons, *J. Electroanal. Chem.* **1973**, 45, 205.
- [127] O.Wolter, J. Willsau, J. Heitbaum, *J. Electrochem. Soc.* **1985**, 132, 1635.
- [128] S. G. Sun, J. Clavilier, *J. Electroanal. Chem.* **1988**, 240, 147.
- [129] A. Miki, S. Ye, M. Osawa, *Chem. Commun.* **2002**, 1500.
- [130] Y. X. Chen, M. Heinen, Z. Jusys, R. J. Behm, *Chem. Phys. Chem.* **2007**, 8, 380.
- [131] Y. X. Chen, M. Heinen, Z. Jusys, R. J. Behm, *Angew. Chem. Int. Ed.* **2006**, 45, 981.
- [132] W. Vielstich, A.Lamm, H. A.Gasteiger, *Handbook of fuel cells: Fundamentals, Technology and Applications* Wiley: Chichester, **2003**, 3, Chapter 1.
- [133] A. Damjanovic, O. J. Murphy, S. Srinivasan, B. E. Conway, *Electrochemistry in Transition* Plenum Press, New York, **1992**, 107.
- [134] A. Damjanovic, V. Brusic, *Electrochim. Acta* **1967**, 12, 615.
- [135] Q. Dong, S. Santhanagopalan, R. E. White, *J. Electrochem. Soc.* **2007**, 154, A888.
- [136] H. A. Gasteiger, S. S. Kocha, B. Sompalli, F. T. Wagner, *Appl. Catal., B* **2005**, 56, 9.
- [137] N. M. Markovic, P. N. Ross, *Surf. Sci. Rep.* **2002**, 45, 121.
- [138] H. Wroblowa, Y. C. Pan, J. Razumney, *J. Electroanal. Chem.* **1976**, 69, 195.
- [139] A. J. Bard, *J. Am. Chem. Soc.* **2010**, 132, 7559
- [140] P. S. Ruvinskiy, A. Bonnefont, C. Pham-Huu, E. R. Savinova, *Langmuir* **2011**, 27, 9018.
- [141] T. S. Ahmadi, Z. L. Wang, T. C. Green, A. Henglein, M. A. El-Sayed, *Science* **1996**, 272, 1924.
- [142] M. Yamada, S. Kon, M. Miyake, *Chem. Lett.* **2005**, 34, 1050.
- [143] J. Solla-Gullon, V. Montiel, A. Aldaz, J. Clavilier, *J. Electroanal. Chem.* **2000**, 491,

69.

- [144] T. Herricks, J. Chen, Y. Xia, *Nano Lett.* **2004**, 4, 2367.
- [145] H. Song, F. Kim, S. Connor, G. A. Somorjai, P. Yang, *J. Phys. Chem. B* **2005**, 109, 188.
- [146] J. Chen, T. Herricks, Y. Xia, *Angew. Chem, Int. Ed.* **2005**, 44, 2589.
- [147] K. Niesz, M. Grass, G. A. Somorjai, *Nano Lett.* **2005**, 5, 2238.
- [148] O. Antoine, Y. Bultel, R. Durand, P. Ozil, *Electrochim. Acta* **1998**, 43, 3681.
- [149] Ch. Venkateswara Rao, B. Viswanathan, *J. Phys. Chem. C* **2010**, 114 (18), 8661.
- [150] M. Shao, A. Peles, K. Shoemaker, *Nano Lett.* **2011**, 11(9), 3714.
- [151] Y. Mu, H. Liang, J. Hu, Li Jiang, L. Wan, *J. Phys. Chem. B* **2005**, 109, 22212.
- [152] L. M. Forbes, A. P. Goodwin, J. N. Cha, *Chem. Mater.* **2010**, 22 (24), 6524.
- [153] Z. Y. Zhou, N. Tian, Z. Z. Huang, D. J. Chen, S. G. Sun, *Faraday Discuss.* **2008**, 140, 81.
- [154] C. K. Tsung, J. N. Kuhn, W. Y. Huang, C. Aliaga, L. I. Hung, G. A. Somorjai, P. D. Yang, *J. Am. Chem. Soc.* **2009**, 131, 5816.
- [155] K. M. Bratlie, H. Lee, K. Komvopoulos, P. D. Yang, G. A. Somorjai, *Nano Lett.* **2007**, 7, 3097.
- [156] R. M. Rioux, H. Song, M. Grass, S. E. Habas, K. Niesz, J. D. Hoefelmeyer, P. Yang, G. A. Somorjai, *Top. Catal.* **2006**, 39, 167.
- [157] H. Lee, S. E. Habas, S. Kweskin, D. Butcher, G. A. Somorjai, P. D. Yang, *Angew. Chem., Int. Ed.* **2006**, 45, 7824.
- [158] C. Wang, H. Daimon, T. Onodera, T. Koda, S. H. Sun, *Angew. Chem., Int. Ed.* **2008**,

47, 3588.

- [159] N. M. Markovic, H. A. Gasteiger, P. N. Ross, *J. Phys. Chem.* **1995**, 99, 3411.
- [160] Z. M. Peng, S.C. Yang, H. Yang, C. Kumar, *Metallic Nano-materials*, Wiley-VCH Verlag, Weinheim, **2009**, 1, Chapter 10.
- [161] X. Gong, Y. Yang, S. Huang, *Chem. Commun.* **2011**, 47, 1009.
- [162] C. Wang, H. Daimon, Y. Lee, J. Kim, S. H. Sun, *J. Am. Chem. Soc.* **2007**, 129, 6974.
- [163] S. I. Lim, I. Ojea-Jimenez, M. Varon, E. Casals, J. Arbiol, V. Puntès, *Nano Lett.* **2010**, 10, 964.
- [164] J. Zhang, J. Y. Fang, *J. Am. Chem. Soc.* **2009**, 131, 18543.
- [165] T. Yu, D. Y. Kim, H. Zhang, Y. Xia, *Angew. Chem. Int. Ed.* **2011**, 50, 2773.
- [166] C. Kim, S. S. Kim, S. Yang, J. W. Han, H. Lee, *Chem. Commun.* **2012**, 48, 6396.
- [167] S. Wasmus, A. Kuver, *J. Electroanal. Chem.* **1999**, 461, 14.
- [168] C. Bock, C. Paquet, M. Couillard, G. A. Botton, B. R. MacDougall, *J. Am. Chem. Soc.* **2004**, 126, 8028.
- [169] T. K. Sau, M. Lopez, D. V. Goia, *Chem. Mater.* **2009**, 21, 3649.
- [170] G. Wu, L. Li, B. Q. Xu, *Electrochim. Acta* **2004**, 50, 1.
- [171] A. N. Gavrilov, E. R. Savinova, P. A. Simonov, V. I. Zaikovskii, S. V. Cherepanova, G. A. Tsirlina, V. N. Parmon, *Phys. Chem. Chem. Phys.* **2007**, 9, 5476.
- [172] C. Roth, N. Benker, T. Buhrmester, M. Mazurek, M. Loster, H. Fuess, D. C. Koningsberger, D. E. Ramaker, *J. Am. Chem. Soc.* **2005**, 127, 14607.
- [173] S. Stoupin, H. Rivera, Z. R. Li, C. U. Segre, C. Korzeniewski, D. J. Casadonte, H. Inoue, E. S. Smotkin, *Phys. Chem. Chem. Phys.* **2008**, 10, 6430.

- [174] Y. Xu, S. Hou, Y. Liu, Y. Zhang, H. Wang, B. Zhang, *Chem. Commun.* 2012, **48**, 2665.
- [175] Y. Kang, C. B. Murray, *J. Am. Chem. Soc.*, **2010**, 132 (22), 7568.
- [176] H. Yang, J. Zhang, K. Sun, S. Zou, J. Fang, *Angew. Chem. Int. Ed.* **2010**, 49, 6848.
- [177] X. Yu, D. Wang, Q. Peng, Y. Li, *Chem. Commun.* **2011**, 47, 8094.
- [178] Y. Kang, J. B. Pyo, X. Ye, T. R. Gordon, B. C. Murray, *ACS Nano*, **2012**, 6(6), 5642.
- [179] Y. M. Liang, H. M. Zhang, Z. Q. Tian, X. B. Zhu, X. L. Wang, B. L. Yi, *J. Phys. Chem. B* **2006**, 110, 7828.
- [180] K. L. Ley, R. X. Liu, C. Pu, Q. B. Fan, N. Leyarowska, C. Segre, E. S. Smotkin, *J. Electrochem. Soc.* **1997**, 144, 1543.
- [181] D. S. Geng, D. Matsuki, J. J. Wang, T. Kawaguchi, W. Sugimoto, Y. Takasu, *J. Electrochem. Soc.* **2009**, 156, B397.
- [182] K. W. Park, J. H. Choi, K. S. Ahn, Y. E. Sung, *J. Phys. Chem. B* **2004**, 108, 5989.
- [183] L. X. Yang, R. G. Allen, K. Scott, P. Christenson, S. Roy, *J. Power Sources* **2004**, 137, 257.
- [184] T. Kawaguchi, Y. Rachi, W. Sugimoto, Y. Murakami, Y. Takasu, *J. Appl. Electrochem.* **2006**, 36, 1117.

Chapter 2

Synthesis of Ultralow Pt Loading Au@Pt/MWCNTs for Formic Acid Electrooxidation and Methanol-Tolerant Oxygen Reduction Reaction

2.1 Background

2.1.1 A brief overview of carbon nanotubes

Since the discovery of multiwall carbon nanotubes (MWCNTs) in 1991, people have applied MWCNTs into a range of different fields such as supercapacitors, fuel cells, lithium ion batteries, accumulators, sensors as well as biomedical applications [1-5] due to their unique physical and chemical properties. [5-11] CNT is an allotrope of carbon like amorphous carbon, graphite and diamond. It can be structurally described as a sheet of graphene rolled into a tube. With regards to the number of layer in the sidewall of MWCNTs, it can be categorized into single-wall carbon nanotubes (SWCNTs), double-wall carbon nanotubes (DWCNTs) and multi-wall carbon nanotubes (MWCNTs), as shown in Figure 2.1. The synthesis of MWCNTs mainly involve the decomposition of carbon sources, such as graphite and hydrocarbon, followed by deposition and growth in the presence of certain metal catalysts.[12, 13] Some of the commonly used methods include chemical vapor deposition (CVD), arc discharge and laser vaporization.

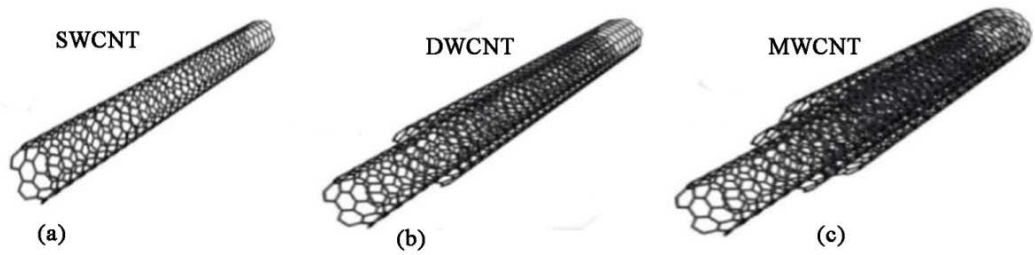


Figure 2.1 Schematic illustrations of different MWCNTs.

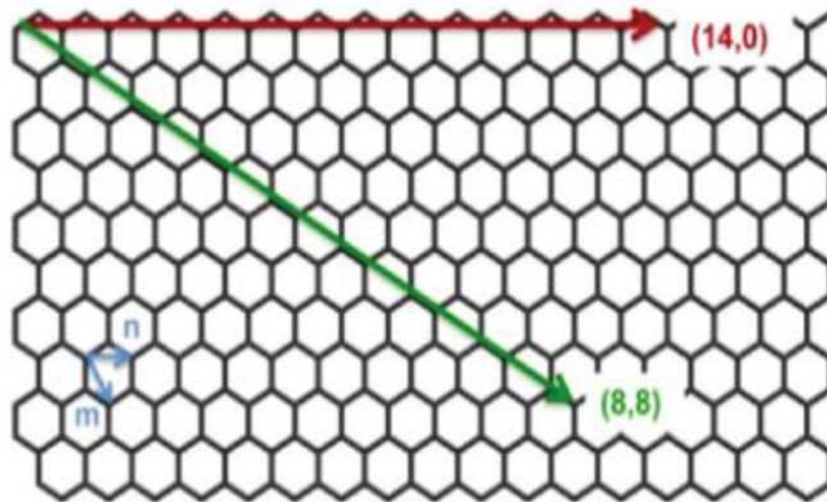


Figure 2.2 Orientation of the carbon network.

2.1.1.1 Physical and chemical properties of MWCNTs

MWCNTs show similar properties to that of graphene to some extent since they are rolled form of graphene. In general, the electronic structure of MWCNTs depends on the details of their microstructure. Additionally, both the cylindrical geometry and an extended π -electron system of the sp^2 carbons bonded in the hexagonal network give rise to different properties as compared to graphene. For example, different ways of rolling up of graphene sheet result in different conductivities ranging from metallic to semiconducting [14] and different numbers of sidewall layers results in variations in Raman scattering. [15] Depending on the wrapping orientation relative to the carbon network, different MWCNTs

can be described by the indices of their chiral vector (n and m , as shown in Figure 2.2). For instance, armchair MWCNTs ($n = m$) usually possess metallic conductivity while Zigzag ($m = 0$) or chiral ($n \neq m$) MWCNTs are semiconductors. To be more specific, the wrapping of the network is presented by the following equation: [16]

$$C = na_1 + ma_2 \quad (2.1)$$

where a_1 and a_2 : unit vectors of the hexagonal network; n and m : integers.

Analysis shows that the MWCNTs are metallic if the value of $n - m$ is an integer. Otherwise, the MWCNTs formed are semiconductors in nature with a band gap of $E_g = 0.9/d$ eV, where d is the diameter of the nanotube. Some noteworthy physical attributes of MWCNTs are summarized in Table 2.1. [16] The synthetic method of MWCNTs determines their quality in terms of crystallinity and impurity contents.[17] Data presented in Table 2.1 apply to high quality MWCNTs. The electrical properties make MWCNTs a promising electrode material which can be applied to the field of electrocatalysis[18] and field effect transistor (FET)-based sensors.[19] Moreover, the high strength of MWCNTs can be exploited in mechanical applications.

Table 2.1 Summary of the physical attributes of MWCNTs

Attribute	Comment
Metallic to semiconductor electrical conductivity, depending on microstructure	No other known molecule has this property
Electrical conductivity: $10^8 \Omega^{-1} \text{ m}^{-1}$	Comparable to that of copper
Thermal conductivity: $10^4 \text{ Wm}^{-1} \text{ K}^{-1}$	> that of diamond
Carrier mobility: $10^4 \text{ cm}^2 \text{ V}^{-1} \text{ s}^{-1}$	> that of GaAs
Supports a current density of 10^9 A cm^{-2}	Due to very weak electromigration
Nanoscale heterojunctions	Common defect that can create an on-tube heterojunction
Young's modulus: 1 TPa	Stiffer than any other known material
Tensile strength: 150 GPa	600 times the strength/weight ratio of steel

In connection with the chemical properties of MWCNTs, some researcher reported a color change of MWCNTs which is originated from the interband excitonic resonance. [20] MWCNTs also exhibit similar properties as metals in showing a redox potential. [21] Therefore, MWCNTs can be used as a reductant [22] or an oxidant [23]. The most striking merit of MWCNTs is the high structural stability and corrosion resistance in acidic and basic solutions [24-26] which, once again, make them a very promising electrode material.

2.1.1.2 Modification of MWCNTs

Ideally, the surface of MWCNTs consists of an extended π -electron system of the sp^2 hybridized carbon hexagonal network resulting in very non-polarity and inert surface which is difficult for further functionalizing. Furthermore, pristine MWCNTs undergo aggregation easily when they are suspended in polar solvents due to bundling caused by van der Waals

interactions, presenting another difficulty for modification. The functionalization of MWCNTs mainly includes covalent and non-covalent modifications. [27] Proper additives were employed in the non-covalent modification which can generate some unique electrical and optical properties. [28] Figure 2.3 shows a typical functionalisation MWCNTs via non-covalent method which utilizes the π - π interaction to introduce amine groups onto the sidewall of MWCNTs. For covalent modification, surface oxidation is commonly used to generate hydroxyl and carboxyl groups for further functionalization as illustrated in Figure 2.4.

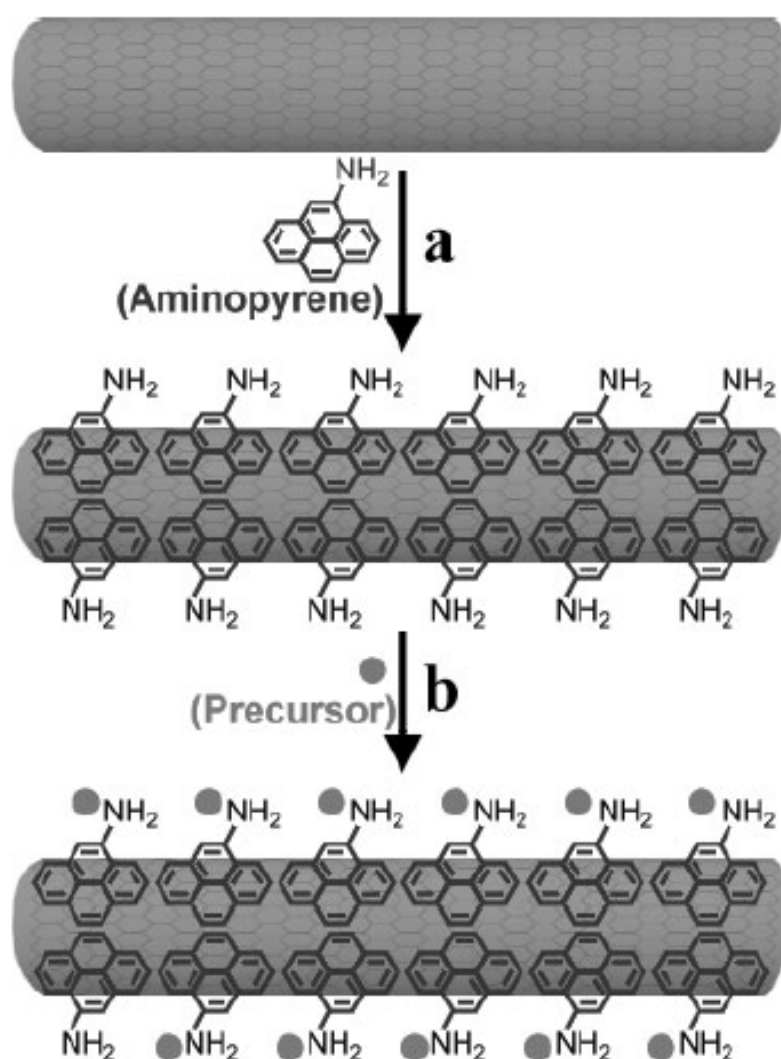


Figure 2.3 Scheme for modification of MWCNTs via non-covalent method. [29]

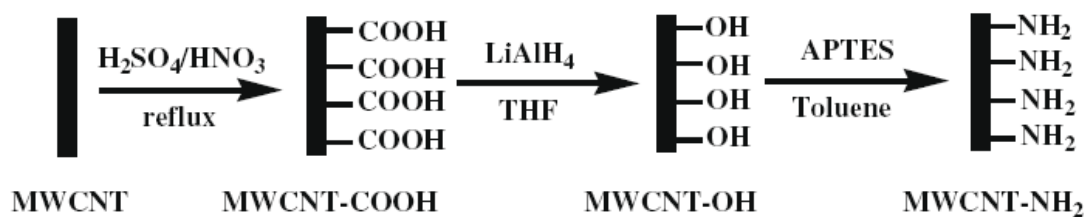


Figure 2.4 Scheme for modification of MWCNTs via covalent method.

2.1.2 Recent development of electrocatalysts for formic acid

Intensive research efforts have been devoted to the electrocatalysts design aiming to enhance the activity as well as the utilization of Pt for formic acid oxidation. There are two major catalysts designs in this connection. The first of which is to synthesize Pt containing mixed metal (Pt-M) alloys. The mechanism of the activity enhancement is still controversial and requires further investigations. For example, even the exact form and surface composition of the most active alloys are still ambiguous. [30-34] For instance, PtBi alloy was reported to show higher activity towards formic acid oxidation as compared to Pt. However, the interaction between Pt and Bi is still unclear though a CO free pathway has been proposed. However, it is widely acceptable that the incorporation of other metal will shift the d-orbitals of Pt leading to a weakened bonding between the poisoning intermediates and the catalysts. Another conclusion drawn is that a second metal can provide oxygenated species at a relatively low potential which help to remove the poisoning intermediates. PtAu alloy is one of the most efficient electrocatalysts for formic acid oxidation since it possesses high activity and durability. [35-37] PtSn [38], PtCu [39] and PtPb [40] were also proven to exhibit enhanced activity compared to their Pt

counterpart. Moreover, trimetallic alloy such as FePtAu [41] were also prepared for electrooxidation of formic acid. Another way to design effective catalyst for the formic acid oxidation is the fabrication of core-shell like structures. Au@Pt structures were extensively prepared by galvanic replacement, [42] thermal treatment, [43] electrostatic self-assembly, [44] and seeds-mediated growth. [45] In addition, using another metal to modify Pt surface was demonstrated to be a better way to enhance the activity. Bismuth, [46] lead, [47] and antimony [48] were proven to be potential candidates to decorate Pt surface in order to enhance its activity towards formic acid oxidation.

2.1.3 Recent development of Pt-based ORR catalyst

The activity enhancement of Pt for ORR can be achieved by shape-controlled synthesis, [49] alloys formation [50] and core-shell structures construction. [51] It was demonstrated that Pt(*hkl*) towards ORR exhibited an increasing activity in the order of Pt(111)<Pt(100)<Pt(110) in sulfuric acid.[52] Sun have successfully prepared Pt nanocrystals of different shapes. [53] The Pt nanocubes shows higher activity compared to its spherical and truncated cubic counterparts. The shape-dependent ORR activity is attributed to the different adsorption capabilities of sulfate ions on the Pt faces of different indices. The binding strength of Pt(111) with sulfate ions is dramatically higher than that of Pt(100) owing to the matching three-fold symmetry of the oxygen atoms and the Pt atoms on (111) layer. [54] Incorporating another metal can also increase the ORR activity. Extensive research efforts have been focused in this regards on the fabrication of Pt-based

alloys such as PtNi, [55,] PtFe, [56] and PtCo [57] for ORR catalysts. It is widely believed that the shift in d-orbitals of Pt by alloying with another metal is one possible reason for the activity enhancement. On the other hand, electrochemical dealloying [58, 59] is also needed to be taken into consideration. It occurs easily during the electrochemical analysis which results in a Pt skeleton shell. Another commonly used strategy for ORR catalyst optimization is a core-shell structure construction with the active component appearing on the outer shell for electrochemical reaction. The core-shell structures can be realized by electrochemical dealloying, [60] galvanic replacement, [61] or seed-mediated growth. [62] Though there is no consensus on the origination of the enhancement of the ORR activity for this sort of catalysts, DFT calculations [63] suggested that the lattice mismatch between the core and the shell may play a critical role.

2.1.4 Synthesis of ultralow Pt loading catalysts

The high cost of Pt catalysts is one of the major bottlenecks for the commercialization of fuel cells. Figure 2.5 shows the relationship between cost of Pt versus the layer thickness for a planar catalyst. [64] The cost of the catalysts can be reduced dramatically via employing a suitable substrate to replace the precious metal underneath. The cost could be cut down for a thousand times if monolayer Pt catalysts could be realized, which is of great significance for the widespread applications of fuel cell devices. Therefore, intensive interest has been concentrated on the design of catalysts with lower Pt loading. Successive reduction [65] is a common way to prepare catalysts with enhanced Pt utilization. Pt was

reduced in the presence of metal nanoparticle seeds (AuNPs in most cases) forming a core shell structure. The amount of the Pt growing on the surface of the seeds could be controlled easily by changing the Pt sources added. Additionally, catalysts with different activity can be obtained by tuning the size of the core employed. [66] Spontaneous deposition is another effective way to fabricate sub monolayer of Pt catalysts. However, it is found to be only available in the cases of Ru@Pt or Ru@Pd synthesis. [67] In the preparation process, Ru(0001) was immersed in the Pt source solution. Reaction occurs on the surface of Ru(0001) with the formation of Pt submonolayer, generating Ru oxide. Recently, underpotential deposit (UPD) and galvanic replacement were employed to prepare monolayer Pt catalysts. [68, 69] Monolayer copper is usually deposited on the surface of a precious metal such as Au, Pd and Pt by underpotential electrodeposition. The monolayer copper was replaced by Pt via galvanic replacement reaction between copper and Pt ions, resulting in the monolayer structure of Pt. The generation of monolayer copper is a key step for the monolayer Pt structure construction. Russell used *in situ* extended X-ray absorption fine structure (EXAFS) to study the UPD process of Cu on Au surface. [70] It was proven to be a morphology dependent process and it is difficult to realize a uniform and completed monolayer copper structure. Stabilization effect induced by the core materials was reported by Adzic. [71] The stability of Pt shell was increased by shifting its oxidation potential positively to which the dissolution of Pt did not take place at the cathodic reaction. Another emerging means for the construction of Pt monolayer structure is through galvanic replacement between metal alloys and Pt ions. [72] This facile method is suitable for low cost and large scale preparation compared to methods involving the UPD

of Cu. However, formation of Pt-M alloy shell was also reported to be dependent on the metal alloys employed and the amount of Pt source used. [73]

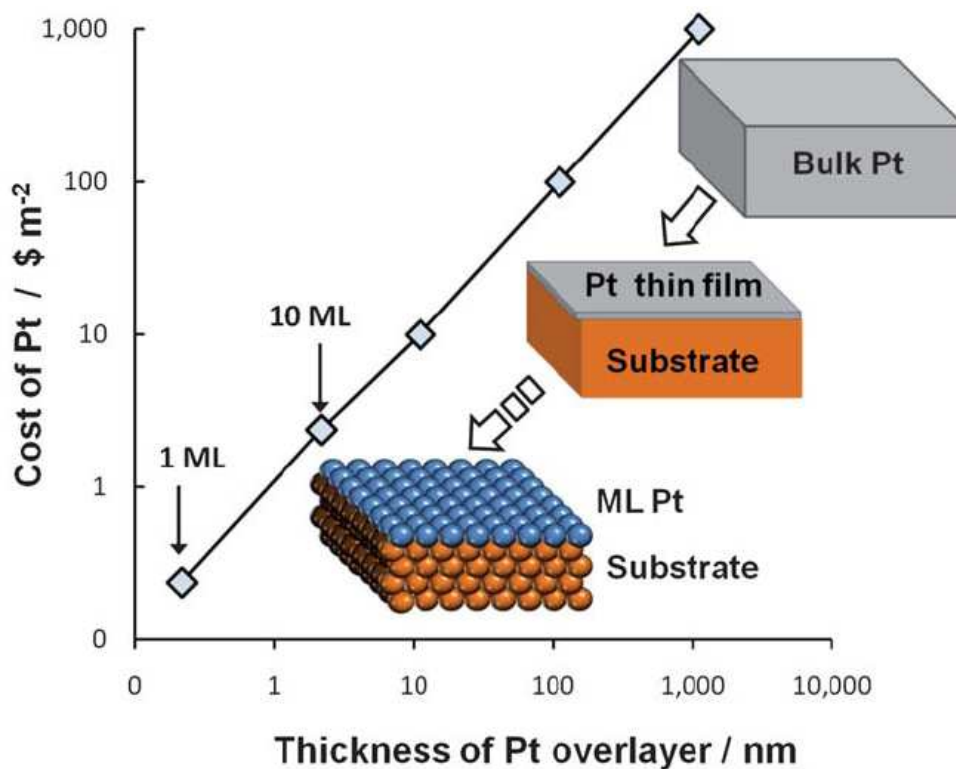


Figure 2.5 Relationship between cost of Pt and overlayer thickness for a planar configuration catalysts

2.2 Synthesis of ultralow loading Pt catalysts for formic acid oxidation and methanol tolerant oxygen reduction reaction

The preparation scheme for Au@Pt/MWCNTs is illustrated in Figure 2.6. Au nanoparticles were first loaded onto the surface of acid-treated MWCNTs forming a Au/MWCNTs composite. Ions adsorption was accomplished by immersing the Au/MWCNTs composite in 0.1M H₂SO₄ containing K₂PtCl₄ or K₂PtCl₆ of different

concentrations. Finally, Au@Pt/MWCNTs composite was obtained via *in situ* electrochemical reduction of the adsorbed Pt ions.

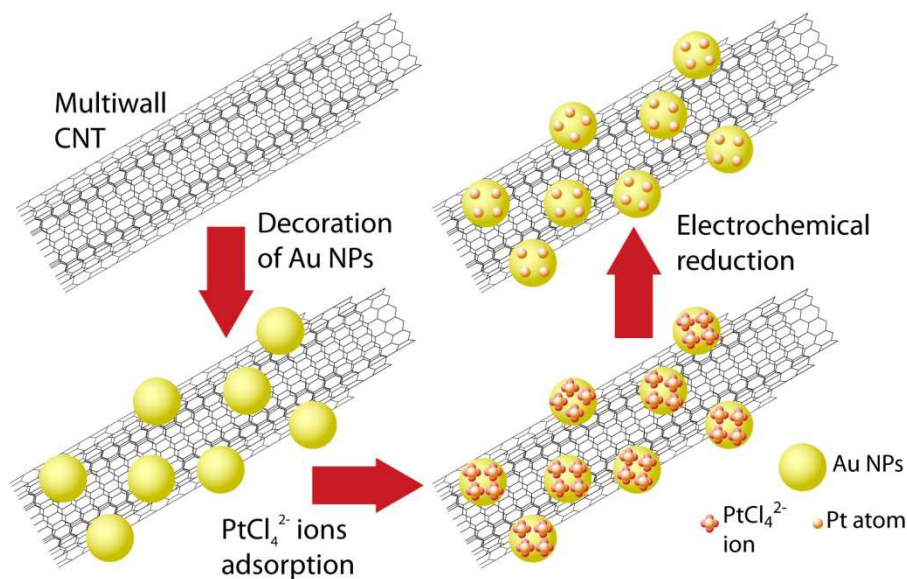


Figure 2.6 Preparation scheme of Au@Pt/MWCNTs composite.

2.2.1 Functionalization of multiwall carbon nanotubes (MWCNTs)

0.1mg of the as-received MWCNTs was dispersed into 50mL of 65% w/w HNO_3 in a 200mL round-bottom flask by sonication for 0.5h. Then the black dispersion was refluxed under 60°C in a oil bath for 12h. Afterwards, the black solid was collected by filtration and washed with deionised water until the pH approaches around 5.8. The treated MWCNTs were dried at 80°C for overnight and kept in a vial for further use.

2.2.2 Synthesis of Au/MWCNTs composite

2.0mg MWCNTs and 85 μ L 1%(w/w) HAuCl₄ solution were suspended in 100mL of dionised water, followed by the addition of 70 μ L ethylene glycol (EG) and 250 μ L sodium citrate. The mixture was sonicated for 30min until a dark dispersion was obtained. Afterwards, 85 μ L of 0.1M NaBH₄ was added as the reducing agent. The ratio between HAuCl₄ and NaBH₄ was kept to 1:10 to ensure a completed reduction of AuCl₄⁻¹ ions. After stirring for 2 hours, the mixture was filtered and washed with deionised water. Afterwards, the Au/MWCNTs was dried in oven at 80°C for 12 hours. For the preparation of Au@Pt/MWCNTs composite as methanol tolerant ORR catalyst, the 1%(w/w) HAuCl₄ used was increased to 340 μ L and 340 μ L of 0.1 M NaBH₄ was employed. Other procedures were remained unchange.

2.2.3 Synthesis of ultralow Pt loading Au@Pt/MWCNTs composite

Au@Pt/MWCNTs composite was fabricated by the so-called ions adsorption and *in situ* electrochemical reduction. Au/MWCNTs (2mg) were dispersed ultrasonically into 0.5mL ethanol. Then 10 μ L of the dispersion was pipetted onto a glass carbon electrode (GCE with diameter of 3mm) and dried in air. Afterwards, the electrode was activated by cyclic voltammograms (CVs) in 0.1M H₂SO₄ between -0.3 and 1.5V until a stable CV curve was obtained. The ion adsorption process was carried out by immersing the electrode with Au/MWCNTs in 0.1M H₂SO₄ containing Pt ions prepared with K₂PtCl₄ or K₂PtCl₆ of different

concentrations. After immersion for 10min, the electrode was washed thoroughly with deionised water and electrochemically reduced at -0.1V for 50s. The Pt source concentrations of the used in the preparation processes were between the range of 0.02 - 20.48mM.

2.2.4 Morphology and phase characterization

Morphology studies were carried out by transmission electron microscopy (TEM FEI Tecnai G2 20) measurement. Samples were dispersed in ethanol and then dropped onto the copper grid with holey formvar and carbon coating. For phase analysis, X-ray powder diffraction (XRD Rigaku 9kW SmartLab) was employed. Samples were casted on a single crystalline silicon support for each measurement. The XRD study was carried out between a 2 theta values of 10 to 90 degree.

2.2.5 Metal loading analysis

Metal loading studies were conducted using inductively coupled plasma mass spectrometer (ICP-MS Agilent 7500ce). After electrochemical studies, the composite on the GCE was transferred to an ultrapure microtube. 1mL aqua regia was added into the microtube and then the mixture was sonicated for 15min to accomplish a complete digestion. Afterwards, the obtained dispersion was centrifuged and the upper solution was separated for ICP measurements. Before injection to ICP-MS, 200 μ L solution was adopted and diluted with 1% HNO₃ to 10mL.

2.2.6 Electrochemical studies

Electrochemical characterizations were carried out at room temperature using a CHI 660D electrochemistry station with a three-electrode system composed of Pt strip and saturated calomel electrode (SCE) as the counter and reference electrodes respectively. The potential presented here are all against SCE reference electrode. Pt deposited on the surface of Au nanoparticles was characterized by cyclic voltammograms in 0.1M H_2SO_4 between -0.3 and 1.5V. The electrolyte was purged with N_2 for 30min before each measurement. The coverage of Pt was estimated in reference to the decrease of Au reduction peaks. The electrocatalytic activity of the as prepared Au@Pt/MWCNTs for formic acid were investigated by CVs between -0.2 and 0.9V and chronoamperometry at 0.15V in 0.1M H_2SO_4 containing 0.05M HCOOH. Methanol tolerant oxygen reduction reaction measurements were conducted in 0.5M O_2 saturated H_2SO_4 in presence or absence of 0.1M methanol using a rotating disk electrode (RDE Pine MSR).

2.3 Results and discussion

2.3.1 MWCNTs functionalization

It is well known that the dispersion of the as-received MWCNTs in water is extremely low due to their high hydrophobicity. Therefore, pretreatment is needed before anchoring metal nanoparticles onto the surface of MWCNTs. The as-received MWCNTs were pretreated with 65% nitric acid under 60°C for 12h. The strong nitric acid oxidizes the

surface of MWCNTs resulting in the generation of carboxyl groups and hydroxyl groups. [74] This procedure significantly improved the dispersion of MWCNTs in water, which is a critical step for the deposit of metal nanoparticles. Figure 2.7 shows a comparison of the dispersion of the as-received MWCNTs and the acid treated MWCNTs. After 20min, aggregation of the as-received MWCNTs was clearly observed while no change could be observed for the acid treated MWCNTs dispersion. This dispersion is highly stable that it can be kept in the sample vial for months without obvious aggregation. The pH value of the acid treated MWCNTs dispersion is slightly lower than that of the non-treated MWCNTs dispersion (5.32 vs 6.86). The weakly acidic nature of the treated MWCNTs dispersion also indicated the presence of carboxyl groups on the surface.

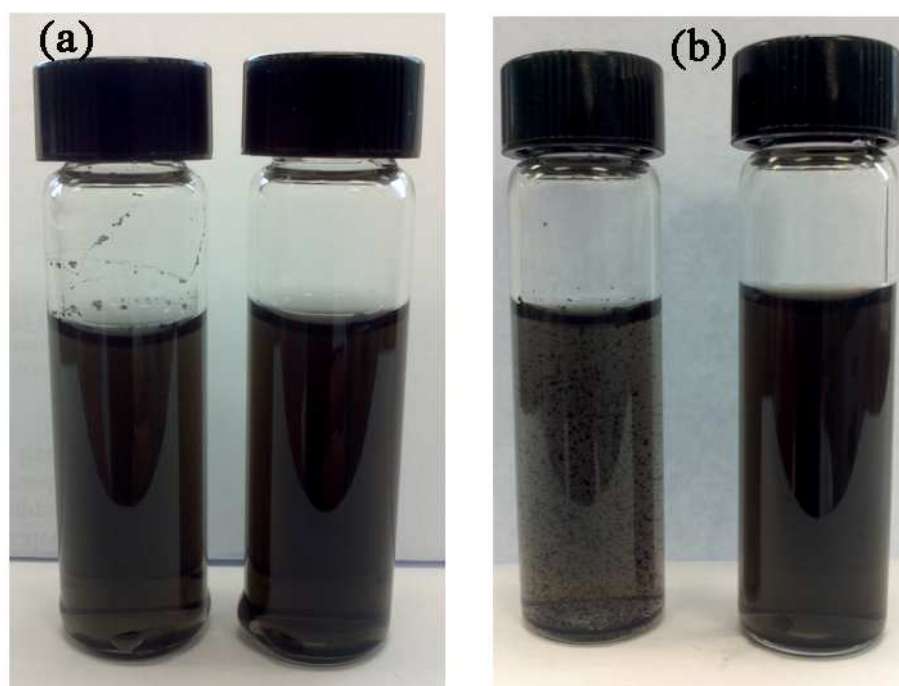


Figure 2.7 Dispersion of MWCNTs in water: (a) freshly prepared MWCNTs dispersion: as-received (left); acid treated (right); (b) after 20min.

2.3.2 Au/MWCNTs composite

Au/MWCNTs composite was prepared via traditional chemical impregnation by using NaBH_4 as the reducing agent. Typical TEM images of the Au/MWCNTs with different loading are presented in Figure 2.8. Au nanoparticles of diameter ranging between 3 to 9 nm were deposited on the surface of MWCNTs. No isolated Au nanoparticles were observed in the background of the TEM image, suggesting that all the nanoparticles were anchored on MWCNTs. It is worthy to notice that no obvious particle size change can be seen even when the Au loading was increased to 30% w/w, Figure 2.9 (a) (b) (c). However, aggregation of the Au nanoparticles occurred when the loading rose to 60% as shown in Figure 2.8 (d).

Since gold is a precious metal, the Au utilization is a critical issue in term of large scale applications. In order to further prove the complete deposition of Au nanoparticles on to the MWCNTs, UV-vis measurement was used to study the filtrate to verify whether there were remaining Au particles after the anchoring process. As shown in Figure 2.10, the absorbance peak at around 510nm which originate from Au nanoparticles vanished after the decoration of MWCNTs. It demonstrated once more that no free Au nanoparticles existed, [75] and was in good agreement with the TEM studies.

The Au/MWCNTs composite was further characterized by XRD, HRTEM and SAED. Figure 2.10 shows the XRD pattern of the as prepared Au/MWCNTs composite. The Au nanoparticles obtained exhibited fcc crystal structure with the diffraction peaks indexed as (111), (200), (311), (220) and (222). [76] The peak at around 26 degree is correspondence to the (002) face of MWCNTs. [77] To further investigate the crystal structure of

Au/MWCNTs, HRTEM and SAED were carried out. In the HRTEM, Figure 2.11 (a), a lattice fringe with the d value of 0.23 was identified which is related to the (111) face of Au nanoparticles. From the SAED image, all diffractions corresponding to that presented in the XRD patterns can be observed.

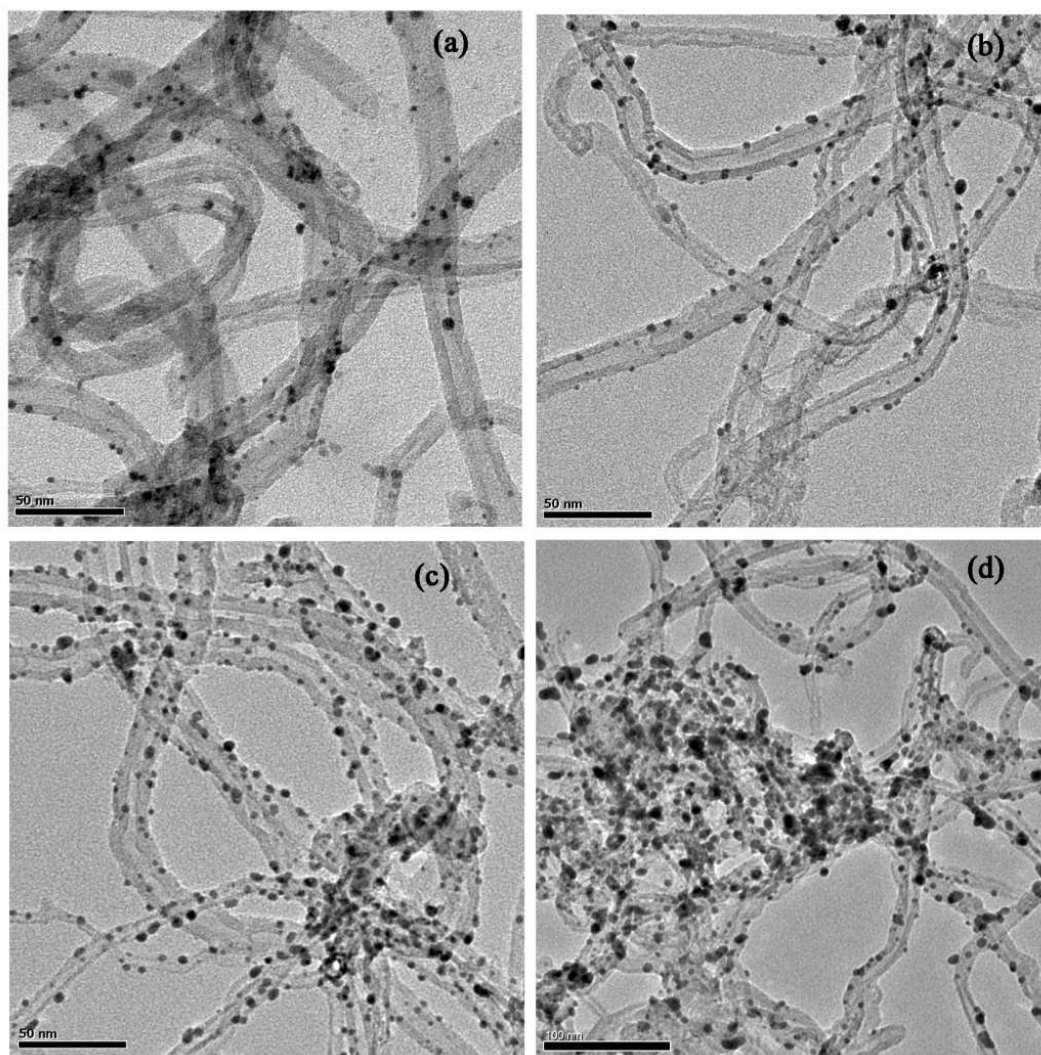


Figure 2.8 TEM images of A/MWCNTs of different Au loading: (a) 10%; (b) 20%; (c) 30%; (d) 60%.

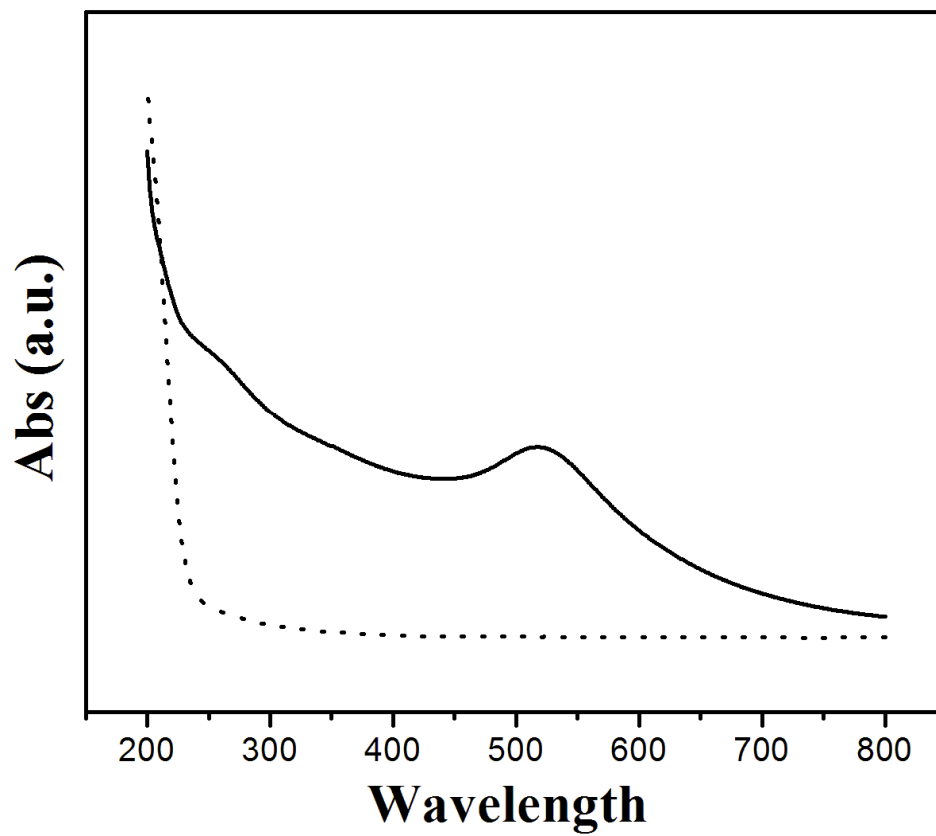


Figure 2.9 UV-visible patterns of gold colloidal (dot line) and filtrate after Au/MWCNTs preparation (solid line).

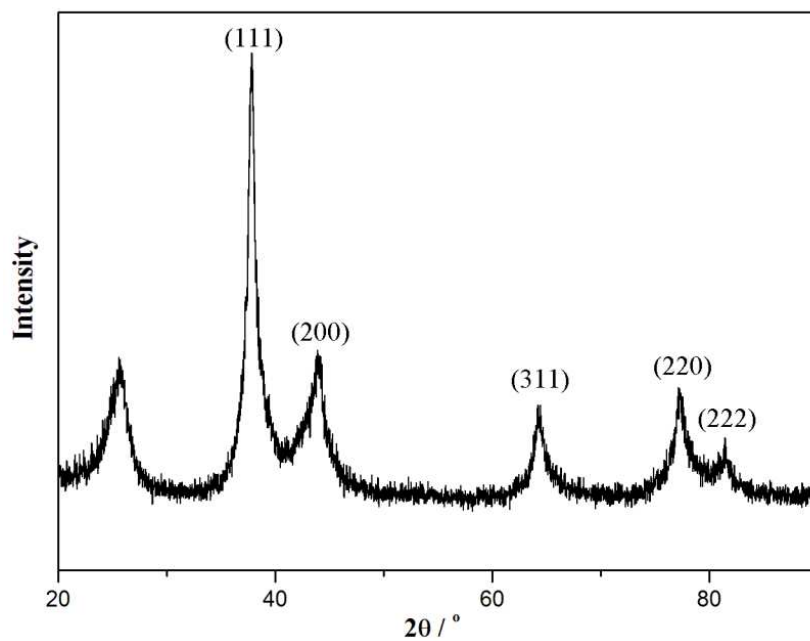


Figure 2.10 XRD pattern of the Au/MWCNTs

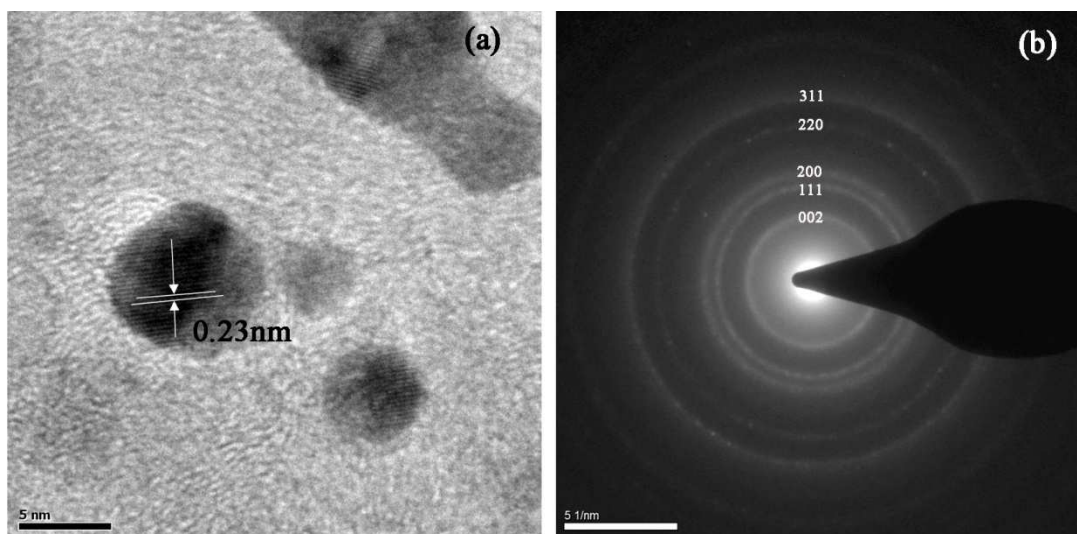


Figure 2.11 HTTEM (a) and SAED (b) of Au/MWCNTs.

2.3.3 Au@Pt/MWCNTs composite

In order to enhance the utilization of Pt, one straight forward way is to synthesize monolayer Pt catalysts. The most common way to prepare single layer Pt structure mainly involves processes of under potential deposit (UPD) of Cu and galvanic replacement reaction between the deposited Cu and Pt. A major disadvantage of these methods is the difficulty in the single layer copper preparation. Up-to-date, there are only few reports on the construction of monolayer Pt structure materials except those which employed UPD and galvanic replacement procedures. Recently, Kingo Itaya and co-workers [78] proved that immersion of an ordered Au(111) electrode in a chloroplatinate solution results in spontaneous and irreversible adsorption of a submonolayer to a monolayer Pt complex on the Au surface. Inspired by this, we proposed a rational design for the construction of

submonolayer Pt decorated Au nanoparticles on multiwall carbon nanotube support by means of ion adsorption and electrochemical reduction.

In order to obtain a clear surface for the ions adsorption process, Au/MWCNTs was first activated by CVs in N₂ saturated 0.1M H₂SO₄ solution until a steady curve was obtained. Then the Au/MWCNTs were transferred to a solution of 0.1M H₂SO₄ containing a Pt source of varying concentrations immediately for the ions adsorption. The immersion time was fixed at 10min. Figure 2.12 shows the CVs of Au/MWCNTs, Pt/C and Au@Pt/MWCNTs in N₂ saturated 0.1M H₂SO₄ solution. Significant changes were observed in the CV curve of Au/MWCNTs after modification. Obviously, the reduction peak for gold oxide at around 0.8V in the backwards scan is decreased due to the coverage of Pt. A broad peak related to Pt oxide reduction at around 0.25V appeared which proved the presence of Pt, almost identical to the CV of Pt/C. However, the typical features for hydrogen adsorption and desorption on Pt in sulfuric acid [79] was only barely observed because of the low loading of Pt. Since the current originating from gold oxide reduction was still present in the CVs, it indicated that a submonolayer structure of Pt was decorated on the surface of gold nanoparticles. This structure was of great significance with regards to the electrooxidation of formic acid and methanol tolerant ORR.

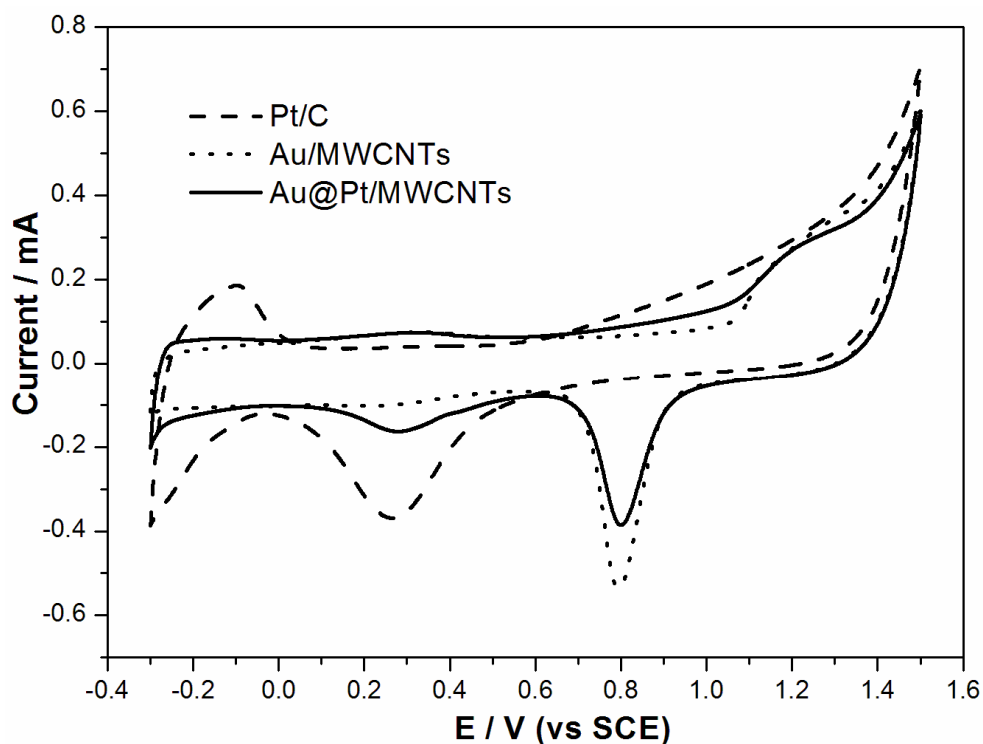


Figure 2.12 Cyclic voltammetric curves in 0.1M N₂ saturated H₂SO₄ solution and Au@Pt/MWCNTs, 50mV/s. Solution for ions adsorption: 0.1M H₂SO₄ + 0.08mM K₂PtCl₄.

To verify the adsorption of Pt ions onto the surface of Au nanoparticles, we must first clarify whether there was interaction between MWCNTs and Pt ions during the ions adsorption process. A control ions adsorption experiment was performed using MWCNTs instead of Au/MWCNTs, after which linear sweep voltammetry (LSV) was used to verify the presence of Pt. The results were showed in Figure 2.13. Apparently, no change in the LSV of MWCNTs after the immersion could be observed. It demonstrated that there was no decoration of Pt ions onto the MWCNTs took place.

Linear sweep voltammetry studies were then employed to prove the adsorption of Pt ion on the surface of Au surface. After 10min immersion in solution of 0.1M H₂SO₄ + 1mM K₂PtCl₄, three consecutive LSVs were conducted, as shown in Figure 2.14. From the first

sweep, the reduction peak of Pt ions around 0.24V was clearly observed. The second sweep started at 1.5V in order to electrochemically oxidize the Pt formed in the first sweep. Similar to the first sweep, the reduction peak corresponding to Pt oxide appeared at the same potential region. In the third sweep, the initial potential was moved to 0.5V, which was not positive enough to electrooxidize Pt. The reduction peak related to Pt oxide can be seen to be missing in the third scan. Combining the above results, we can conclude that the presence of Au was critical for Pt ions adsorption. In order to obtain direct evidence for the adsorbed Pt ions on the surface of Au nanoparticles, X-ray photoelectron spectroscopy (XPS) was carried out. For the sample preparation, Au/MWCNTs were dipped into solution of 0.1M H₂SO₄ + 0.1mM K₂PtCl₄ for 10min but without reduction subsequently. The XPS pattern is showed in Figure 2.15. The 4f_{7/2} and 4f_{5/2} peaks at 72.2 and 75.1eV which can be attributed to PtCl₄²⁻ comparable to metallic Pt with the value of 70.9 and 74.3eV. [80-82] Although a positive shift of binding energy was reported for Pt in AuPt alloy, [83] this can not be accounted for the positive shift in this case as no reducing agent was added.

It has been reported that the driving force for the adsorption of PtCl₄²⁻ on Au surface was the strong interaction between Au and chlorine. [84] We aim to verify this statement by replacing PtCl₄²⁻ with PdCl₄²⁻ in the ions adsorption process since they share similar molecular structure in solution state. As shown in Figure 2.16, similar to its platinum analogue, Au oxide reduction peak at around 0.8V was decreased due to the coverage of Pd; the hydrogen desorption signal was clearly observed even though the signal for that of hydrogen adsorption was featureless. Additionally, a weak peak related to Pd oxide reduction appeared at about 0.4V. These results provided further support the conclusion that

strong interaction between Au and chlorine was the main reason for the metal chloride ions adsorbing on to the Au surface, as seen from the similar reactivity of Pt and Pd halides.

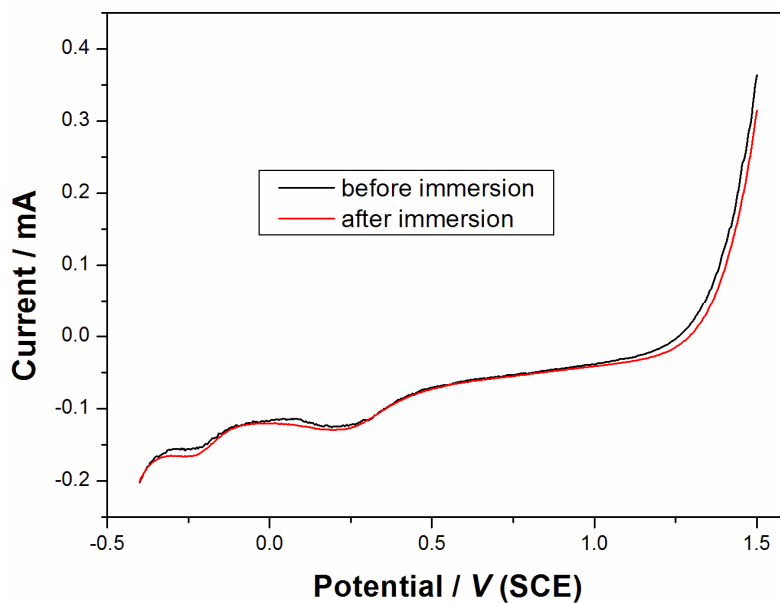


Figure 2.13 LSVs of MWCNTs before and after the immersion in 0.1M H_2SO_4 + 0.1mM K_2PtCl_4 for 10min.

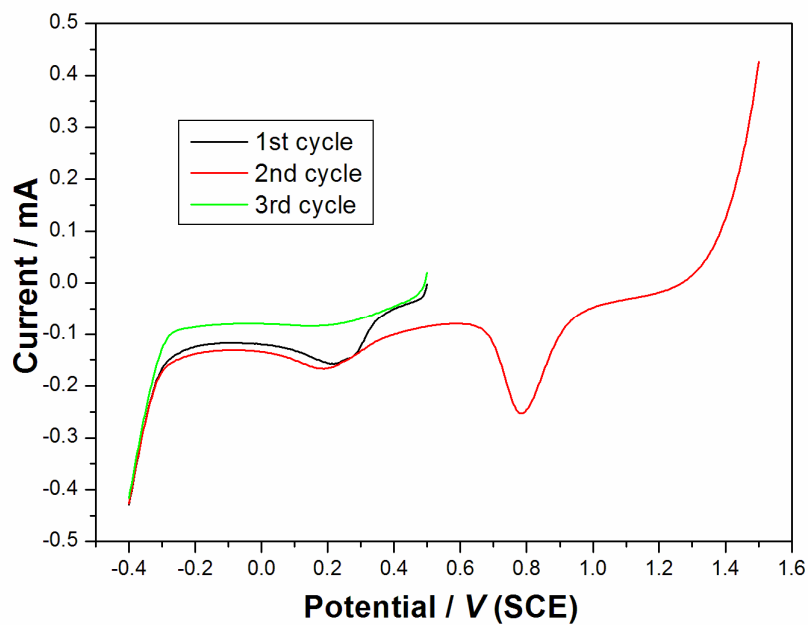


Figure 2.14 LSVs of Au/MWCNTs before and after the immersion in 0.1M H_2SO_4 + 0.1mM K_2PtCl_4 for 10min.

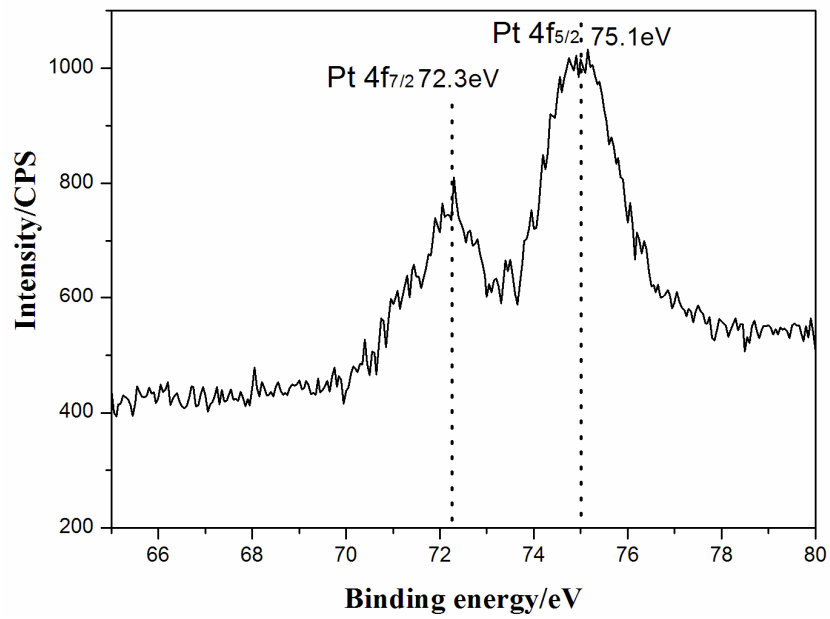


Figure 2.15 XPS pattern of Pt, sample preparation: Au/MWCNTs composite was immersed in 0.1mM K_2PtCl_4 + 0.1M H_2SO_4 for 10min, the composite was separated by filtration and washed thoroughly with deionised water and dried in air for XPS measurement.

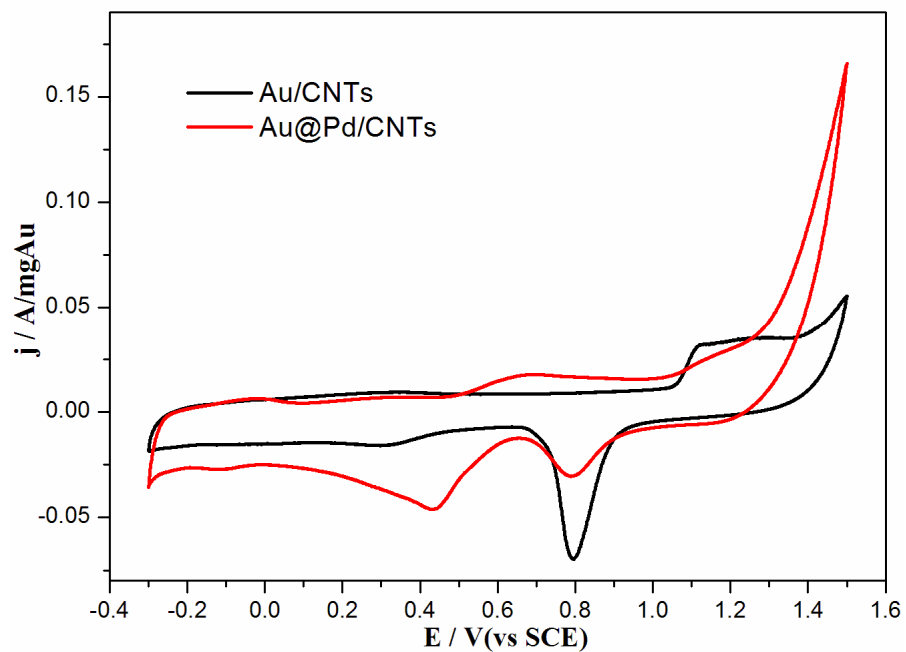


Figure 2.16 CVs of Au/MWCNTs and Au@Pd/MWCNTs in 0.1M N_2 saturated H_2SO_4 .

Based on the mechanism discussed previously, the Au@Pt catalyst obtained should possess a sub-monolayer Pt structure on the surface of Au nanoparticles. In order to control the Pt coverage on this basis, ion adsorption experiments were carried out with different K_2PtCl_4 concentrations. As the concentration of K_2PtCl_4 increase, more Pt should have decorated on to the surface of Au, which can be indicated by both the increasing Pt oxide reduction peak and the decrease of the Au oxide peak (Figure 2.17(A)). The Pt coverage was calculated by the amount of decrease of the Au oxide peak. [85] As shown in the inset of Figure 2.17(A), a good linear relation between the Pt coverage and the K_2PtCl_4 concentration was obtained within the estimated error. It suggests that the coverage of Pt can be tuned by varying the Pt source concentration during the ions adsorption process, similar to the results attained by C. K. Rhee et al. [86] Nevertheless, a state close to saturation was reached when the concentration is raised to 20.48mM since no apparent increase in Pt coverage can be obtained by increasing the concentration of K_2PtCl_4 further. Indeed, the ca. 2% decrease in coverage observed at 81.92mM K_2PtCl_4 concentration also suggests that the adsorption reached a plateau at the K_2PtCl_4 concentration of 20.48mM. On the other hand, the Pt coverage can also be controlled by repeating the adsorption-electrochemical reduction processes. As shown in Figure 2.17(B), the Pt coverage increased as we repeated the ion adsorption after each electrochemical reduction. A coverage of about 87.8% was achieved as cycles was repeated for 11 times. In order to obtain a series of coverage, different K_2PtCl_4 concentrations were chosen: 0.08mM $K_2PtCl_4 + 0.1M H_2SO_4$ for the first 7 cycles, 0.32mM $K_2PtCl_4 + 0.1M H_2SO_4$ for the eighth and the ninth immersions and 1.28mM $K_2PtCl_4 + 0.1M H_2SO_4$ for the tenth immersion and

finally 5.12mM K_2PtCl_4 + 0.1M H_2SO_4 for the eleventh immersion. Noticeably, for the concentration of 0.08mM, a maximum coverage of around 65.5% was observed as there was no apparent increase in coverage between the seventh immersion and the sixth immersion. However, increasing the concentration resulted in further increase on the coverage. These results imply that it is feasible that the Pt coverage can be controlled by other means other than merely changing the Pt ions concentration. Moreover, repeating immersion at a relatively low concentration for a high coverage is significant for the reducing the use of Pt in the production process.

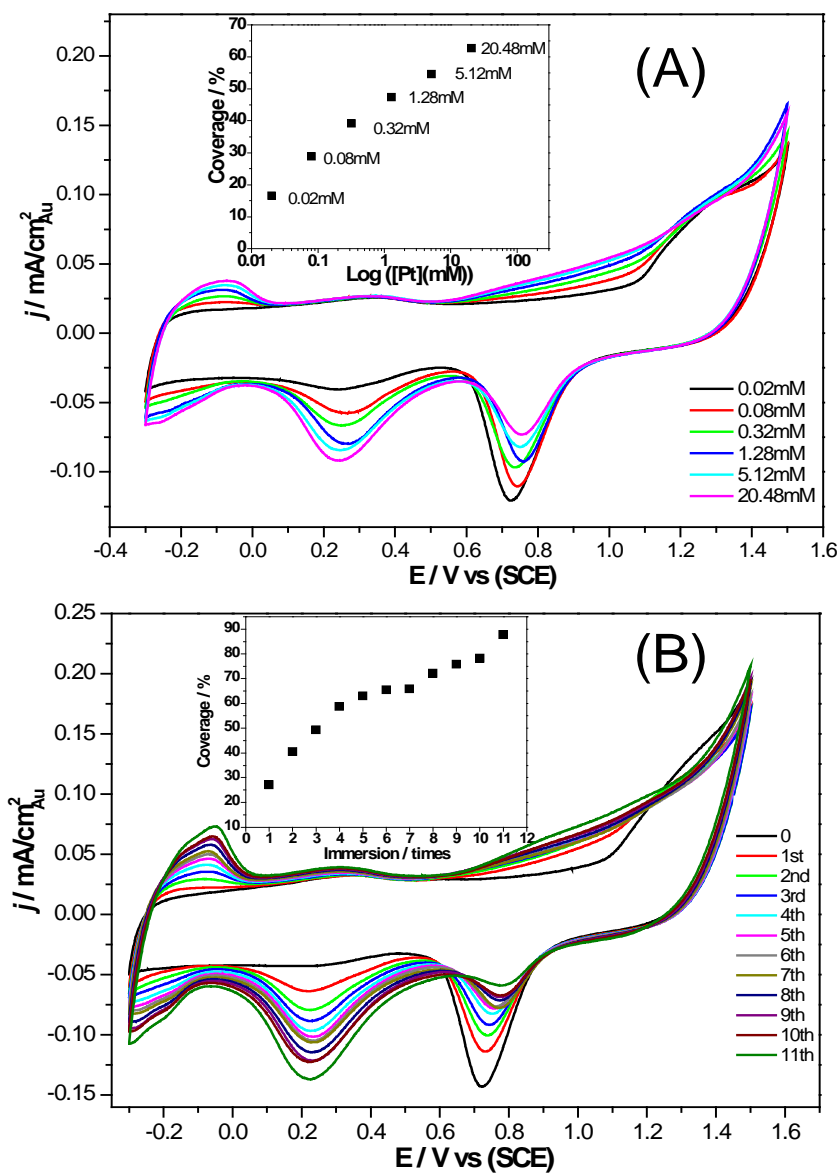


Figure 2.17 CVs of Au@Pt/MWCNTs in 0.1M H₂SO₄ prepared in 0.1M H₂SO₄ containing K₂PtCl₄ of different concentrations (A) and repeating ions adsorption times in 0.08mM K₂PtCl₄ + 0.1M H₂SO₄ for the first seven times immersions and 0.32mM K₂PtCl₄ + 0.1M H₂SO₄ for eighth and ninth immersions and 1.28mM K₂PtCl₄ + 0.1M H₂SO₄ for the tenth immersion and 5.12mM K₂PtCl₄ + 0.1M H₂SO₄ for the eleventh immersion, 50mV/s.

Pt is widely used as the catalytic materials in fuel cell devices. Nevertheless, the limited natural abundance and in turn the high cost of Pt pose challenges for widespread applications of fuel cells. Therefore, submonolayer or monolayer construction of Pt will be of great influence in this respect. It is difficult to characterize the submonolayer structure on the surface of Au nanoparticles by employing traditional techniques such as TEM, HRTEM, SAED, XRD, EDS since the Pt loading is too low. In contrast, electrochemical techniques are surface mediated method with very high sensitivity. Therefore, we for the first time use cyclic voltammetry to aim verification of the sub-monolayer Pt structure on the surface of Au. With regards to the synthetic process, it resulted in two effects upon the decoration of Pt: the decrease of gold surface area, ΔS_{Au} , and the increase of Pt surface area, ΔS_{Pt} . The change in surface areas of Au and Pt can be well represented by the charge transfer during the related electrochemical processes in CVs. [87] Again, considering the preparation scheme, if sub-atomic layered Pt structure was achieved, the decrease in Au surface area should equal to the increase in Pt surface area. This is due to the fact that a single layer of Pt atoms are laid directly on top of the Au surface in an ideal scenario. It can be presented as:

$$\frac{\Delta S_{Au}}{\Delta S_{Pt}} = \frac{(C_{Au}/c_{Au})}{(C_{Pt}/c_{Pt})} = \frac{(C_{Au}c_{Pt})}{(C_{Pt}c_{Au})} = \frac{420C_{Au}}{400C_{Pt}} = 1.05\left(\frac{C_{Au}}{C_{Pt}}\right) = 1 \quad (2.1)$$

Thus

$$\left(\frac{C_{Au}}{C_{Pt}}\right) = 0.95 \quad (2.2)$$

where C_{Au} and C_{Pt} stand for the charge for the Au oxide and Pt oxide reduction, respectively; the specific numbers, 420 and 400, are the surface oxide reduction charge of polycrystalline

Au and Pt. [87] Figure 2.18(A) presents the plot of ΔS_{Pt} as a function of ΔS_{Au} , derived from figures obtained from different $PtCl_4^{2-}$ concentrations. A slope of 0.993 was obtained upon linear fit, which is close enough to 1 within calculation error. [87] Similarly, very good linear relation of ΔS_{Pt} and ΔS_{Au} was also observed when Au@Pt/MWCNTs was prepared through repeating immersion cycles, Figure 2.18(B). A slope of 0.992 was obtained. These results proved that the as synthesized Au@Pt/MWCNTs possess sub-monolayer Pt structure. Table 2.2 and Table 2.3 present the summaries of C_{Au} / C_{Pt} derived from the various CV measurements. Considering that the standard error for electrochemical measurement is 10%, one could consider that the data are in good agreement with equation (2.2). Based on these analyses, a conclusion can be drawn that sub-atomic layer to monolayer Pt structure was successfully attained by the so called ions adsorption-*in situ* electrochemical reduction approach. The proposed adsorption scheme for the increase of Pt coverage on the surface of gold nanoparticles is illustrated in Figure 2.19.

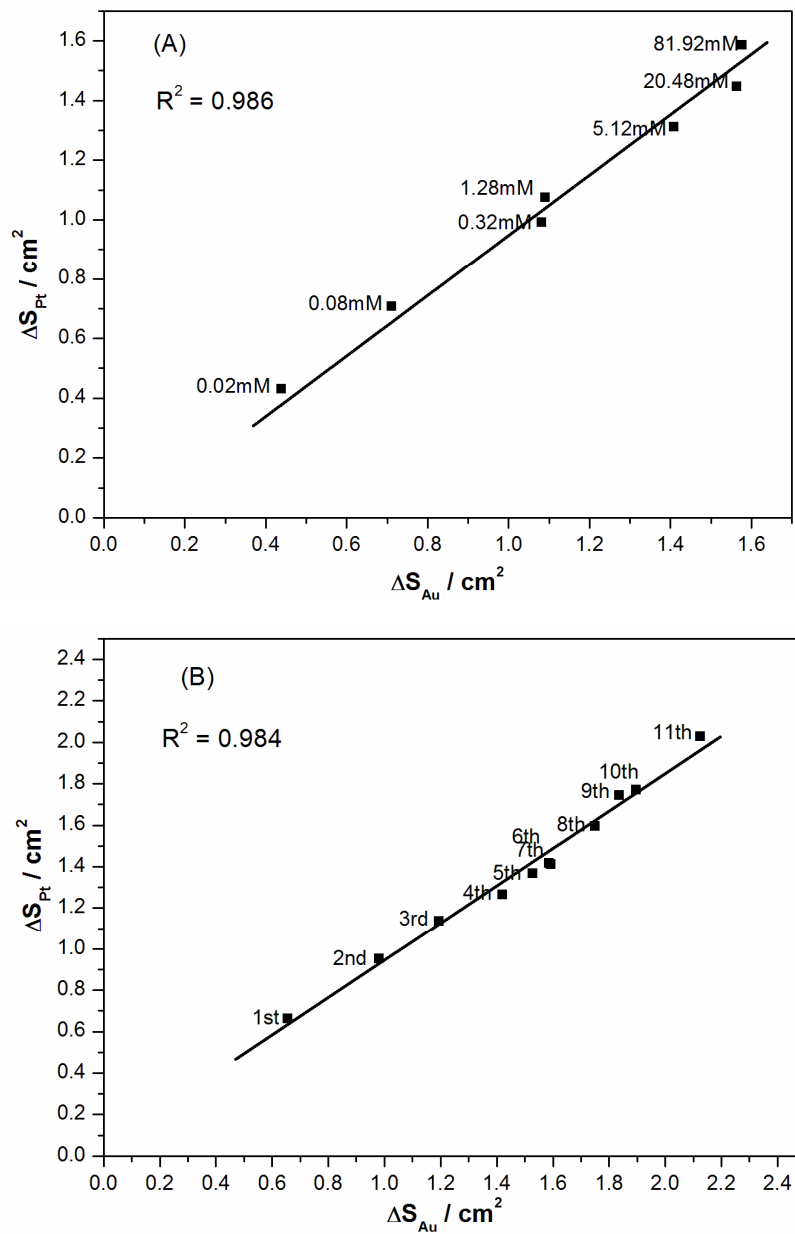


Figure 2.18 Relationship between of the decrease of Au surface area and the increase of Pt surface area: (A) data derived from different Pt ions concentrations; (B) data corresponding to repeating immersion cycles.

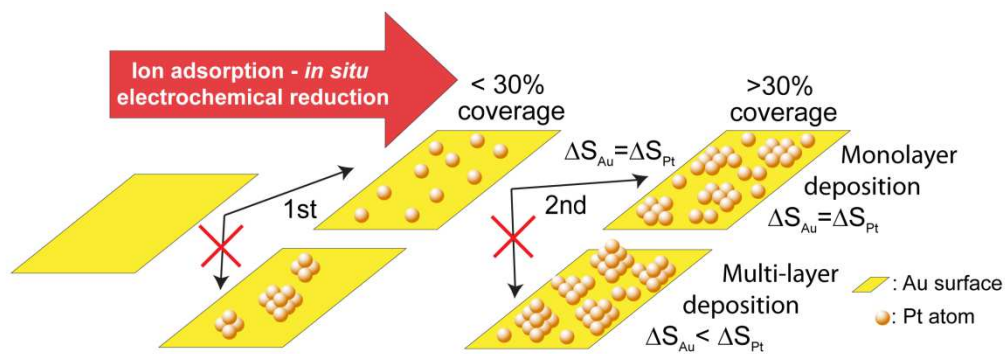


Figure 2.19 Schematic illustration of the consecutive ions adsorption – *in situ* electrochemical reduction.

Table 2.2 Summary of data derived from CVs of Au@Pt/MWCNTs prepared through different K_2PtCl_4 concentrations.

C / mM	Decrease of Au oxide reduction peak $\Delta C_{Au} / \times 10^{-4} C$	Increase of Pt oxide reduction peak $\Delta C_{Pt} / \times 10^{-4} C$	$\Delta C_{Au} / \Delta C_{Pt}$	Coverage / %
0.02	1.754	1.812	0.97	16.5
0.08	2.846	2.976	0.97	28.9
0.32	4.328	4.168	1.04	39.2
1.28	4.359	4.518	0.96	47.4
5.12	5.631	5.507	1.02	54.6
20.48	6.255	6.077	1.03	62.7
81.92	6.308	6.660	0.95	60.4

Table 2.3 Summary of data derived from CVs of Au@Pt/MWCNTs prepared through consecutive immersion cycles

NO. of cycles	C / mM	Decrease of Au oxide reduction peak $\Delta C_{Au} / \times 10^{-4} C$	Increase of Pt oxide reduction peak $\Delta C_{Pt} / \times 10^{-4} C$	$\Delta C_{Au} / \Delta C_{Pt}$	Coverage / %
1	0.08	2.621	2.792	0.94	27.1
2	0.08	3.927	4.005	0.98	40.6
3	0.08	4.776	4.775	1.00	49.3
4	0.08	5.68	5.318	1.06	58.7
5	0.08	6.109	5.750	1.06	63.1
6	0.08	6.342	5.951	1.06	65.5
7	0.08	6.372	5.927	1.07	65.8
8	0.32	6.994	6.702	1.04	72.2
9	0.32	7.338	7.335	1.00	75.8
10	1.28	7.581	7.290	1.04	78.2
11	5.12	8.500	8.526	1.00	87.8

2.3.4 Electrochemical oxidation of formic acid

As mentioned in the background section that formic acid electrooxidation on Pt occurred mainly through three pathways: direct oxidation (dehydrogenation), indirect pathway (dehydration) and the formate pathway. A deeper evaluation of the reaction is required before any discussion in greater details. Figure 2.20 shows the CV of commercial Pt/C in 0.1M H₂SO₄ + 0.05M HCOOH. There were two peaks in the forward scan. The weak broad peak (peak I) between 0.2 to 0.4V is originated from direct oxidation of formic acid and indirect oxidation is responsible for the relatively strong peak at around 0.7V (peak II). [88]

As demonstrated by *in situ* IR studies, the dissociation of formic acid occurs at potential under the onset of peak II, identified by the presence of CO_{ad} IR signal, [89] which in turn indicates that that peak II correlates to the indirect oxidation pathway. Meanwhile, Pt oxide

was formed resulting in the decrease in current in the region following peak II as shown by Figure 2.12. In the reverse scan, only one peak appeared due to the direct oxidation of formic acid after the reduction of Pt oxide formed in the positive-going sweep. The considerable hysteresis and the significant difference of the positive and negative going scans were generally ascribed to the hysteresis in the formation and the reduction of the surface Pt oxide in high potential region, and the oxidation or build-up of the poisoning CO_{ad} layer in the lower potential range. [90-93]

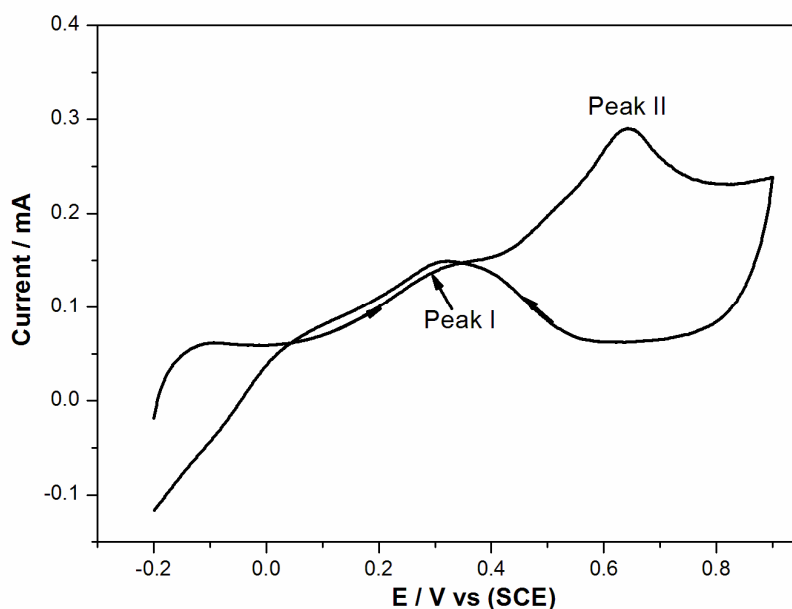


Figure 2.20 CV of Pt/C in 0.1M H_2SO_4 + 0.025M HCOOH , 50mV/s.

The electrochemical properties of the as prepared Au@Pt/MWCNTs catalysts towards formic acid oxidation were analyzed by CVs in 0.1M H_2SO_4 + 0.025M HCOOH . The result was shown in Figure 2.21. The shape of the CV closely resembles that of the Pd/C catalyzed formic acid oxidation which was reported to favor dehydrogenation of formic

acid without the formation of CO. [94, 95] Comparing Figure 2.20 with Figure 2.21, only one peak at around 0.4V corresponding to the direct oxidation of formic acid can be observed in the forward scan. Moreover, the current behavior in both forward and backward scans were nearly identical, indicating vast improvement for formic acid oxidation over pure Pt catalyst. [96] Direct oxidation of formic acid on Pt-based catalysts has been reported recently. [97-99] It was generally believed that the elimination of CO during formic acid oxidation on Pt was due to a so-called ensemble effect of Pt atoms. [100] Dehydrogenation of formic acid requires only 1-2 Pt atoms while the dehydration occurs over greater atom ensemble size (above 3). As in the case of Au@Pt/MWCNTs, Pt ions were first absorbed on the surface of Au and then *in situ* electrochemically reduced. The resulting submonolayer Pt structure may consist of isolated Pt atom since the lattice mismatch of Au and Pt is small. Therefore, the dehydration of formic acid was mostly eliminated.

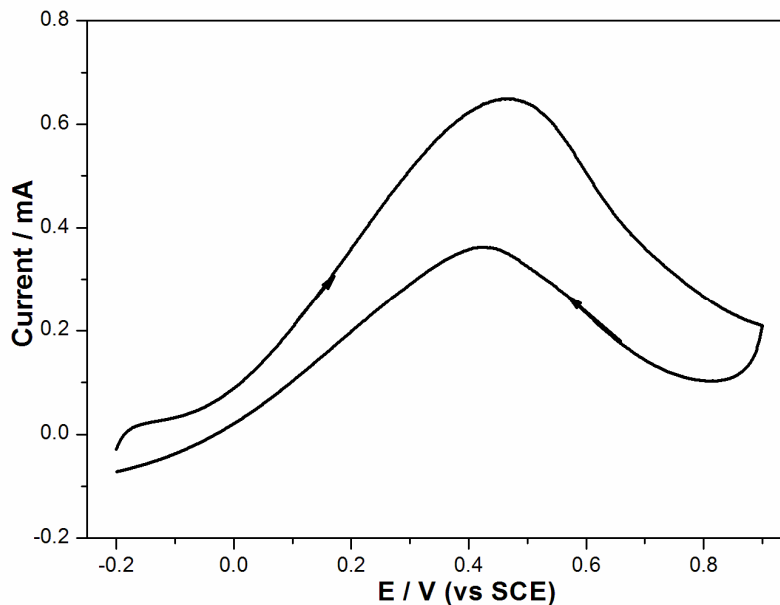


Figure 2.21 CV of Au@Pt/MWCNTs in 0.1M H₂SO₄ + 0.025M HCOOH, 50mV/s;
Solution for ions adsorption: 0.1M H₂SO₄ + 0.08mM K₂PtCl₄.

Base on the mechanism of formic acid oxidation on Pt, the coverage of Pt on the gold surface may have a significant influence on the electrocatalytic behavior of Au@Pt/MWCNTs. Further investigations regarding this prospect were performed. As proven previously, the electrocatalysts with different Pt coverage can be obtained by using a variety of concentrations of the Pt sources in the ions adsorption process or repeating ions adsorption. Figure 2.22 shows the electrochemical properties of the as prepared Au@Pt/MWCNTs catalysts. Interestingly, indirect oxidation of formic acid can be observed in the curve 2.22(d) when the concentration of K₂PtCl₄ was increased to 1.28mM. Further increase of Pt on the Au surface resulted in even more indirect oxidation of formic acid as indicated by the increase of the dehydration peak, as shown in curve (e) and (f). The increasing ratio of between peak II and peak I also (from 0.76 in (d) to 0.88 in (f))

suggested that more formic acid was oxidized through dehydration. These were consistent with results obtained by other researchers. [97, 101] As the Pt coverage increases, the proportion of ensemble structure of Pt atoms on the gold surface increases, which led to a higher proportion of indirect oxidation in the formic acid oxidation reaction. In addition, electrooxidation of formic acid on Au@Pt/MWCNTs prepared via repeated immersions was also carried out. As shown in Figure 2.23, similar results were observed. As the Pt coverage increase, the indirect oxidation related peak rises while the peak corresponding to direct oxidation decrease. The CV of a 88.4% Pt coverage (Figure 2.23(f)) actually resembles the shape of Pt/C.

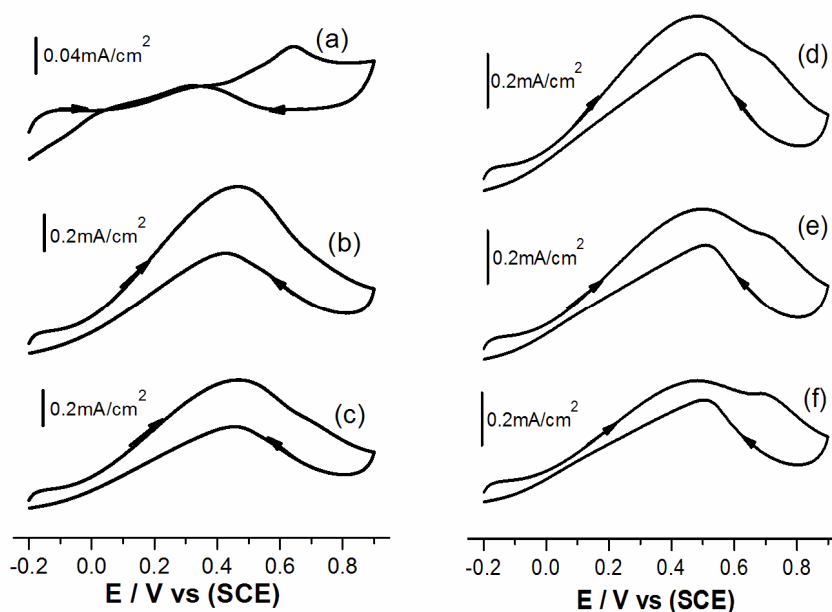


Figure 2.22 CVs in $0.1\text{H}_2\text{SO}_4 + 0.025\text{M HCOOH}$ of (a) Pt/C and Au@Pt/MWCNTs fabricated from PtCl_4^{2-} of different concentrations with different coverage: (b) 0.08mM , 28.9% ; (c) 0.32mM , 39.2% ; (d) 1.28mM , 47.4% ; (e) 5.12mM , 54.6% ; (f) 20.48mM , 62.7% .

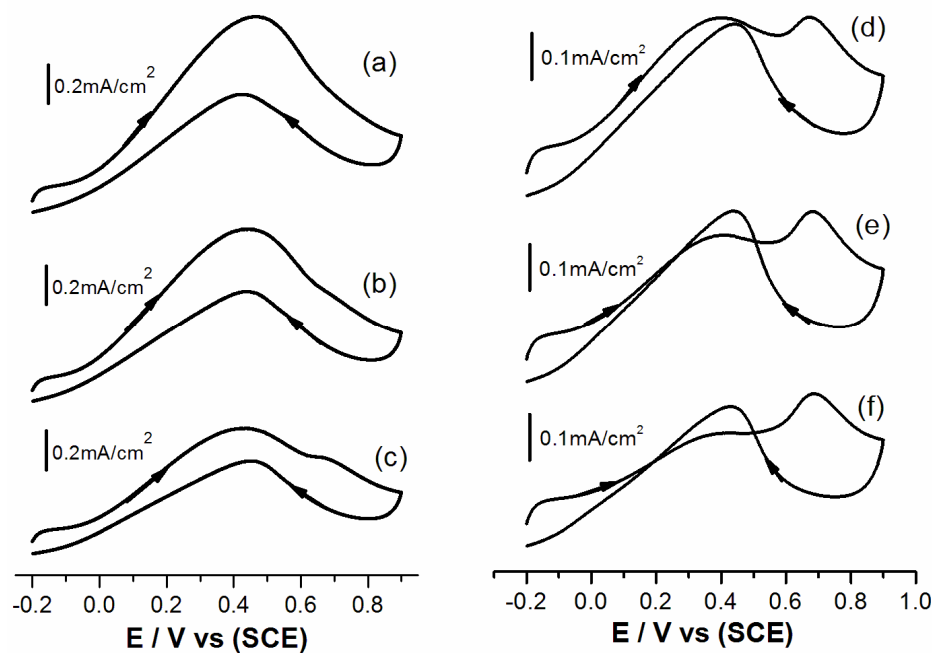


Figure 2.23 CVs in 0.1M H₂SO₄ + 0.025M HCOOH of Au@Pt/MWCNTs prepared through repeating adsorption-reduction cycles with increasing Pt coverage: (a) 28.9%; (b) 45.2%; (c) 59.2%; (d) 72.8%; (e) 81.6%; (f) 88.4%.

The stability of the electrocatalysts for fuel cells is a critical issue especially in terms of large scale applications. Since the loading of Pt in the submonolayer Pt catalyst is extremely low, thus its durability would be a key concern. We investigated the stability of our catalysts by scanning the catalyst in 0.1M H₂SO₄ + 0.025M HCOOH between -0.2 to 0.9V for 2000 cycles. As shown in Figure 2.24, the activity of Au@Pt/MWCNTs and Pt/C decrease after the accelerated durability test (ADT). The activity loss for Au@Pt/MWCNTs was 14% at the peak potential while the loss for Pt/C was around 40%. There are two major proposed causes for the gradual loss of electrochemical activity: (1) dissolution of Pt which led to Ostwald ripening; [102] and (2) Pt sintering by particles migration and agglomeration. [103] Both situations would result in the electrochemical active surface area (ECSA) loss

and thus degradation in the catalysts' performance. Therefore, we used CVs to study the ESCA loss before and after the accelerated durability test. As shown in Figure 2.25, no significant change in the CV of Au@Pt/MWCNTs could be observed after the durability test whereas the current signal for hydrogen adsorption-desorption and Pt oxide reduction show apparent decrease in the CV of Pt/C. It suggested that the ECSA loss in Pt/C is more severe compared to the Au@Pt/MWCNTs. The superior stability of the our catalysts may be ascribed to the better electrochemical resistance of the Au support in an acid medium since the reversible potential for Au was more positive than that of Pt under the same condition.

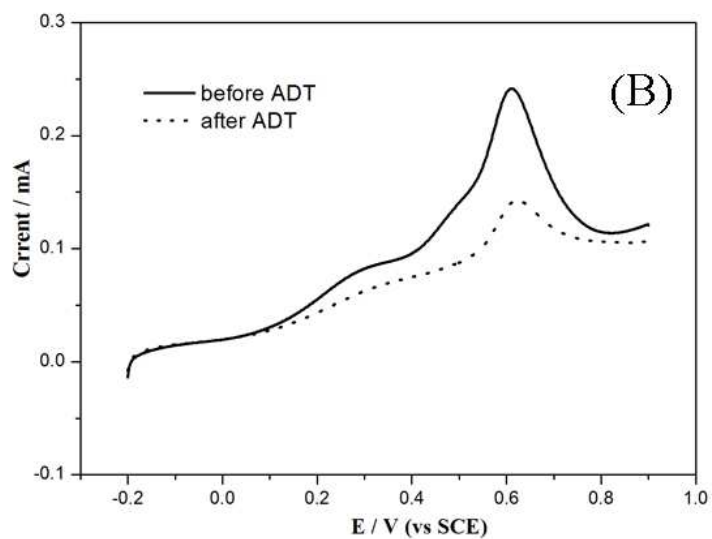
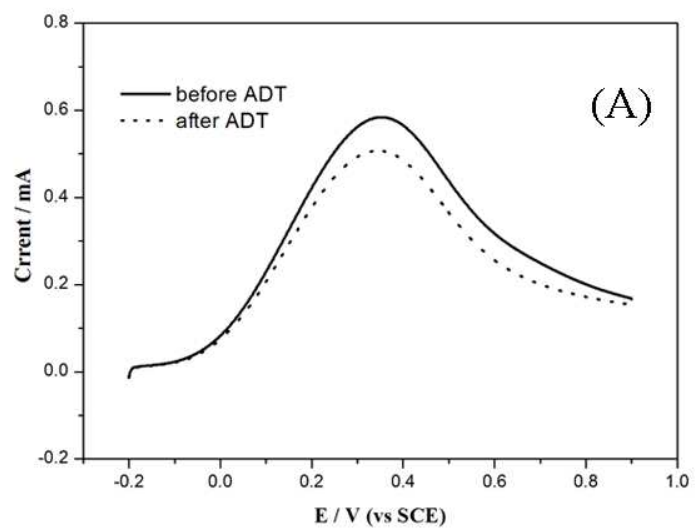


Figure 2.24 (A) LSV of Au@Pt/MWCNTs before and after accelerated durability test; (B) LSV of Pt/C before and after accelerated durability test; in 0.025M HCOOH + 0.1M H₂SO₄, 50mV/s.

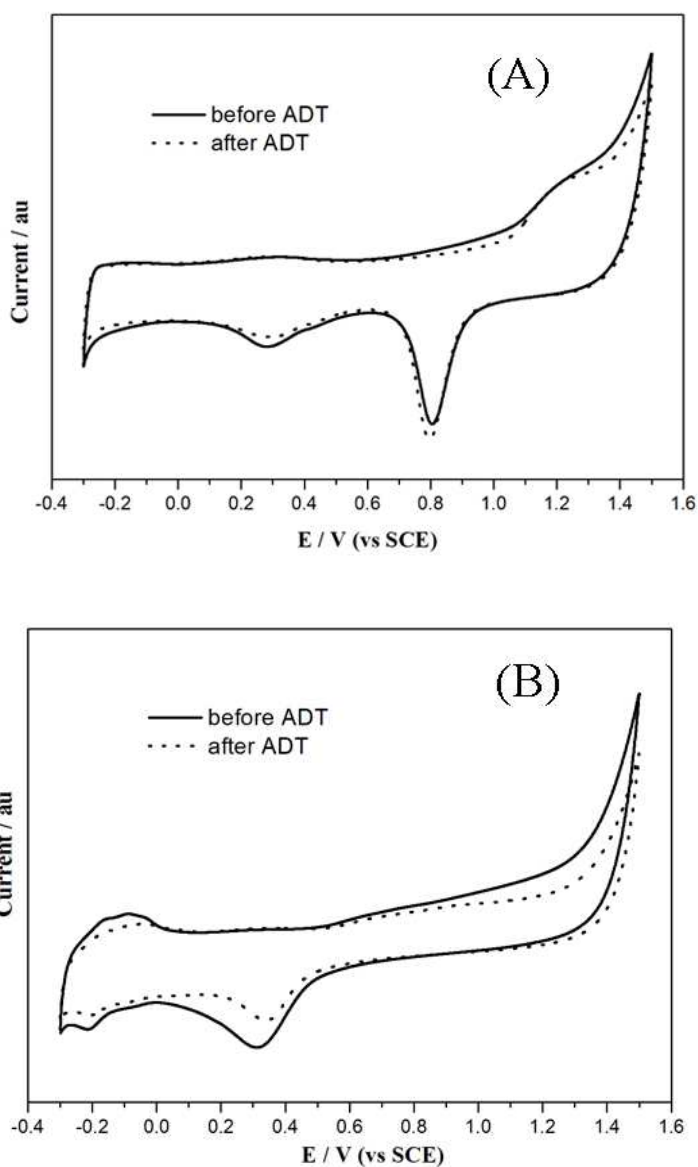


Figure 2.25 (A) CVs of Au@Pt/MWCNTs before and after accelerated durability test; (B) CV of Pt/C before and after accelerated durability test; in 0.1M N₂ saturated H₂SO₄, 50mV/s.

2.3.5 Methanol tolerant ORR catalysis

Recently, there are a few literatures reporting the synthesis of methanol tolerant catalysts. Zhao and co-workers [104] synthesized ordered mesoporous graphitic carbon

supporting Pt nanostructure as a highly active and methanol tolerant ORR catalysts. A. K. Shulka fabricated a Pt-Au alloy cathode catalyst for DMFCs which showed better methanol-resistant performance compared to its pure Pt counterpart.[105] Unfortunately, the Pt loading in both cases is too high for large scale application. With regard to the loading of the submonolayer Pt catalyst, Au@Pt/MWCNTs were quite promising as ORR electrocatalysts. Based on Matthew's calculation, [100] we expected that the as prepared submonolayer Pt structure may exhibit good performance for a methanol resistant ORR catalysis reaction. Inspired by this consideration, we investigated the electrochemical oxidation of methanol using our catalysts. As shown in Figure 2.26, interestingly, Au@Pt/MWCNTs with coverage below 40% showed almost no activities towards methanol oxidation ((b) and (c)) while those with higher coverage was active for methanol oxidation. Catalysts prepared through repeated immersions also displayed similar behavior for methanol oxidation (Figure 2.27). A closer look at the comparison between the activity of commercial Pt/C and the Au@Pt/MWCNTs was presented in Figure 2.28. The specific area activity of Au@Pt/MWCNTs for methanol oxidation was three times higher compared to that of the Pt/C catalysts. In the meantime, based on these results, it can be suggested that the Au@Pt/MWCNTs with lower Pt coverage, namely below 40%, may potentially have potential applications in methanol resistance ORR electrocatalysts for direct methanol fuel cells.

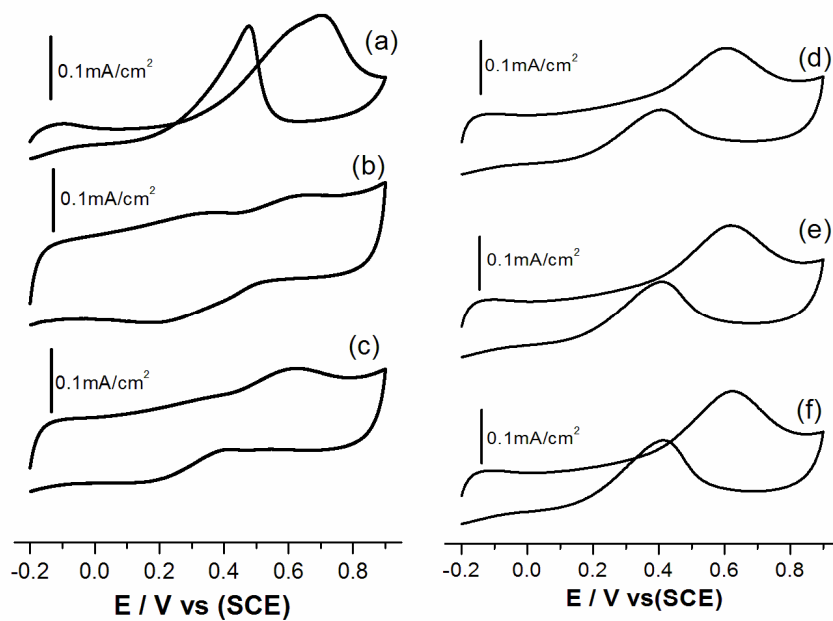


Figure 2.26 CVs in 0.1M H_2SO_4 + 0.1M methanol of (a) Pt/C and Au@Pt/MWCNTs fabricated from PtCl_4^{2-} of different concentrations with different coverage: (b) 0.08mM, 28.9%; (c) 0.32mM, 39.2%; (d) 1.28mM, 47.4%; (e) 5.12mM, 54.6%; (f) 20.48mM, 62.7%.

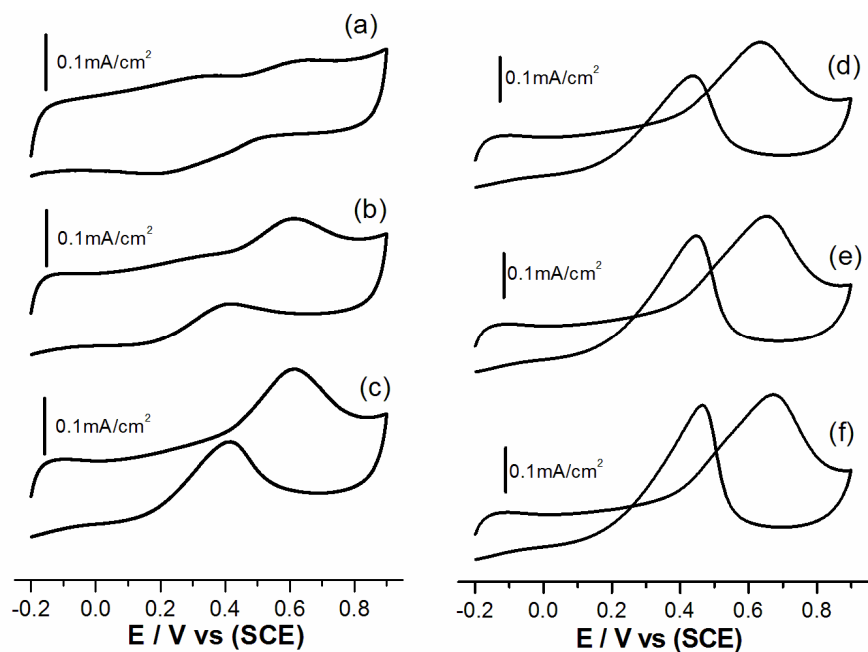


Figure 2.27 CVs in 0.1M H₂SO₄ + 0.1M methanol of Au@Pt/MWCNTs prepared through repeating adsorption-reduction with increasing Pt coverage: (a) 28.9%; (b) 45.2%; (c) 59.2%; (d) 72.8%; (e) 81.6%; (f) 88.4%.

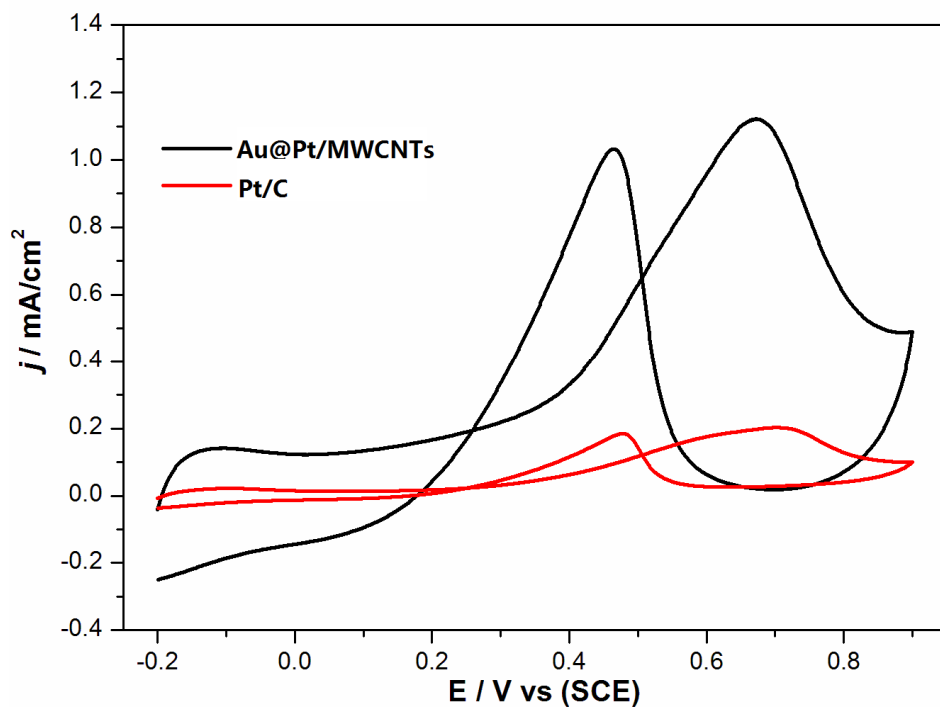


Figure 2.28 CVs in 0.1M H₂SO₄ + 0.1M methanol of Pt/C (red) and Au@Pt/MWCNTs with 88.4% Pt coverage (black), 50mV/s.

We analyzed the methanol resistance performance of the Au@Pt/MWCNTs with 27.9% Pt coverage by linear sweep voltammetry (LSV) measurement in the presence and absence of 0.1M methanol on a rotating disk electrode. From Figure 2.29, one can observe no change in the LSV curves in both cases. It indicates that the presence of methanol have no influence on the ORR catalysis. This result is in good agreement with the CV study in Figure 2.26 and Figure 2.27 that Au@Pt/MWCNTs with relatively lower Pt coverage show no activity for methanol oxidation. Furthermore, the addition of methanol induced a 40mV over potential for the ORR at the same current density as in the case of Pt/C. These results suggest that the as prepared catalyst has great potential for methanol tolerant ORR in direct methanol fuel cells. To provide further evidence for the methanol tolerant properties of the submonolayer Pt structure, chronoamperometric measurements were conducted in the presence of 0.1M methanol. The result is shown in Figure 2.30. The current-time (i-t) chronoamperometric response for Pt/C shows an obvious decrease (about 34.9%) in current upon the addition of 0.1M methanol. In contrast, the amperometric response from Au@Pt/MWCNTs remains unchanged even upon the addition of methanol. Therefore, the as prepared submonolayer Pt catalyst has better methanol tolerance than typical Pt/C electrocatalyst. Figure 2.31 shows the ORR polarization curve of the as prepared Au@Pt/MWCNTs in O₂ saturated 0.5M H₂SO₄. The current was corrected in reference to the area of Pt. The specific area activity of the submonolayer Pt catalyst is much higher than that of the commercially available Pt/C, and the specific mass activity at 0.45V has also shown a two-fold increase.

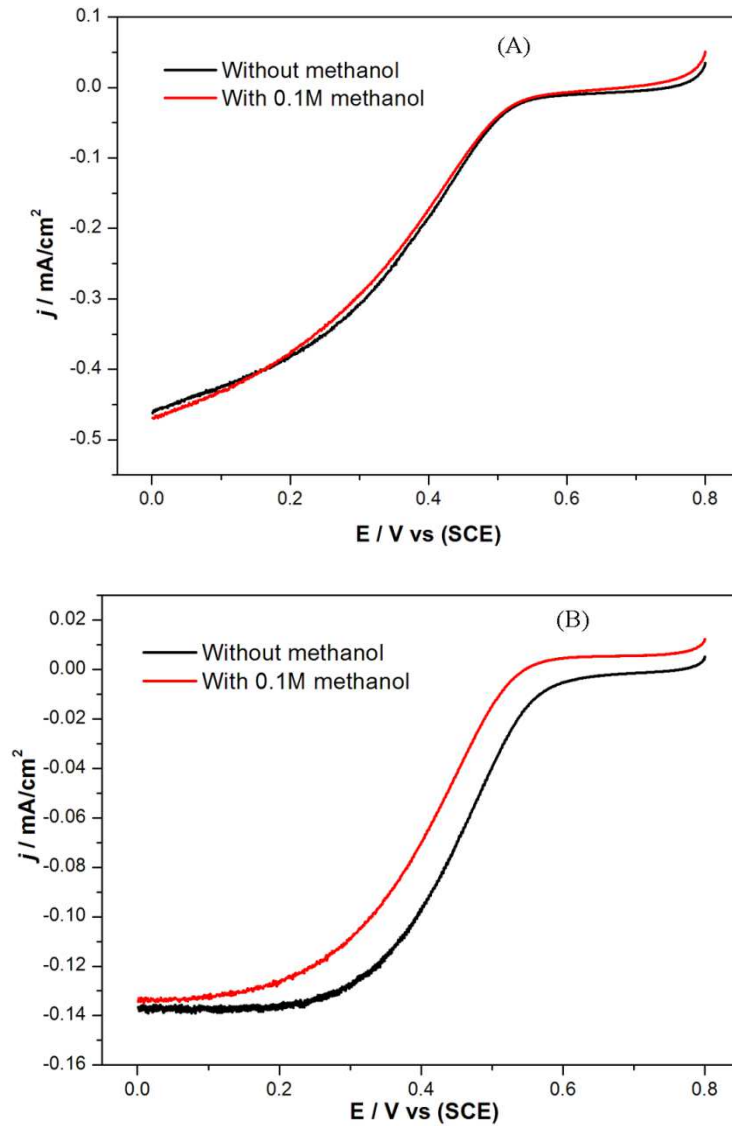


Figure 2.29 (A) LSV of Au@Pt/MWCNTs with 27.9% Pt coverage in 0.5M H₂SO₄ with and without 0.1M methanol, 10mV/s, 1600rpm; (B) LSV of Pt/C in 0.5M H₂SO₄ with and without 0.1M methanol, 10mV/s, 1600rpm.

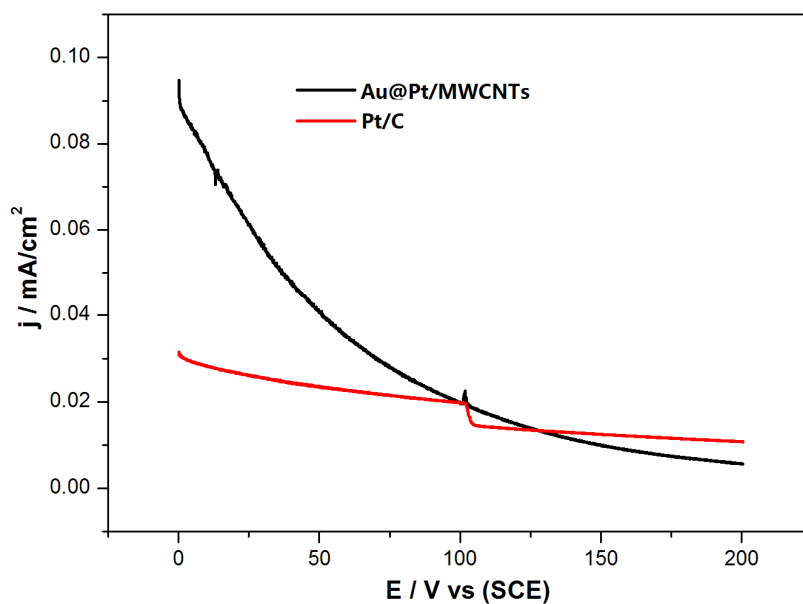


Figure 2.30 I-t curves at 0.5V in 0.5M O₂-saturated H₂SO₄ of Au@Pt/MWCNTs and Pt/C in the presence of 0.1M methanol: methanol was added after 100s.

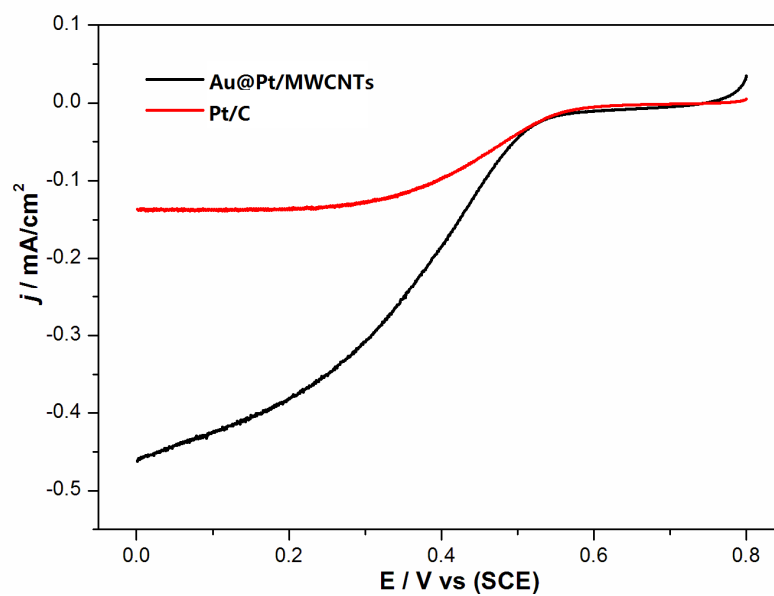


Figure 2.31 ORR polarization curves of Au@Pt/MWCNTs and Pt/C in O₂-saturated 0.5M H₂SO₄, 10mV/s, 1600rpm.

2.4 Summary

To summarize, ultralow loading Au@Pt/MWCNTs electrocatalyst was synthesized by a so-called ions adsorption and *in situ* electrochemical reduction method. The as prepared composites were used as electrocatalysts for formic acid oxidation and methanol tolerant oxygen reduction reaction.

- (1) MWCNTs were pretreated with concentrated nitric acid. The dispersion of MWCNTs in water had improved significantly after the acid treatment due to the formation of oxygen containing function groups on the surface of MWCNTs. In addition, the function groups would serve as the anchoring site for the deposition of Au nanoparticles.
- (2) Au/MWCNTs composite was prepared via traditional chemical impregnation. Complete deposition of Au nanoparticles on MWCNTs was confirmed by UV-vis measurement. TEM analyses illustrated that the particle size was in range of 4 to 9 nm. Au loading on Au/MWCNTs composite could be easily controlled by varying the amount of Au source, but some aggregations were observed in high loading. XRD study demonstrated that Au nanoparticles exhibit a fcc structure.
- (3) Au@Pt/MWCNTs composite was fabricated by ions adsorption and *in situ* electrochemical reduction. Linear sweep voltammetry and XPS were used to confirm the adsorption of Pt ions on to the surface of Au nanoparticles. The driving force for adsorption of the Pt chloride ions on to the Au surface is the strong interaction between Au and chlorine. The key role of chlorine atom in the ions adsorption process was proven by replacing the platinum chloride with palladium chloride based on the similar

adsorption mechanism. The submonolayer Pt structure on the surface of Au nanoparticles were verified for the first time by cyclic voltammetry. Electrochemical studies demonstrated that the Pt coverage can be controlled by varying the concentration of the Pt ions in the adsorption process or repeated immersions. Direct oxidation of formic acid occurred on the catalysts with lower Pt coverage, namely less than 40%, whereas both direct and indirect pathway took place on those with higher Pt coverage due to the ensemble effect. The Au@Pt/MWCNTs electrocatalyst possess higher stability as compared to commercial Pt/C catalyst which make Au@Pt/MWCNTs promising electrocatalysts for direct formic acid fuel cells.

- (4) Catalyst with lower Pt coverage showed excellent performance for methanol tolerant ORR catalysis since it was inactive towards methanol. Both the CV and chronoamperometric studies provided evidences for this conclusion. In addition, the specific area activity of ORR showed a tow-fold enhancement when compared to the commercial Pt/C catalyst.

References

- [1] J. W. Mintmire, B. I. Dunlap, C. T. White, *Phys. Rev. Lett.* **1992**, 68, 631.
- [2] M. R. Falvo, G. J. Clary, R. M. Taylor, V. Chi, F. P. Brooks, S. Washburn, R. Superfine, *Nature* **1997**, 389, 582.
- [3] S. Iijima, T. Ichihashi, *Nature* **1993**, 363, 603.
- [4] R. Saito, M. Fujita, G. Dresselhaus, M. S. Dresselhaus, *Phys. Rev. B* **1992**, 46, 1804.
- [5] S. Iijima, *Nature* **1991**, 354, 56.
- [6] M. S. Dresselhaus, G. Dresselhaus, P. C. Eklund, *Science of Fullerenes and Carbon Nanotubes*, Academic Press, San Diego, **1996**.
- [7] Y. Gogotsi, *Nano-materials Handbook* Boca Raton, FL, CRC Press, **2006**.
- [8] M. J. O'Connell, *Carbon Nanotubes: Properties and Applications* Boca Raton, FL, CRC Press, **2006**.
- [9] Y. Gogotsi, *Nanotubes and Nanofibres* Boca Raton, FL, CRC Press, **2006**.
- [10] D. N. Futaba, K. Hata, T. Yamada, T. Hiraoka, Y. Hayamizu, Y. Kakudate, O. Tanaike, H. Hatori, M. Yumura and S. Iijima, *Nat. Mater.* **2006**, 5, 987.
- [11] P. Simon, Y. Gogotsi, *Nat. Mater.* **2008**, 7, 845.
- [12] H. Dai, *Surf. Sci.* **2002**, 500, 218.
- [13] T. Guo, P. Nikolaev, A. G. Rinzler, D. Tomanek, D. T. Colbert, R. E. Smalley, *J. Phys.Chem.* **1995**, 99, 10694.
- [14] Jan M. Schnorr, Timothy M. Swager, *Chem. Mater.*, **2011**, 23 (3), 646.
- [15] M. S. Dresselhaus, G. Dresselhaus, R. Saito, A. Jorio, *Phys. Rep.* **2004**, 409(2), 47.
- [16] M. Baxendale, *J. Mater. Sci-mater. el.* **2003**, 14, 657.

- [17] R. Saito, G. Dresselhaus, M. S. Dresselhaus, *Physical Properties of Carbon Nanotubes* Imperial College Press, London, **1998**.
- [18] J. Li, H. T. Ng, A. Cassell, W. Fan, H. Chen, Q. Ye, J. Koehne, J. Han, M. Meyyappan, *Nano Lett.* **2003**, 3, 597.
- [19] C. E. Banks, T. J. Davies, G. G. Wildgoose, R. G. Compton, *Chem. Commun.* **2005**, 829.
- [20] E. H. Hároz, B. Y. Lu, P. Nikolaev, S. Arepalli, R. H. Hauge, J. Kono, *J. Am. Chem. Soc.* **2012**, 134, 4461.
- [21] M. Zheng, B. A. Diner, *J. Am. Chem. Soc.* **2004**, 126, 15490.
- [22] H. C. Choi, M. Shim, S. Bangsaruntip, H. Dai, *J. Am. Chem. Soc.* **2002**, 124, 9058.
- [23] Y. Xue, H. Chen, D. Yu, S. Wang, M. Yardeni, Q. Dai, M. Guo, Y. Liu, F. Lu, J. Qu, L. Dai, *Chem. Commun.* **2011**, 47, 11689.
- [24] D. P. He, C. Zeng, C. Xu, N. C. Cheng, H. G. Li, S. C. Mu, M. Pan, *Langmuir* **2011**, 27, 5582.
- [25] D. P. He, S. C. Mu, M. Pan, *Carbon* 2011, 49, 82.
- [26] W. M. Zhang, P. Sherrell, A. I. Minett, J. M. Razal, J. Chen, *Energy Environ. Sci.* **2010**, 3, 1286.
- [27] B. Baykal, V. Ibrahimova, G. E. Erman Bengu, D. Tuncel, *Chem. Commun.* **2010**, 46, 6762.
- [28] Y. K. Kang, O. Lee, P. Deria, S. H. Kim, T. Park, D. A. Bonnell, J. G. Saven, M. J. Therien, *Nano Lett.* **2009**, 9, 1414.
- [29] X. Li, Y. Liu, L. Fu, L. Cao, D. Wei, Y. Wang, *Adv. Funct. Mater.* **2006**, 16, 2431.

- [30] T. J. Schmidt, H. A. Gasteiger, R. J. Behm, *Electrochem. Commun.* **1999**, 1, 1.
- [31] H. A. Gasteiger, N. M. Markovic, P. N. Ross, *J. Phys. Chem.* **1995**, 99, 8290.
- [32] E. Casado-Rivera, Z. Gal, A. C. D. Angelo, C. Lind, F.J. DiSalvo, H. D. Abruna, *Chem. Phys. Chem.* **2003**, 4, 193.
- [33] J. W. Long, R. M. Stroud, K. E. Swider-Lyons, D. R. Rolison, *J. Phys. Chem. B* **2000**, 104, 9772.
- [34] D. R. Rolison, P. L. Hagans, K. E. Swider, J. W. Long, *Langmuir* **1999**, 15, 774.
- [35] J. Wang, D. F. Thomas, A. Chen, *Chem. Commun.* **2008**, 5010.
- [36] S. Zhang, Y. Shao, G. Yin, Y. Lin, *J. Power Sources* **2010**, 195, 1103.
- [37] S. Zhang, Y. Shao, H. Liao, J. Liu, I. A. Aksay, G. Yin, Y. Lin, *Chem. Mater.* **2011**, 23, 1079.
- [38] Z. Liu, X. Zhang, *Electrochem. Comm.* **2009**, 11, 1667.
- [39] D. Xu, S. Bliznakov, Z. Liu, J. Fang, N. Dimitrov, *Angew. Chem. Int. Ed.* **2010**, 49, 1282.
- [40] D. J. Chen, Z. Y. Zhou, Q. Wang, D. M. Xiang, N. Tian, S. G. Sun, *Chem. Commun.* **2010**, 46, 4252.
- [41] S. Zhang, S. Guo, H. Zhu, D. Su, S. Sun *J. Am. Chem. Soc.*, **2012**, 134 (11), 5060.
- [42] X. Gu, X. Cong, Y. Ding, *Chem. Phys. Chem.* **2010**, 11, 841.
- [43] Z. Peng, H. Yan, *Nano Res.* **2009**, 2, 406.
- [44] S. Zhang, Y. Shao, G. Yin, Y. Lin, *Angew. Chem. Int. Ed.* **2010**, 49, 2211.
- [45] N. Kristian, Y. Yu, P. Gunawan, R. Xu, W. Deng, X. Liu, X. Wang, *Electrochim. Acta* **2009**, 54, 4916.

- [46] Q. S. Chen, Z. Y. Zhou, F. J. Vidal-Iglesias, J. Solla-Gullon, J. M. Feliu, S. G. Sun, *J. Am. Chem. Soc.*, **2011**, 133 (33), 12930.
- [47] X. Yu, P. G. Pickup, *Electrochim. Acta* **2010**, 55, 7354.
- [48] B. Peng, J. Y. Wang, H. X. Zhang, Y. H. Lin, W. B. Cai, *Electrochem. Comm.* **2009**, 11, 831.
- [49] Zh. Chen, M. Waje, W. Li, Y. Yan, *Angew. Chem.* **2007**, 46, 4060.
- [50] Y. Tan, J. Fan, G. Chen, N. Zheng, Q. Xie, *Chem. Commun.* **2011**, 47, 11624.
- [51] V. Mazumder, M. Chi, K. L. More, S. Sun, *Angew. Chem. Int. Ed.* **2010**, 122, 9558 .
- [52] N. M. Markovic, H. A. Gasteiger, P. N. Jr. Ross, *J. Phys. Chem.* **1995**, 99, 11.
- [53] C. Wang, H. Daimon, T. Onodera, T. Koda, S. Sun, *Angew. Chem.* **2008**, 120, 3644 .
- [54] M. E. Gamboa-Aldeco, E. Herrero, P. S. Zelenay, A. Wieckowski, *J. Electroanal. Chem.* **1993**, 348, 451.
- [55] C. Wang , M. Chi , G. Wang , D. V. D. Vliet, D. Li , K. More, H. H. Wang, J. A. Schlueter, N. M. Markovic, V. R. Stamenkovic, *Adv. Funct. Mater.* **2011**, 21, 147.
- [56] S. Guo, S. Sun, *J. Am. Chem. Soc.* **2012**, 134 (5), 2492.
- [57] S. Koh, J. Leisch, M. F. Toney, P. Strasser, *J. Phys. Chem. C* **2007**, 111, 3744-3752
- [58] Jiang-lan Shui , * Chen Chen , and James C. M. Li, *Adv. Funct. Mater.* **2011**, 21, 3357.
- [59] V. R. Stamenkovic, B. Fowler, B. S. Mun, G. Wang, P. N. Ross, C. A. Lucas, N. M. Markovic, *Science* **2007**, 315, 493.
- [60] P. Mani, R. Srivastava, P. Strasser, *J. Phys. Chem. C* **2008**, 112, 2770.
- [61] M. Shao, K. Shoemaker, A. Peles, K. Kaneko, L. Protsailo, *J. Am. Chem. Soc.* **2010**,

132 (27), 9253.

- [62] K. M. Yeo, S. Choi, R. M. Anisur, J. Kim, I. S. Lee, *Angew. Chem. Int. Ed.* **2011**, 50, 745.
- [63] J. X. Wang, H. Inada, L. Wu, Y. Zhu, Y. M. Choi, P. Liu, W. P. Zhou, R. R. Adzic, *J. Am. Chem. Soc.* **2009**, 131, 17298.
- [64] D. V. Esposito, J. G. Chen, *Energy Environ. Sci.* **2011**, 4, 3900
- [65] S. Wang, Noel Kristian, S. Jiang, X. Wang, *Nanotechnology* **2009**, 20, 25605.
- [66] D. Zhao, B. Q. Xu, *Phys. Chem. Chem. Phys.* **2006**, 8, 5106.
- [67] S. R. Brankovic, J. McBreen, R. R. Adzic, *J. Electroanal. Chem.* **2001**, 503, 99.
- [68] Y. D. Jin, Y. Shen, S. J. Dong, *J. Phys. Chem. B* **2004**, 108, 8142.
- [69] S. Cheng, R. E. Rettew, M. Sauerbrey, F. M. Alamgir, *ACS Appl. Mater. Interfaces* **2011**, 3, 3948.
- [70] S. W. T. Price, J. D. Speed, P. Kannan, A. E. Russell, *J. Am. Chem. Soc.* **2011**, 133, 19448.
- [71] K. Sasaki, H. Naohara, Y. Cai, Y. M. Choi, P. Liu, M. B. Vukmirovic, J. X. Wang, R. R. Adzic, *Angew. Chem. Int. Ed.* **2010**, 49, 8602.
- [72] D. Wang, H. L. Xin, Y. C. Yu, H. S. Wang, E. Rus, D. A. Muller, H. D. Abruna, *J. Am. Chem. Soc.* **2010**, 132 (50), 17664.
- [73] J. H. Yang, W. Zhou, C. H. Cheng, J. Y. Lee, Z. Liu, *ACS Appl. Mater. Inter.* **2010**, 2, 119.
- [74] T. W. Ebbesen, H. Hirua, M. E. Bisher, M. M. J. Treacy, J. L. Shreeve-Keyer, R. C. Haushalter, *Adv. Mater.* **1996**, 8, 155.

- [75] Y. Shia, R. Yang, P. K. Yueta, *Carbon* **2009**, 47, 1146.
- [76] Y. Huang, X. Zhou, M. Yin, C. Liu, W. Xing, *Chem. Mater.* **2010**, 22, 5122.
- [77] J. Li, Y. Liang, Q. Liao, X. Zhu, X. Tian, *Electrochim. Acta* **2009**, 54, 1277.
- [78] Y. Nagahara, M. Hara, S. Yoshimoto, J. Inukai, S. L. Yau, K. Itaya, *J. Phys. Chem. B* **2004**, 108, 3224.
- [79] D. Q. Yang, S. Sun, J. P. Dodelet, E. Sacher, *J. Phys. Chem. C* **2008**, 112, 11717.
- [80] S.Y. Uhm, S.T. Chung and J. Y. Lee, *Electrochem. Commun.* **2007**, 9, 2027.
- [81] D. R. Blasini, D. Rochefort, E. Fachini, L. R. Alden, F. J. DiSalvo, C. R. Cabrera, H. D. Abruna, *Surf. Sci.* **2006**, 600, 2670.
- [82] S. C. Hall, V. Subramanian, G. Teeter, B. Rambabu, *Solid State Ionics* **2004**, 175,809.
- [83] M. Yin, Y. J. Huang, L. Liang, J. Liao, C. Liu, W. Xing, *Chem. Commun.* **2011**, 47, 8172.
- [84] H. F. Waibel, M. Kleinert, L. A. Kibler, D. M. Kolb, *Electrochim. Acta.* **2002**, 47, 1461.
- [85] S. Trasatti, O. A. Petrii, *Pure Appl. Chem.* **1991**, 63, 711.
- [86] S. Kim, C. Jung, J. Kim, C. K. Rhee, S. M. Choi, T. H. Lim, *Langmuir* **2010**, 26(6), 4497.
- [87] D. V. Esposito, S. T. Hunt, Y. C. Kimmel, J. G. Chen, *J. Am. Chem. Soc.* **2012**, 134, 3025.
- [88] S. Zhang, Y. Shao, G. Yin, Y. Lin, *Angew. Chem. Int. Ed.* **2010**, 49, 2211.
- [89] Y. X. Chen, S. Ye, M. Heinen, Z. Jusys, M. Osawa, R. J. Behm, *J. Phys. Chem. B* **2006**, 110, 9534.

- [90] H. Okamoto, W. Kon, Y. Mukoyama, *J. Phys. Chem. B* **2004**, 108, 4432.
- [91] H. A. Kozłowska, B. E. Conway, W. B. A. Sharp, *J. Electroanal. Chem.* **1973**, 43, 9.
- [92] T. Iwasita, X. Xia, H. D. Liess, W. Vielstich, *J. Phys. Chem. B* **1997**, 101, 7542.
- [93] G. Q. Lu, A. Crown, A. Wieckowski, *J. Phys. Chem. B* **1999**, 103, 9700.
- [94] W. P. Zhou, *J. Phys. Chem. B* **2006**, 110, 13393.
- [95] J. Ge, *J. Phys. Chem. C* **2007**, 111, 17305.
- [96] E. C. Rivera, *Chem. Phys. Chem.* **2003**, 4, 193.
- [97] N. Kristian, Y. Yan, X. Wang, *Chem. Commun.* **2008**, 353.
- [98] S. Zhang, Y. Shao, G. Yin, Y. Lin, *Angew. Chem. Int. Ed.* **2010**, 49, 2211.
- [99] R. Wang, C. Wang, W. B. Cai, Y. D. *Adv. Mater.* **2010**, 22, 1845.
- [100] M. Neurock, M. Janik, A. Wieckowski, *Faraday Discuss.* **2008**, 140, 363.
- [101] S. Kim, C. Jung, J. Kim, C. K. Rhee, S. M. Choi, T. H. Lim, *Langmuir* **2010**, 26(6), 4497.
- [102] P. J. Ferreira, G. J. la O, Y. Shao-Horn, D. Morgan, R. Makharia, S. Kocha, H. A. Gasteiger, *J. Electrochem. Soc.* **2005**, 152, A2256.
- [103] K. Hartl, M. Nesselberger, K. J. J. Mayrhofer, S. Kunz, F. F. Schweinberger, G. Kwon, M. Hanzlik, U. Heiz, M. Arenz, *Electrochim. Acta* **2010**, 56, 810.
- [104] Z. X. Wu, Y. Y. Lu, Y. Y. Xia, P. A. Webley, D. Y. Zhao, *J. Am. Chem. Soc.* **2012**, 134 (4), 2236.
- [105] G. Selvarani, S. V. Selvaganesh, S. Krishnamurthy, G. V. M. Kiruthika, P. Sridhar, S. Pitchumani, A. K. Shukla, *J. Phys. Chem. C* **2009**, 113, 7461.

Chapter 3

Synthesis of Hollow PtAg Nanostructures with Excellent Electrocatalytic Performances

3.1 Background

3.1.1 An overview of hollow nanostructures

Owing to their fascinating physical and chemical properties originating from the nanoscale size, nanostructures have attracted enormous interest in the last few decades. [1] Thanks to the recent advancement in nanotechnologies, a wide range of nanostructures have been successfully prepared including nanostars, [2, 3] nanorods, [4, 5] nanocubes, [6-8] nanospheres [9] and nanowires. [10] Among them, hollow nanostructure is one of the emerging significant members in nanoscience. With regards to the morphology of the hollow nanostructures, it consists of hollow-spheres, nanotubes, hollow-nanocubes and hollow-octaheron and so forth. Compared to its solid nanostructure counterparts, hollow structures show features such as high specific surface area, high pore volume ratio, low density, easy permeability and enhanced reactivity. [11-13] Therefore, it holds potential applications as drug-delivery carriers, [14] biomedical diagnostic agents, [15] cell imaging agents, [16] and catalyts. [17] For example, to name but a few, hollow Pd nanospheres have been employed in catalyzing Suzuki cross coupling reaction that showed higher performance than Pd nanoparticles. [18] Au nanocages have been proven to be an ideal candidate for photothermally triggered drug release agent in tissues owing to their strong

surface plasmon absorption. [19] Pt hollow spheres exhibited higher activity for both oxygen reduction reaction (ORR) and methanol oxidation reaction (MOR) than its solid analogues. [20-23] Noble metal such as Pt and Pd nanocages showed enhanced catalytic efficiency for the reduction reaction of 4-nitrophenol resulting from the nanocage effect. [24]

3.1.2 Synthesis of hollow nanostructures

There are many techniques to generate hollow nanostructures which mainly involve the sacrificial templates as the precursors. For example, polymer and inorganic spheres, [25-28] microemulsion droplets, [29] vesicles, [30] and liquid droplets [31] were all been employed as the templates. After the desirable materials are deposited on to the surface of the templates, the templates would be removed which results in the hollow structures. For this reason, the morphology of the remaining hollow structure largely depends on the template. Therefore, the design of the templates is a key step for the fabrication of the hollow structures. However, in recent years, newly developed methods have emerged for the preparation of hollow structures. Base on a brief literature review, we categorize the methods as follows.

3.1.2.1 Hard template assist synthesis

Hard template assistance synthesis usually involves a template such as polymers, [32] silica, [33] titanium oxide [34] and metal nanoparticles [35] as the precursor. There are mainly two main steps in the hard template assistance preparation. For example, Figure 3.1

shows the preparation process of PtRu hollow structure using the porous carbon as the template. The desirable shell materials are deposited on to the surface of the template by chemical reduction. Afterwards, the templates are removed generating the hollow structures. The methods used to remove the template materials needed to be chosen carefully in order to obtain decent hollow structures. Normally, polymer and carbon templates were removed simply by calcinations at 500-600 °C; other precursors were cleared up by chemical dissolution. The morphology of the resulting hollow structure obviously depends on the precursor. The thickness of the shell can be easily controlled just by varying the amount of the relevant materials employed. The disadvantage of this method is mainly that of the tedious and complicated preparation of the templates. In addition, the post-synthetic treatment for the removal of the templates may sometimes destroy the hollow structures.

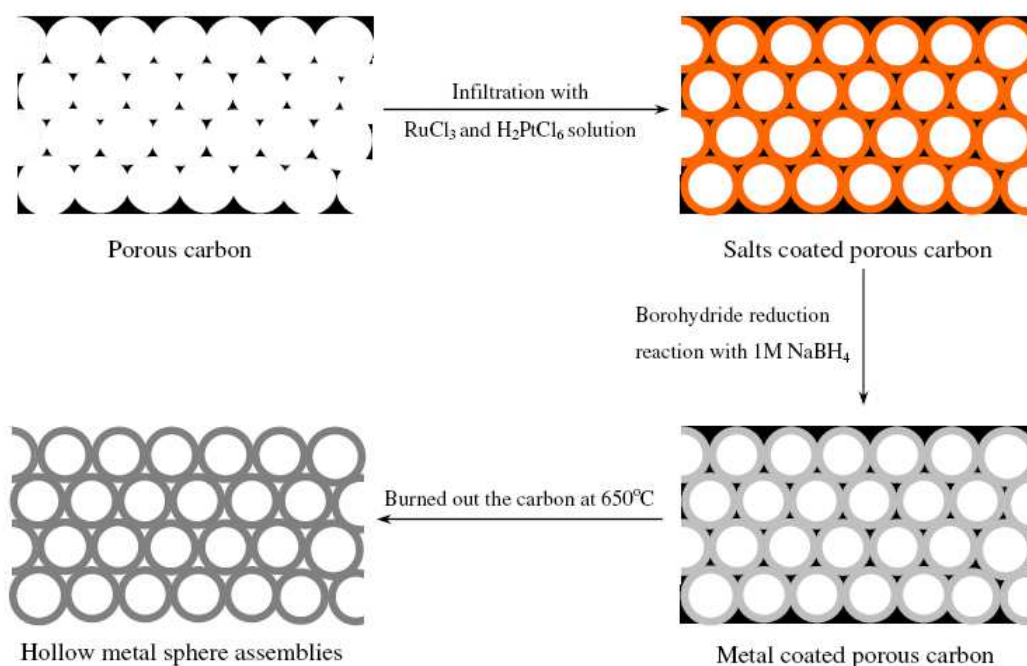


Figure 3.1 Schematic illustration of PtRu hollow spheres synthesis. [36]

3.1.2.2 Soft template assist synthesis

In contrast to the hard template assistance synthesis, soft template assistance preparation employs template such as micelles, [37] vesicles, [38-40] and emulsions [42] as the precursors for hollow structure construction. The word “soft” originates from the physical state of the templates as oppose to the solid templates in the hard template assisted preparation. Generally, this approach is suitable for the synthesis of semiconducting hollow structures such as silica, [43] CdS [44] and SnO₂. [45] A typical fabrication process is illustrated in Figure 3.2. In this case, sodium dodecyl sulfate (SDS) was adopted as the micelle template. Pt ions and Pd ions are adsorbed on to the SDS micelle surface by electrostatic attraction. Hollow spheres can be obtained by simply washing away the SDS after the metal ions reduction. Compared to the hard template synthesis, the soft templates can be removed easily with little impact on the final hollow structures. However, the soft templates consist of surfactants which may introduce contaminations to the final products.

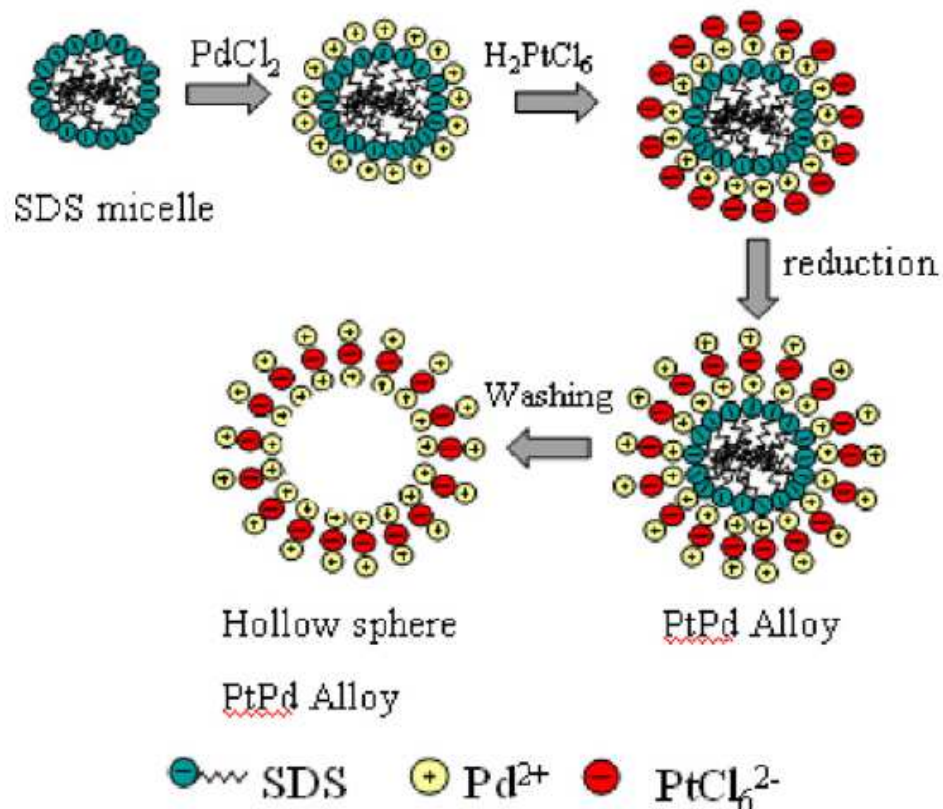


Figure 3.2 Schematic illustration of PtPd hollow spheres synthesis. [46]

3.1.2.3 Galvanic displacement involved synthesis

Inspired by Xia's pioneering work, great advancement have been achieved in nano-hollow structures preparation through galvanic displacement reaction. [47] In this synthetic process, nanostructures of a metal with low electrochemical potential are first synthesized as the sacrificial templates. The desirable, or the shell materials, metal source ions are subsequently introduced into the as prepared template dispersion. Galvanic replacement takes place resulting in the hollow nanostructure formation. The driving force for the reaction is the electrochemical potential difference between the respective metals involved. Template metals behave as the cathode while metals with higher electrochemical

potential serve as the anode. Therefore, transition metal such as Co, [48, 49] Ni, [50, 51] Ag [52, 53] and even Pd [54 55] are usually employed as the sacrificial template. In the cases of Co and Ni, an oxygen free atmosphere is needed in order to avoid surface oxidation of the template which would then inhibit the galvanic displacement reaction. Since the final hollow structures usually exhibited similar morphology to the employed templates, therefore, by controlling the morphology of the templates, nanostructures such as hollow sphere, [56] nanotubes, [57] and hollow cubic [58] can be easily synthesized. Moreover, the thickness of the shell of the hollow structures could be tuned just as easily by changing the amount of the relevant metal source similar to other preparation methods.

3.1.2.4 Other synthetic methods

Apart from the approaches mentioned above, there are other means of the preparation of hollow structures which are worthy of our notice, for instance, photochemical synthesis [59] and electrochemical methods. [60] Ag@Pt core shell structure was first prepared and then photo-excavated by picosecond laser pulses resulting in a hollow Pt spheric structure. [61] The thermalized photon energy of Pt Plasmon induces the core Ag to melt and effuse out, since Ag has lower melting and boiling temperature than Pt. This technique can eliminate any chance of contamination by silver chloride as in the case of galvanic displacement. Electrochemical methods such as electrodeposition and electrochemical anodizing have been proven to be versatile approaches for the preparation of hollow structures. Ce doped ZnO hexagonal nanotubes and nanocages were successfully fabricated

using electrodeposition by Li's group. [62] TiO₂ nanotubes can be synthesized through anode electrolysis of Ti electrode in a glycol aqueous solution. [63] Compared to other approaches, electrochemical methods are simple, quick and economical.

3.1.3 Mechanism of the formation of hollow structure through galvanic displacement

An enormous amount of works have been done in regards to the preparation of hollow structures through galvanic replacement, nevertheless, the hollow structure formation mechanism was rather poorly understood. Xia's group was one of the pioneers, in this context, to investigate the mechanism by using Ag/Au as a typical case study. The galvanic replacement reaction was run similar to a titration with the HAuCl₄ solution being added into the Ag templates gradually. Products at different stages were analyzed by TEM, SEM and elemental analysis. [64] Galvanic reaction was initiated locally at the high-energy sites of the Ag template such as defects, surface steps or hole rather than on the entire surface. [65] As the reaction proceeded, more Ag atoms dissolve out through the pinhole formed in the previous stage. The stripping electrons migrated to the surface which would then be captured by AuCl₄⁻ ions, forming Au atom on the surface. As this process was repeated over time, hollow structures were formed. TEM and electron diffraction analysis confirmed that the as formed shell consisted of an Ag/Au alloy instead of an Ag and Au phase separated regime. This observation can be explained by the mutual solubility of Ag and Au in their lattices especially with the high diffusion rate at the reaction temperature. [66, 67] Further

increase in the amount of HAuCl_4 would result in dealloying causing the collapse of the shell structures. [68] Similar to initiate stage of the reaction, dealloying occurred at the active sites of the as formed shell structures. Therefore, great caution was needed in determining the amount of HAuCl_4 used for synthesizing the Au hollow structures. To use cubic Ag template as an example, the whole process is illustrated in Figure 3.3.

In this chapter, Ag nanoparticles were employed as the precursor to synthesis of PtAg hollow nanostructure. The reason why Ag was used as the template is that Ag nanoparticles are quite stable in water in an ambient atmosphere. Therefore, it offers great ease in the preparation process.

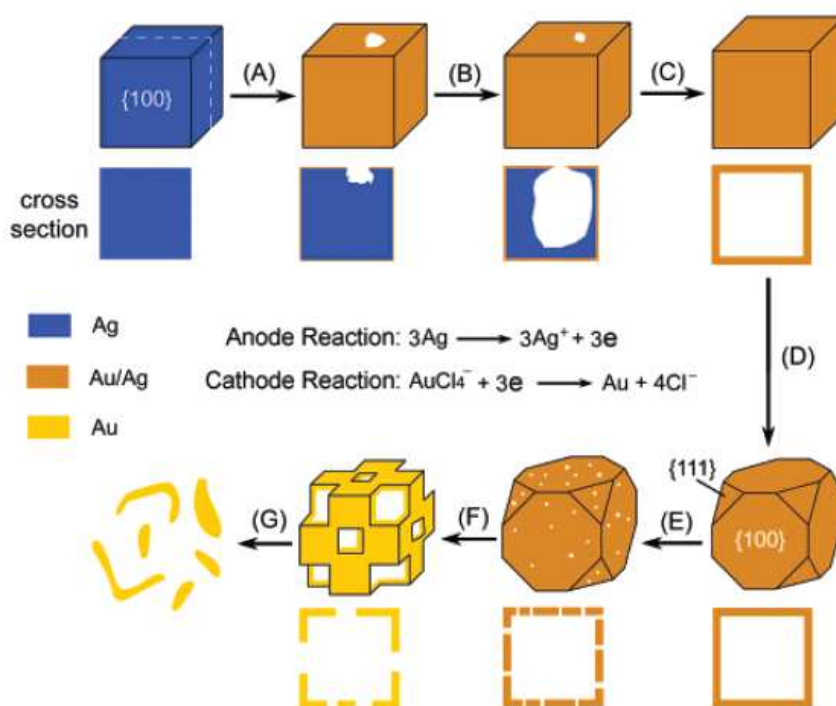


Figure 3.3 Schematic illustration summarizing all morphological and structural changes involved in the galvanic replacement reaction between silver nanocubes and an aqueous HAuCl_4 solution. [64]

3.2 Synthesis of PtAg hollow spheres

3.2.1 Preparation of Ag nanoparticles template

Ag nanoparticles template was prepared by seed mediated growth under room temperature. In a typical process for Ag seeds synthesis, 600 μ L of 0.1M AgNO₃ solution was mixed with 300mL of 0.5mM sodium citrate aqueous solution. Then 3mL of freshly prepared 0.1M NaBH₄ was added dropwise to the mixture while stirring. The colorless solution turned bright yellow indicating the formation of Ag nanoparticles. Afterwards, the solution was further stirred for a further 2h to decompose the remaining NaBH₄. For the growth process, a relatively weak reducing agent, NH₂OH·HCl, was used. 3.0mL of 0.2M NH₂OH·HCl solution was added into the above seed solution. After stirring for 5min, 750 μ L of 0.1M AgNO₃ solution was added. The mixture was then stirred for 12h to ensure the completion of the growth process.

3.2.2 Synthesis of the PtAg hollow spheres

30mL of the above template colloidal solution was heated to 60°C in an oil bath for 10min. A predetermined amount of K₂PtCl₄ solution was added with continuous stirring. Immediate color change was observed upon the addition of K₂PtCl₄ solution. Thereafter, the solution was kept stirring for 1h. The product was then separated by centrifugation at 6000rpm for 20min. In order to remove any by-product and the unreacted silver, the black solid was washed with 35% ammonium hydroxide and 5M HNO₃ solution consecutively

respectively. Typically, the obtained black solid was dispersed into 3mL of 35% ammonium hydroxide by sonication for 15min. The resulting crude product was centrifuged and washed with 6mL deionised water twice. The final black solid was washed with 3mL of 5M HNO₃ solution once and 6mL deionised water twice and was dried at 60°C overnight afterwards.

3.2.3 UV-visible spectroscopic measurement

In order to prove the successful formation of a PtAg shell on the surface of Ag nanoparticles, UV-visible spectroscopic studies were conducted at a HP 8453 spectrometer. 100µL of the Ag colloidal solution was transferred to the cell and diluted to 4mL with deionised water. The absorption spectrum was recorded between 200 to 800nm. In the same manner, measurements for the PtAg solution after the reaction were also conducted for comparison.

3.3.4 Physical characterizations

X-Ray powder diffraction analyses were conducted on a Rigaku Smartlab diffractometer. The sample was placed on a silicon substrate for measurement and the 2 theta range was chosen at the region between 20 and 90 degree. Morphology studies were carried out by transmission electronic microscopy (FEI Tecnai G2 20). Samples were prepared by dropping the relevant dispersion onto a carbon and Formvar copper grid for the observation. Energy dispersive X-ray spectra (EDS) and selected electron diffraction

(SAED) were also carried out during the TEM studies. Surface analyses were also performed by X-ray photoelectron spectrum (XPS) measurement.

3.3.5 Electrochemical analysis

All electrochemical performance tests were conducted at room temperature condition and were performed in a three-electrode setting on CHI 660D electrochemical station. Saturated calomel electrode (SCE) and Pt plate were used as the reference electrode and the counter electrode respectively. To prepare the working electrode, 1mg sample was mixed with 795 μ L deionised water, 200 μ L isopropanol and 5 μ L of 0.05% nafion by sonication to form a homogeneous ink. 2 μ L of the ink was casted to the glass carbon electrode (GCE) using a micropipette to yield a total metal loading of 2 μ g. The working electrode was cycled at 50mV/s between -0.24 and 1.0V in a N₂ saturated 0.1M H₂SO₄ solution until a stable CV curve was obtained. The last cycle was used to determine the hydrogen adsorption-desorption charge which was related to the Pt electrochemical active surface area (ECSA). For the formic acid activity test, the working electrode was transferred to a cell containing 0.1M H₂SO₄ + 0.05M HCOOH electrolyte solution. A CV between -0.2 to 1.0V was recorded when it reached a stable state after several cycles. For the methanol oxidation activity study, the electrolyte solution was changed to 0.1M H₂SO₄ + 0.1M methanol. Chronoamperometric studies were performed in the same electrolytes as with that of the activity tests under relevant potential.

3.4 Results and discussion

3.4.1 UV-visible spectroscopic analyses

UV-vis spectroscopic measurement is a common technique to study the silver related chemistry since it shows the absorbance which originate from the surface plasmon resonance (SPR). [69] The UV-vis spectroscopic studies before and after the galvanic replacement with different amount of K_2PtCl_4 were shown in Figure 3.4. The amount of the Ag colloidal was kept constant at 30mL (0.45mM) in the galvanic displacement process to enable direct comparison. As the amount of K_2PtCl_4 increased, the absorbance corresponding to Ag silver decreased suggesting that the Pt atoms were being deposited on to the surface of the Ag nanoparticles. [70] A flat line was observed when the amount was raised to 650 μ L, which indicated that all silver was completely removed. The gradually decrease of the Ag-related absorbance peak implied the formation of hollow structure.

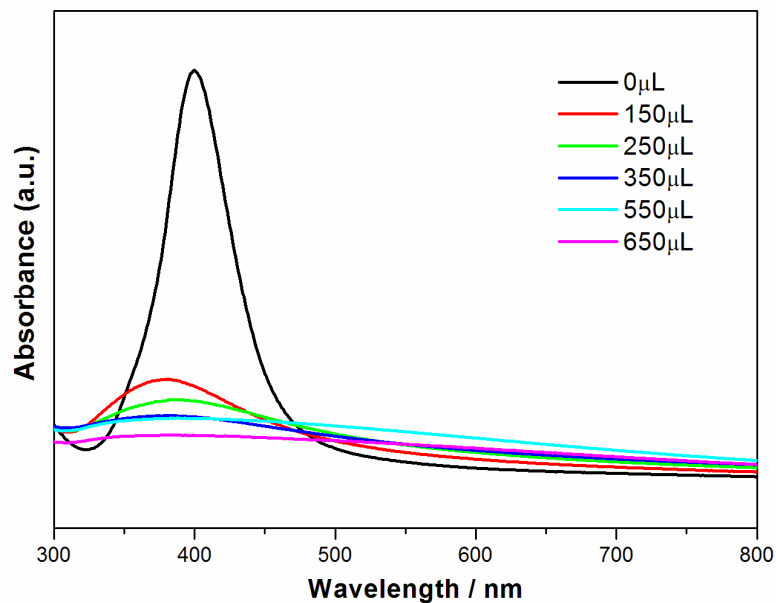


Figure 3.4 UV-vis spectra of the Ag colloidal solutions after reaction with different amount of 25mM K_2PtCl_4 .

3.4.2 Morphology characterization

3.4.1.1 Ag template observation

TEM measurement is typically used for morphology determination. Figure 3.5 shows the TEM image of the Ag templates. The Ag templates displayed nanosphere morphology with a diameter ranging from 20 to 50nm. From the HRTEM, shown in Figure 3.6(a), the lattice fringe with a d value of 0.24nm was observed, which corresponded to the (111) face of silver. The SAED measurement confirmed that the as prepared Ag templates exhibited a fcc structure with the appearance of diffraction rings corresponding to (111), (200), (220), (311). The template preparation is a key step of the hollow structures design since the morphology of the hollow structure, in most cases, would resemble that of the templates.

Moreover, the size of the templates plays a crucial role in the construction of the hollow structure since small particles can not be used as templates for the preparation of hollow spheres.

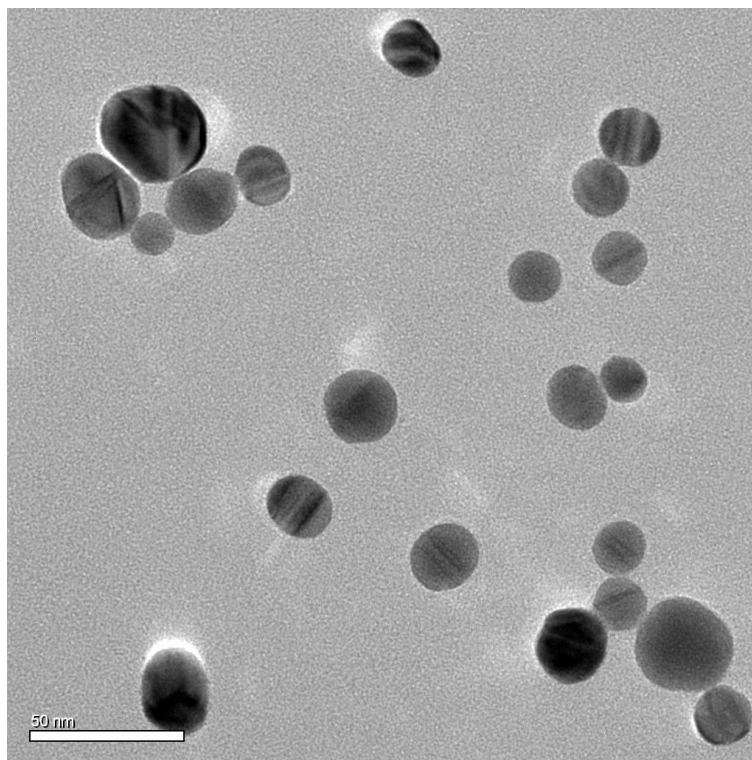


Figure 3.5 TEM image of Ag templates.

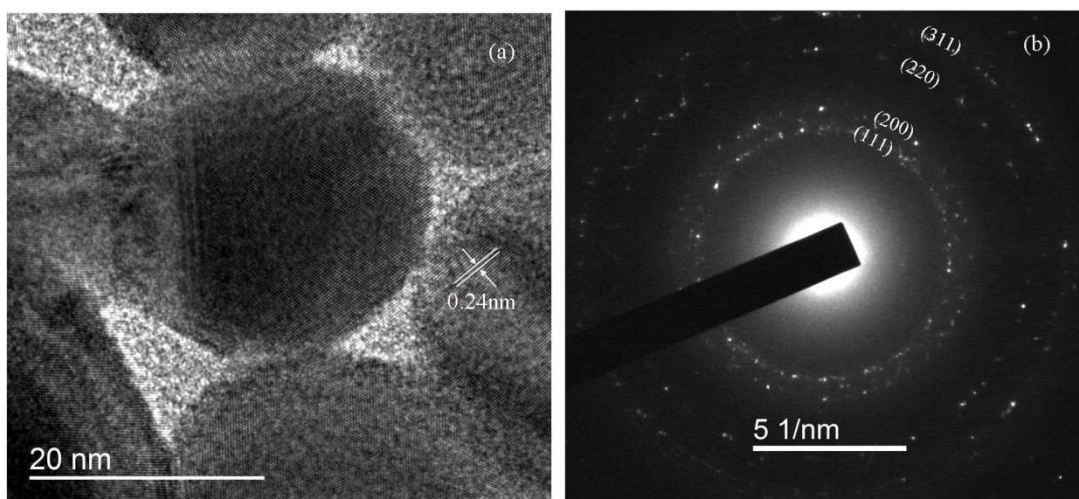


Figure 3.6 HRTEM (a) and SAED (b) of the Ag template nanoparticles.

3.4.1.2 PtAg hollow structures observation

As proposed from the UV-vis analyses, the newly formed Pt atoms gradually deposited on to the surface of the Ag templates. TEM studies were used to further confirm this conclusion. In similar manner, we carried out the galvanic displacement with different amount of 25mM K_2PtCl_4 solution with a fixed amount of template colloidal solution (30mL, 0.45mM). The results were shown in the Figure 3.7. A trend can be easily observed: as the amount of K_2PtCl_4 increased, more hollow structures could be seen. Additionally, the surface of the hollow spheres is rougher when a high amount of K_2PtCl_4 was used. During the galvanic replacement reaction, AgCl was the major by product which would contaminate the PtAg hollow structures. [71] Though it was proposed that the AgCl would dissolve in a relatively high temperature, [72] chlorine could still be detected in the EDS analysis of the purified hollow spheres as shown in Figure 3.8. Therefore, the remaining solid core at low amount K_2PtCl_4 preparation may be attributed to the unreacted Ag and AgCl. [35]

Another trend can be observed from Figure 3.7: the thickness of the hollow sphere increased as the amount of K_2PtCl_4 added was raised. To improve the clarity, samples were washed with ammonium hydroxide and 5M nitric acid respectively to remove any AgCl and unreacted silver. The relationship between the thickness of the hollow spheres and the amount of K_2PtCl_4 added can be obviously observed in Figure 3.9. Table 3.1 presents the summary of the thickness of the resulting hollow nanospheres prepared from different amount of K_2PtCl_4 . The thickness increased from ca. 2.3 nm to ca. 7.5 nm as the K_2PtCl_4 precursor amount rose from 150 μ L to 550 μ L. Based on this observation, one can conclude

that the thickness of the hollow sphere can be controlled just by simply varying the volume of K_2PtCl_4 source. A closer look at the thickness derived from different amount of K_2PtCl_4 source, one can observe that hollow spheres with lower thickness consist of a smooth surface while those of relatively high thickness compose of continuous aggregated nanoparticles growing on the smooth outer surface. This provides further proof for the hollow structure formation mechanism: active silver atoms first react with Pt ions, newly formed Pt atoms then deposited on to the surface of the Ag templates forming pinholes. As the reaction proceeded, silver dissolved out from the pinholes while Pt atoms continuously deposited onto the surface, which resulted in the hollow structures. Unlike the case of Au, when excess amount of Pt ions were used, dealloying did not occur. We increased the K_2PtCl_4 volume to 650 μL and verified the presence of excess Pt ions in the filtrate by ICP-MS measurement. In contrast to the dealloying in the case of Au, [73] the hollow spheres did not change. This is of great significance when the hollow structures were used as electrocatalysts since the large surface area can be well preserved for the electrochemical catalytic reaction.

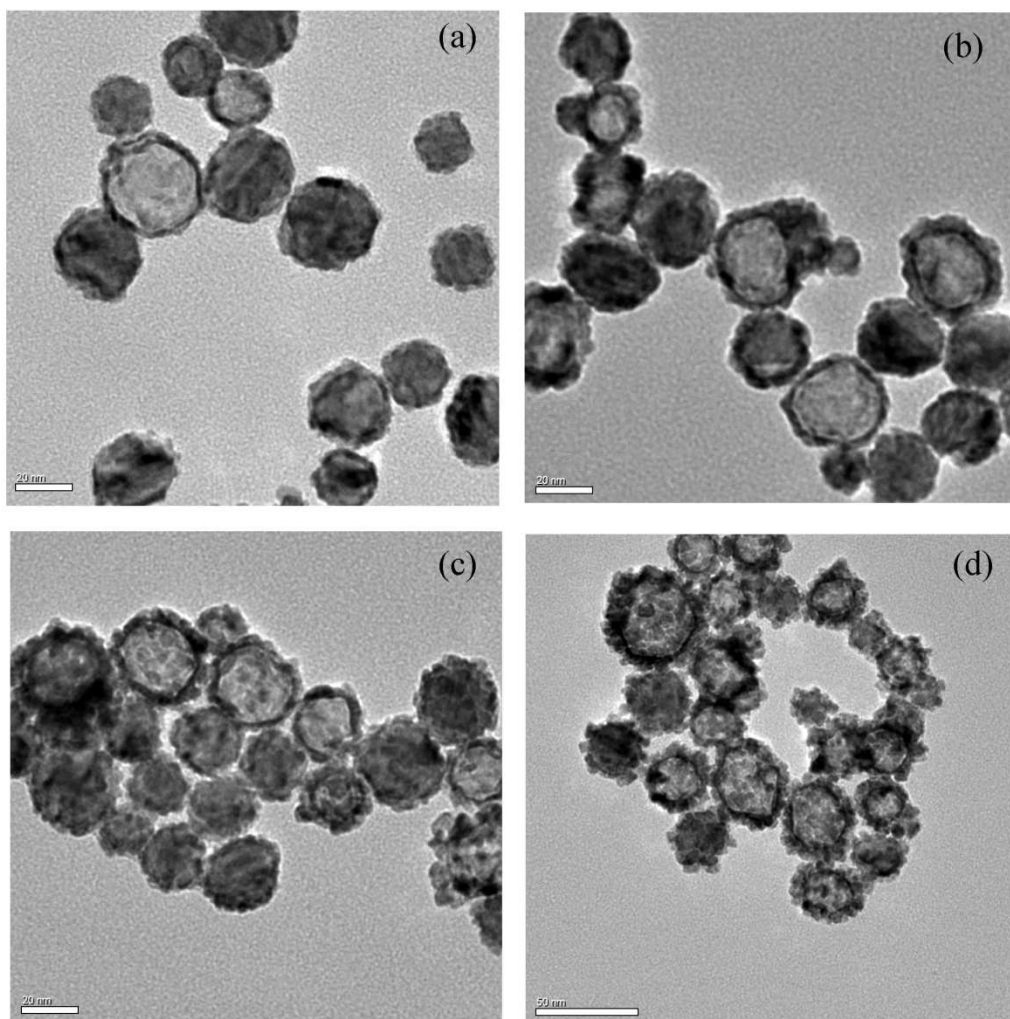


Figure 3.7 TEM images of PtAg hollow sphere prepared with different volume of 25mM K_2PtCl_4 before washing: (a) 150 μ L; (b) 250 μ L; (c) 350 μ L; (d) 550 μ L.

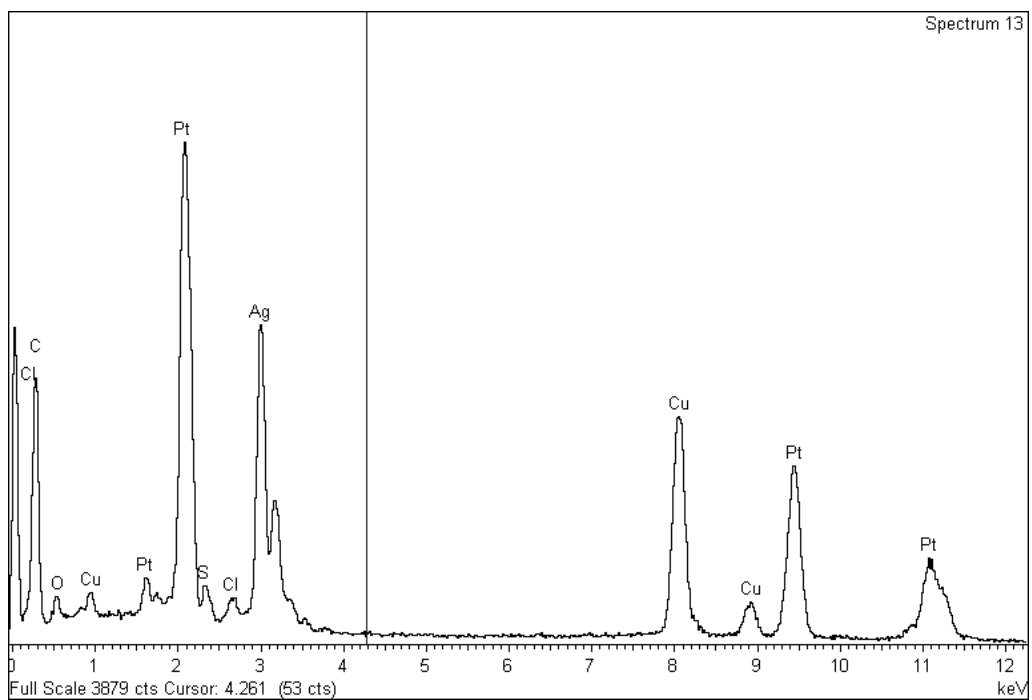


Figure 3.8 EDS spectrum of PtAg hollow structures before washing, sample prepared from 250 μ L of 25mM K_2PtCl_4 solution.

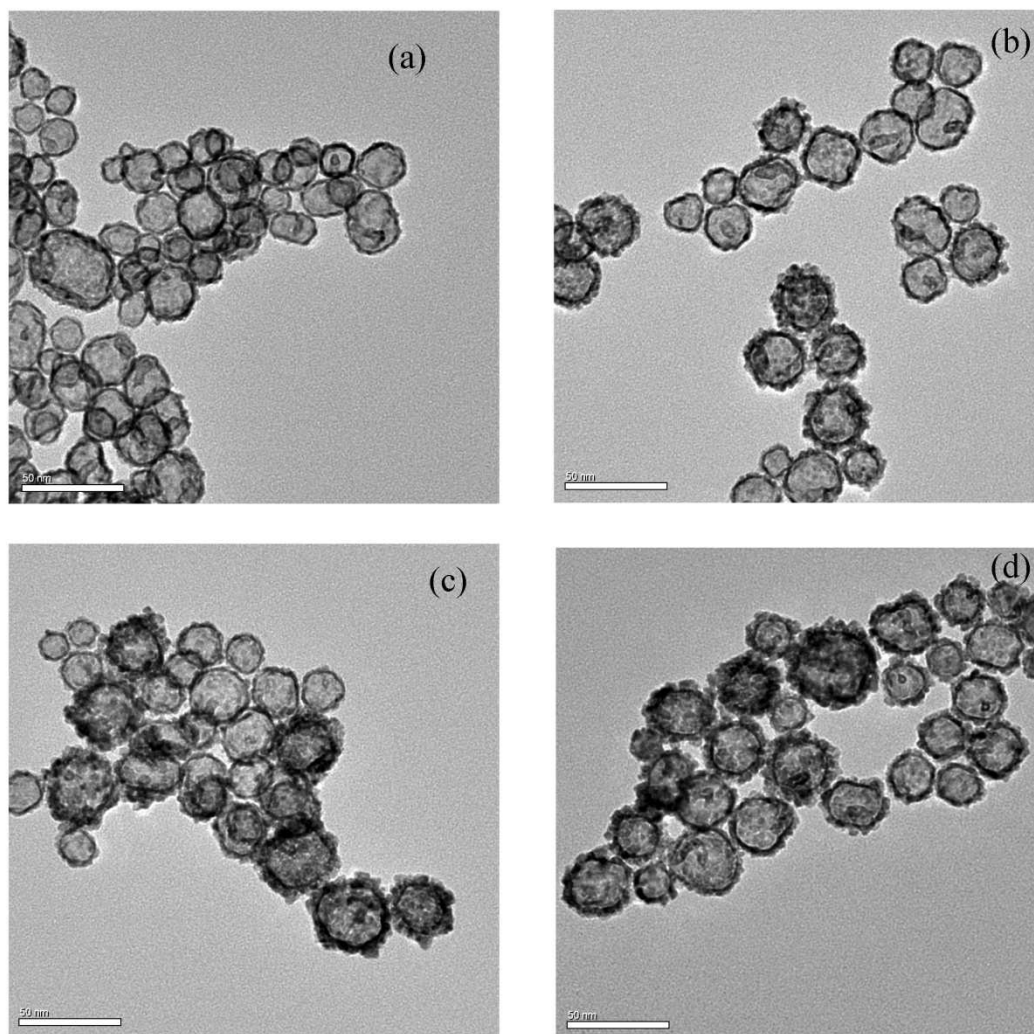


Figure 3.9 TEM images of PtAg hollow sphere prepared with different volume of 25mM K_2PtCl_4 solution after being washed by ammonium hydroxide and nitric acid: (a) 150 μ L; (b) 250 μ L; (c) 350 μ L; (d) 550 μ L.

Table 3.1 Data summary derives from TEM studies

25mM K_2PtCl_4 used/ μ L	Shell thickness/nm
150	2.3 ± 0.1
250	3.6 ± 0.1
350	5.1 ± 0.1
550	7.5 ± 0.2

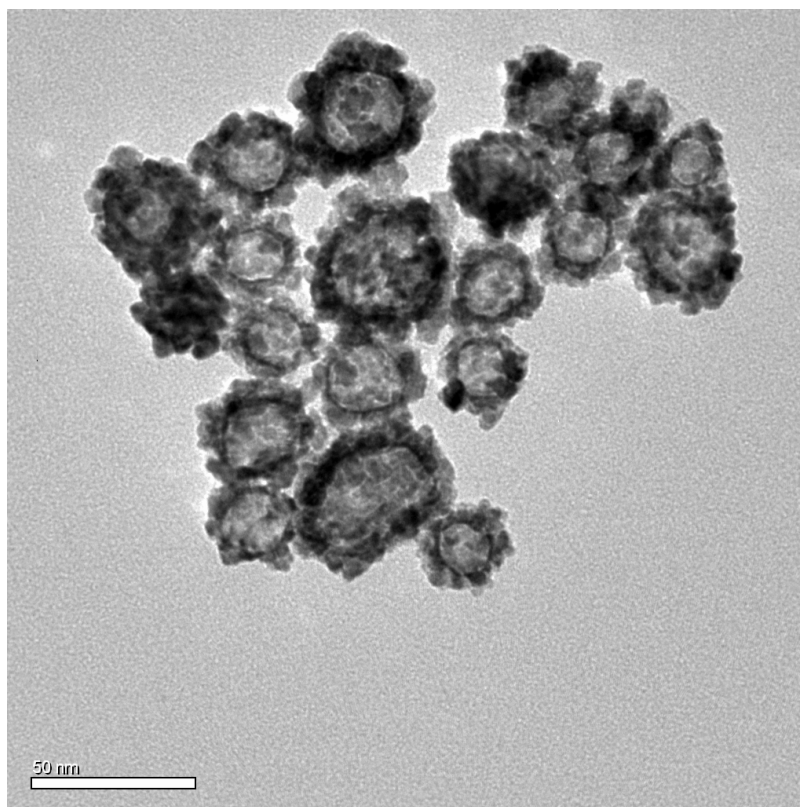


Figure 3.10 TEM images of PtAg hollow sphere prepared with 800 μ L of 25mM K_2PtCl_4 solution,

3.4.3 Structural analyses

3.4.3.1 XRD studies

To obtain the structural information of the as prepared PtAg hollow composite, XRD characterization was carried out. The results are shown in Figure 3.11, along with the diffraction pattern of silver and platinum as reference. The pattern of PtAg hollow structure exhibited diffraction peaks of (111), (200), (220), and (311) at 2 theta values of 39.1 $^\circ$, 45.7 $^\circ$, 67.1 $^\circ$ and 80.1 $^\circ$, respectively. The peaks indicated that the PtAg hollow structure took up a face-centered cubic structure. [74] A detailed comparison of the

diffraction patterns between Pt, Ag and PtAg hollow spheres was presented in Table 3.2. All diffraction peaks of PtAg are located in between the peaks of that of the patterns of Ag and Pt, implying the formation of PtAg alloy resulted from the galvanic displacement reaction. Moreover, there were no noticeable diffraction peaks related to Ag or Pt as compared to the references suggesting that there was a good degree of alloying between Pt and Ag. [75, 76]

3.4.3.2 HRTEM and SAED measurements

High resolution transmission electron microscopy (HRTEM) and selected area diffraction (SAED) are commonly used approaches for structural analyses for alloy nanocrystal. The PtAg hollow structures were further investigated by HRTEM and SAED to confirm the formation of PtAg alloy. The results were shown in Figure 3.12. The fringes spacing of 2.29Å, 2.30Å, 2.31Å can be observed in Figure 3.12(a), which was corresponding to the (111) face of the PtAg hollow structure. [77] It was noteworthy that all these values are located between that of Pt (2.26 Å) and Ag (2.35 Å), again, demonstrating the formation of PtAg alloy resulting from the galvanic replacement reaction. [77] The incorporation of Ag atoms enlarged the d value of the (111) face of Pt. In the SAED pattern, Figure 3.12(b), it displays the diffraction rings originating from (111), (200), (220), (311) faces of the PtAg alloy with the d-space value of 2.33 Å, 2.01 Å, 1.43 Å and 1.21 Å. The HRTEM and SAED results were in good consistence with the XRD measurements.

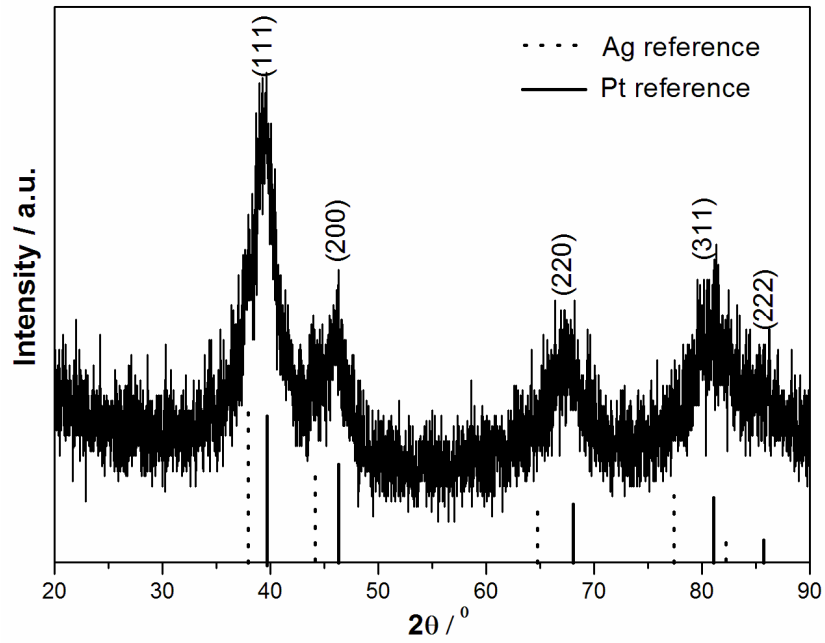


Figure 3.11 XRD pattern of the PtAg hollow structure.

Table 3.2 Data summary derived from XRD studies

Face	Pt ^o	Ag ^o	PtAg ^o
(111)	39.7	38.0	39.1
(200)	46.3	44.3	45.7
(220)	68.3	64.8	67.1
(311)	81.2	77.5	80.1
(222)	85.7	82.2	---

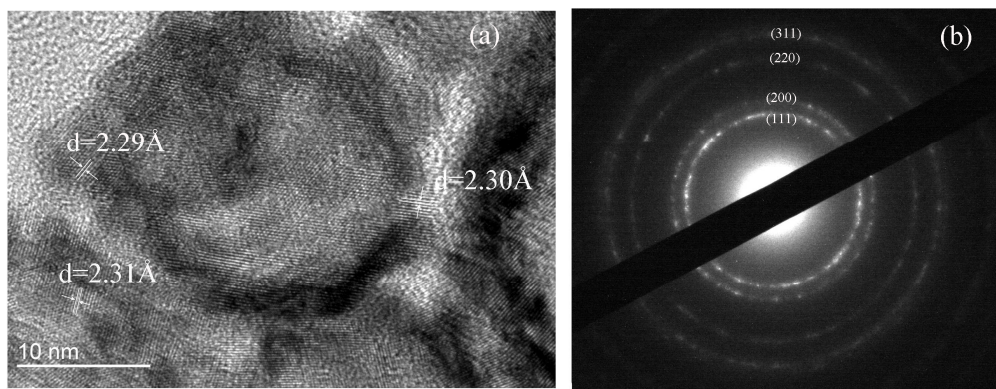


Figure 3.12 HRTEM image and SAED pattern of PtAg hollow structure.

3.4.3.3 XPS characterization

Further investigation on the PtAg hollow structure and the interaction between Pt and Ag were made by X ray photoelectron spectrum analyses (XPS). The results were presented in Figure 3.13. With reference to pure Pt and Ag, the binding energy of Pt in the hollow structure shifted to higher values while that of Ag shifted to lower values, implying the formation of PtAg alloy. [78] The positive shift in binding energy of Pt indicated an increase of 5d-orbitals vacancy, which is of great significance for the enhancement of electrocatalytic activity. An atomic ratio of 4.39:1 between Pt and Ag was obtained. With regards to the PtAg alloy preparations, it was reported that PtAg alloy was difficult to form because Pt does not readily undergo solid-solid diffusion with Ag. [79] However, on the other hand, PtAg alloy had been successfully fabricated by co-reduction of Pt and Ag metal sources. [80] In our case, the PtAg alloy formation by galvanic displacement was well proven by analyses such as XRD, HRTEM, SAED and XPS.

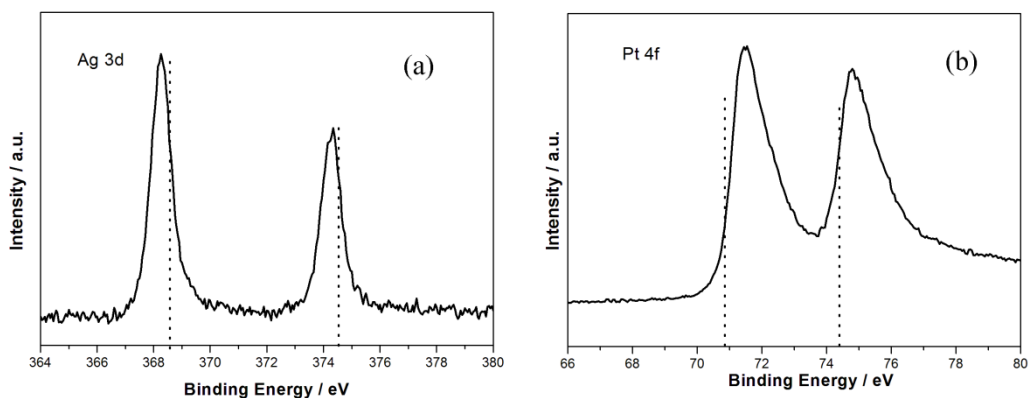


Figure 3.13 XPS spectra of the as-prepared PtAg hollow structure: (a) Ag; (b) Pt; The dotted line represented the binding energy for pure Ag and Pt metal, respectively.

3.4.4 Composition analyses

The composition of the as-prepared PtAg alloy was crucial for its electrochemical performance. [70] One straightforward way to control the atomic ratio between Pt and Ag in the PtAg alloy synthesis is to change the respective amount of the Pt and Ag metal sources used in a co-reduction approach. [81] In the case of galvanic replacement, we carried out the experiments by varying the ratio between PtCl_4^{2-} and Ag colloid, aiming to tune ratio of Pt and Ag in the resulting PtAg alloy hollow structure. The results are presented in Table 3.3. The atomic ratio between Pt and Ag in the hollow structure was found to be in range of 4.3 to 7.2. No distinct trend can be observed from Table 1. On the other hand, the galvanic displacement reactions at various temperatures were also conducted in hope of changing the composition of the PtAg alloy. The results were shown in Table 3.4. Similar results were obtained. The composition variation may be caused by the multiple steps involved in the preparation. For instance, the washing with nitric acid

might have induced dealloying of the PtAg nanostructures.

Table3.3 Atomic ratio between Pt and Ag*

25mM K ₂ PtCl ₄ / μ L	Pt/Ag(precursor)	Pt/Ag(product)
150	0.28	7.25
250	0.46	6.76
450	0.83	5.27
550	1.02	4.77
650	1.20	6.57

*The amount of Ag colloidal was fixed: 0.45mM, 30mL.

Table3.4 Atomic ratio between Pt and Ag**

Temperature/ $^{\circ}$ C	Pt/Ag
0	8.91
20	5.31
60	4.81
90	5.91

**The amount of Ag colloidal and K₂PtCl₄ were fixed, Ag: 0.45mM, 30mL; K₂PtCl₄: 25mM, 550 μ L.

3.4.5 Electrochemical characterizations

3.4.5.1 CVs in H₂SO₄

Platinum shows some typical features in CV in an acid medium including the hydrogen adsorption-desorption, Pt oxidation and reduction. Therefore it is a common approach to study Pt related materials. Figure 3.14 shows the CV of PtAg alloy and commercially available Pt black in N₂ saturated 0.1M H₂SO₄. From the CV of Pt black, one can observe hydrogen adsorption and desorption related to different faces. The peaks with more negative value corresponds to the (111) face and those appeared in more positive potential originates from the (200) face. [82, 83] However, in contrast, it was not featured in the CV of PtAg because the incorporation of Ag into the Pt lattice could decrease the crystallinity of the surface. Therefore, in the hydrogen region we could not observe the relevant H₂ adsorption-desorption peaks as in the case of Pt black. It was worth noticing that the electrochemical active area (ECSA) of PtAg hollow spheres is larger than that of Pt black, which was proven by both the hydrogen region and the Pt oxide reduction current signal. The ECSA can be calculated by the following equation: [84, 85]

$$\text{ECSA} = Q_{\text{H}}/mq_{\text{H}} \quad (3.1)$$

where Q_{H} is charge transfer for H_{upd} adsorption, m is the amount of metal loading, and q_{H} (210 $\mu\text{C}/\text{cm}^2$) is the charge for monolayer hydrogen adsorption on Pt surface. A value of 18.7m²/g of ECA was obtained for the PtAg hollow spheres compared to 14.9m²/g for Pt black.

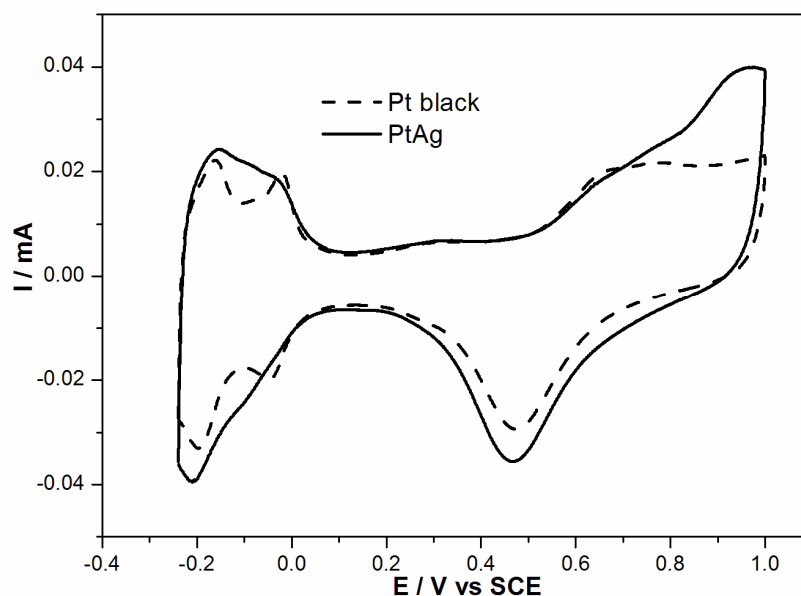


Figure 3.14 CVs of Pt black and PtAg hollow structure in N_2 saturated 0.1M H_2SO_4 solution, 50mV/s.

3.4.5.2 Electrooxidation of methanol and formic acid

The advantages of the PtAg hollow structures for electrochemical catalysis includes: (1) large ECSA would result in higher activity; (2) the utilization of the precious metal could be enhanced significantly since the cores were free of metal; and finally (3) the incorporation of Ag has apparently increase the 5d-orbitals vacancy of Pt which could weaken the interaction of Pt and poisoning intermediates (mainly CO), thus leading to an enhancement of catalytic capability. [86] To investigate the electrochemical performance of the as prepared PtAg hollow structure alloy, methanol and formic acid electrooxidations were carried out in 0.1M H_2SO_4 . Figure 3.15 shows the electrooxidation activity of methanol and formic acid. To aid direct comparisons, identical experiments were conducted for Pt black. The current values were normalized to the mass of the Pt. For the activity study of methanol (Figure 3.16(a)), the PtAg alloy displayed improved reactivity compared to that

of commercially available Pt black. A factor of 1.8 times enhancement was calculated from the current intensity at 0.5V as shown in Figure 3.16. Significant improvement was observed in case of formic acid oxidation as shown in Figure 3.15(b). The onset potential for formic acid oxidation negatively-shifted for about 40mV on PtAg alloy as compared to that of Pt black. A broad peak appeared at the forward scan in the CV of PtAg while the dehydration of formic acid (shoulder at 0.2-0.4V) and oxidation of CO (peak at around 0.62V) were clearly seen in the CV of Pt black. [87] It suggests that less poisoning intermediates were formed on the surface of PtAg alloy. The activity for formic acid oxidation at 0.3V was enhanced by five-fold as compared to Pt black (Figure 3.16).

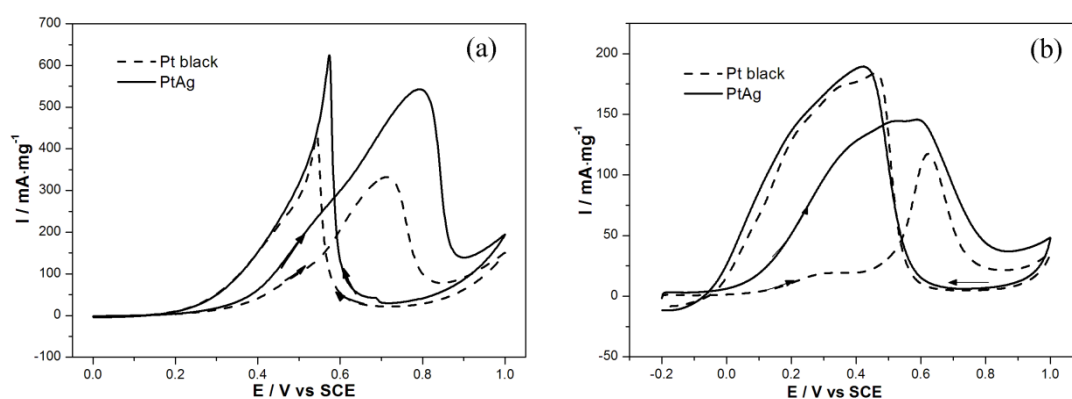


Figure 3.15 CVs of Pt black and PtAg alloy in (a): 0.1M H₂SO₄ + 0.1M methanol; (b): 0.1M H₂SO₄ + 0.05M HCOOH, 50mV/s; Current was normalized to the mass of Pt.

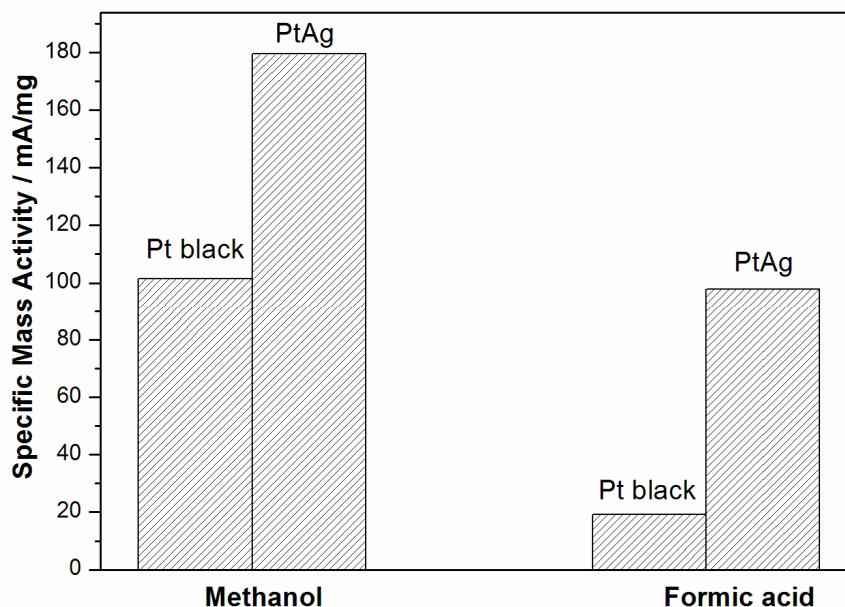


Figure 3.16 Specific mass activity comparisons of PtAg and Pt black.

3.4.5.3 Chronoamperometric studies

In order to investigate the long term electrocatalytic performance of the PtAg alloy hollow structure, chronoamperometric studies were carried out. At a fixed potential, due to continuous oxidation of the respective fuels there would be an accumulation of intermediates on the surface of the catalysts, which would decrease the current and degrade the performance of the catalysts. [88] As shown in Figure 3.17, the activity of PtAg for both methanol and formic acid was much higher than that of Pt black in throughout the measurement. A closer look shows that the current decrease for PtAg for methanol and formic acid oxidations were 18.6% and 12.8%, respectively, whereas the equivalent calculations for Pt black were 55.2% and 38.9%. It revealed that the PtAg alloy possesses higher stability compared to commercial Pt black. These results can be linked to the higher poison tolerance of the PtAg alloy, which can be furthermore ascribed to the electronic

effect caused by the incorporation of Ag as confirmed by the XPS study.

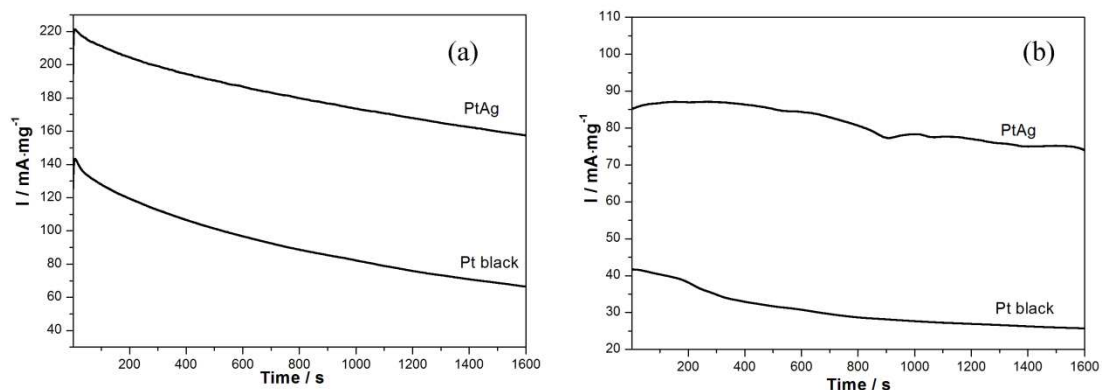


Figure 3.17 Chronoamperometric responses of PtAg alloy and Pt black recorded at (a) 0.5V, 0.1M H_2SO_4 + 0.1M methanol; (b) 0.3V, 0.1M H_2SO_4 + 0.05M HCOOH.

3.5 Summary

To summarize, an excellent electrocatalyst PtAg in the form of hollow structure was successfully synthesized by galvanic replacement reaction using the Ag nanoparticles as the template.

- (1) Ag template was prepared by a seed-mediated growth approach. Ag nanoparticle seeds were obtained by chemical reduction with sodium borohydride as the reducing agent. The growth process was performed under a weak reducing agent, $\text{NH}_2\text{OH} \cdot \text{HCl}$ at room temperature.
- (2) The galvanic displacement reaction was conducted at 60°C . The thickness of the hollow sphere can be easily controlled by simply changing the volume of Pt source added. EDS study revealed that the ratio of Pt and Ag was in a range of 4.2 to 7.2 but was found to be difficult to tune by either varying the precursors ratio or reaction

temperature. Both the XRD and XPS analysis confirmed the alloying of Pt and Ag.

- (3) Electrochemical investigations revealed that the as prepared PtAg alloy displays higher activity and stability towards methanol and formic acid oxidation compared to commercially available Pt black.

References

- [1] U. Kreibig, M. Vollmer, *Optical Properties of Metal Clusters Springer Series in Materials Science 25* **1995**, 25, 125.
- [2] T. S. Ahmadi, Z. L. Wang, T. C. Green, A. Henglein, M. A. El-Sayed, *Science* **1996**, 272, 1924.
- [3] M. A. Mahmoud, C. E. Tabor, M. A. El-Sayed, Y. Ding, Z. L. Wang, *J. Am. Chem. Soc.* **2008**, 130, 4590.
- [4] N. R. Jana, L. Gearheart, C. J. Murphy, *J. Phys. Chem. B* **2001**, 105, 4065.
- [5] B. Nikoobakht, M. A. El-Sayed, *Chem. Mater.* **2003**, 15, 1957.
- [6] Y. G. Sun, Y. N. Xia, *Science* **2002**, 298, 2176.
- [7] M. A. Mahmoud, M. A. El-Sayed, *J. Phys. Chem. C* **2008**, 112, 14618.
- [8] M. A. Mahmoud, B. Snyder, M. A. El-Sayed, *J. Phys. Chem. Lett.* **2010**, 1, 28.
- [9] P. L. Freund, M. Spiro, *J. Phys. Chem.* **1985**, 89, 1074.
- [10] K. K. Caswell, C. M. Bender, C. Murphy, *Nano Lett.* **2003**, 3, 667.
- [11] Y. G. Sun, B. Mayers, Y. N. Xia, *Adv. Mater.* **2003**, 15, 641.
- [12] Q. Zhang, W. S. Wang, J. Goebel, Y. D. Yin, *Nano Today* **2009**, 4, 494.
- [13] M. S. Yavuz, Y. Y. Cheng, J. Y. Chen, C. M. Cobley, Q. Zhang, M. Rycenga, J. W. Xie, C. Kim, K. H. Song, A. G. Schwartz, L. V. Wang, Y. N. Xia, *Nat. Mater.* **2009**, 8, 935.
- [14] E. Mathiowitz, J. S. Jacob, Y. S. Jon, G. P. Carino, D. E. Chickering, P. Chaturvedi, C. A. Santos, K. Vijayaraghavan, S. Montgomery, M. Bassett, C. Morrell, *Nature* **1997**, 386, 410.

- [15] J. Chen, F. Sacki, B. Wiley, H. Cang, M. J. Cobb, Z. Li, L. Au, H. Zhang, M. J. Kimmey, X. Li, Y. Xia, *Nano Lett.* **2005**, 5, 473.
- [16] X. Mei, D. Chen, N. Li, Q. Xu, J. Ge, H. Li, B. Yang, Y. Xu, J. Lu, *Soft Matter.* **2012**, 8, 5309.
- [17] M. A. Mahmoud, W. Qian, M. A. El-Sayed, *Nano Lett.* **2011**, 11, 3285.
- [18] S. W. Kim, M. Kim, W. Y. Lee, T. Hyeon, *J. Am. Chem. Soc.* **2002**, 124, 7642.
- [19] J. Chen, D. Wang, J. Xi, L. Au, A. Siekkinen, A. Warsen, Z. Y. Li, H. Zhang, Y. Xia, X. Li, *Nano Lett.* **2007**, 7, 1318.
- [20] Z. W. Chen, M. Waje, W. Z. Li, Y. S. Yan, *Angew. Chem., Int. Ed.* **2007**, 46, 4060.
- [21] H. M. Chen, R. S. Liu, M. Y. Lo, S. C. Chang, L. D. Tsai, Y. M. Peng, J. F. Lee, *J. Phys. Chem. C* **2008**, 112, 7522.
- [22] H. P. Liang, H. M. Zhang, J. S. Hu, Y. G. Guo, L. J. Wan, C. L. Bai, *Angew. Chem., Int. Ed.* **2004**, 43, 1540.
- [23] S. J. Guo, S. J. Dong, E. Wang, *Chem. Eur. J.* **2008**, 14, 4689.
- [24] M. A. Mahmoud, F. Saira, M. A. El-Sayed, *Nano Lett.* **2010**, 10, 3764.
- [25] F. Caruso, R. A. Caruso, H. Mohwald, *Science* **1998**, 282, 1111.
- [26] Z. Dai, L. Dahne, H. Mohwald, B. Tiersch, *Angew. Chem.* **2002**, 114, 4191.
- [27] K. P. Velikov, A. Blaaderen, *Langmuir* **2001**, 17, 4779.
- [28] A. B. Bourlinos, M. A. Karakassides, D. Petridis, *Chem. Commun.* **2001**, 1518.
- [29] D. Walsh, B. Lebeau, S. Mann, *Adv. Mater.* **1999**, 11, 324.
- [30] T. Nakashima, N. Kimizuka, *J. Am. Chem. Soc.* **2003**, 125, 6386.
- [31] H. T. Schmidt, A. E. Ostafin, *Adv. Mater.* **2002**, 14, 532.

- [32] Z. Yang, Z. Niu, Y. Lu, Z. Hu, C. C. Han, *Angew. Chem. Int. Ed.* **2003**, 42, 1943.
- [33] Y. Xia, R. Mokaya, *J. Mater. Chem.* **2005**, 15, 3126.
- [34] S. Guo, S. Dong, E. Wang, *J. Phys. Chem. C* **2009**, 113, 5485.
- [35] J. Yang, J. Y. Lee, H. P. Too, S. Valiyaveetil, *J. Phys. Chem. B* **2006**, 110, 125.
- [36] H. Wang, Y. W. Li, S. J. Cho, X. D. Li, D. P. Kim, *Micropor. Mesopo. Mat.* **2009**, 117, 208–212
- [37] C. E. Fowler, D. Khushalani, S. Mann, *J. Mater. Chem.* **2001**, 11, 1968.
- [38] H. T. Schmidt, A. E. Ostafin, *Adv. Mater.* **2002**, 14, 532.
- [39] D. H. W. Hubert, M. Jung, A. L. German, *Adv. Mater.* **2000**, 12, 1291.
- [40] H. P. Hentze, S. R. Raghavan, C. A. McKelvey, E. W. Kaler, *Langmuir* **2003**, 19, 1069.
- [41] T. Hirai, S. Hariguchi, I. Komasaawa, R. J. Davey, *Langmuir* **1997**, 13, 6650.
- [42] M. M. Wu, G. G. Wang, H. F. Xu, J. B. Long, F. L. Y. Shek, S. M. F. Lo, I. D. Williams, S. H. Feng, R. R. Xu, *Langmuir* **2003**, 19, 1362.
- [43] C. E. Fowler, D. Khushalani, S. Mann, *Chem. Commun.* **2001**, 2028.
- [44] J. X. Huang, Y. Xie, B. Li, Y. Liu, Y. T. Qian, S. Y. Zhang, *Adv. Mater.* **2000**, 12, 808.
- [45] F. Du, Z. Guo, G. Li, *Mater. Lett.* **2005**, 59, 2563.
- [46] Y. Y. Chua, Z. B. Wang, Z. Z. Jiang, D. M. Gu, G. P. Yin, *J. Power Sources* **2012**, 203, 17.
- [47] Y. Sun, B. Mayers, Y. Xia, *Nano Lett.* **2002**, 2, 481.
- [48] Q. Sun, S. Wang, R. Wang, *J. Phys. Chem. C* **2012**, 116, 5352.
- [49] X. W. Zhou, Q. S. Chen, Z. Y. Zhou, S. G. Sun, *J. Nanosci. Nanotechnol.* **2009**, 9,

2392.

- [50] Q. Sun, Z. Ren, R. Wang, N. Wang, X. Cao, *J. Mater. Chem.* **2011**, 21, 1925.
- [51] H. Li, H. Lin, Y. Hu, H. Li, P. Li, X. Zhou, *J. Mater. Chem.* **2011**, 21, 18447.
- [52] C. L. Lee, H. P. Chiou, C. M. Syu, C. R. Liu, C. C. Yang, C. C. Syu, *Int. J. Hydrogen Energ.* **2011**, 36, 12706.
- [53] V. Bansal, A. P. O'Mullane, S. K. Bhargava, *Electrochem. Comm.* **2009**, 11, 1639.
- [54] H. Zhang, M. Jin, H. Liu, J. Wang, M. J. Kim, D. Yang, Z. Xie, J. Liu, Y. Xia, *ACS Nano* **2011**, 5(10), 8212.
- [55] J. W. Hong, S. W. Kang, B. S. Choi, D. Kim, S. B. Lee, S. W. Han, *ACS Nano* **2012**, 6 (3), 2410.
- [56] H. P. Liang, H. M. Zhang, J. S. Hu, Y. G. Guo, L. J. Wan, C. L. Bai, *Angew. Chem. Int. Ed.* **2004**, 43, 1540.
- [57] Y. Bi, G. Lu, *Electrochem. Comm.* **2009**, 11, 45.
- [58] J. Zeng, Q. Zhang, J. Chen, Y. Xia, *Nano Lett.* **2010**, 10(1), 30.
- [59] F. Bai, Z. Sun, H. Wu, R. E. Haddad, X. Xiao, H. Fan, *Nano Lett.* **2011**, 11, 3759.
- [60] Z. Peng, H. You, J. Wu, H. Yang, *Nano Lett.* **2010**, 10, 1492.
- [61] S. J. Kim, C. S. Ah, D. J. Jang, *Adv. Mater.* **2007**, 19, 1064.
- [62] G. R. Li, X. H. Lu, W. X. Zhao, C. Y. Su, Y. X. Tong, *Cryst. Growth Des.* **2008**, 8(4), 1276.
- [63] X. Lu, G. Wang, T. Zhai, M. Yu, J. Gan, Y. Tong, Y. Li, *Nano Lett.* **2012**, 12, 1690.
- [64] Y. Sun, Y. Xia, *J. Am. Chem. Soc.* **2004**, 126, 3892.
- [65] Z. L. Wang, *J. Phys. Chem. B* **2000**, 104, 1153.

- [66] S. K. Wonnell, J. M. Delaye, M. Bibole, Y. Limoge, *J. Appl. Phys.* **1992**, 72, 5195.
- [67] T. Shibata, B. A. Bunker, Z. Zhang, D. Meisel, C. F. Vardeman, J. D. Gezelter, *J. Am. Chem. Soc.* **2002**, 124, 11989.
- [68] J. Erlenbacher, M. J. Aziz, A. Karma, N. Dimitrov, K. Sieradzki, *Nature* **2001**, 410, 450.
- [69] J. Zeng, Y. Zheng, M. Rycenga, J. Tao, Z. Y. Li, Q. Zhang, Y. Zhu, Y. Xia, *J. Am. Chem. Soc.* **2010**, 132, 8552.
- [70] D. Zhao, B. Yan, B. Q. Xu, *Electrochem. Comm.* **2008**, 10, 884.
- [71] Y. N. Tan, J. Yang, J. Y. Lee, D. I. C. Wang, *J. Phys. Chem. C* **2007**, 111, 14084.
- [72] Y. Sun, Y. Xia, *J. Am. Chem. Soc.* **2004**, 126, 3892.
- [73] X. Lu, H. Y. Tuan, J. Chen, Z. Y. Li, B. A. Korgel, Y. Xia, *J. Am. Chem. Soc.* **2007**, 129, 1733.
- [74] J. B. Xu, K. F. Hua, G. Z. Sun, C. Wang, X. Y. Lv, Y. J. Wang, *Electrochem. Commun.* **2006**, 8, 982.
- [75] Z. M. Peng, H. Yang, *J. Solid State Chem.* **2008**, 181, 1546.
- [76] L. Vegard, H. Dale, *Zeits. Krist.* **1928**, 67, 148.
- [77] Y. Y. Feng, J. H. M, G. R. Zhang, G. Liu, B. Q. Xu, *Electrochem. Comm.* **2010**, 12, 1191.
- [78] Y. Y. Feng, G. R. Zhang, J. H. Ma, G. Liu, B. Q. Xu, *Phys. Chem. Chem. Phys.* **2011**, 13, 3863.
- [79] M. Batzill, B. E. Koel, *Surf. Sci.* **2004**, 553, 50.
- [80] Z. Peng, H. You, H. Yang, *Adv. Funct. Mater.* **2010**, 20, 3734.

- [81] C. L. Lee, Y. J. Chao, C. H. Chen, H. P. Chiou, C. C. Syu, *International Journal of Hydrogen Energy* **2011**, 36, 15045.
- [82] P. N. Ross, *Surf. Sci.* **1981**, 102, 463.
- [83] M. N. Markovic, P. N. Ross, *Surf. Sci. Rep.* **2002**, 45, 117.
- [84] T. J. Schmidt, H. A. Gasteiger, G. D. Stab, P. M. Urban, D. M. Kolb, R. J. Behm, *J. Electrochem. Soc.* **1998**, 145 (7), 2354.
- [85] B. Lim, M. Jiang, P. H. C. Camargo, E. C. Cho, J. Tao, X. Lu, Y. Zhu, Y. Xia, *Science* **2009**, 324 (5932), 1302.
- [86] S. Schwamborn, M. Bron, W. Schuhmann, *Electroanal.* **2011**, 23, 3, 588.
- [87] X. Gu, X. Cong, Y. Ding, *Chem. Phys. Chem.* **2010**, 11, 841.
- [88] B. Liu, J. H. Chen, C. H. Xiao, K. Z. Cui, L. Yang, H. L. Pang, Y. F. Kuang, *Energ. Fuel.* **2007**, 21, 1365.

Chapter 4

Synthesis and Characterization of Pd@PdPt/MWCNTs

Core-Shell Structure for Electrocatalysis

4.1 Introduction

4.1.1 A brief overview of core-shell structure in electrocatalysis

For a heterogeneous reaction, the catalyst plays a critical role which can decrease the activation energy required for the generation of the intermediate states. Precious metals, such as Au, Pd and Pt, are crucial to electrochemical catalysis owing to their high activity and excellent durability. However, their limited natural abundance and high cost is one of the major challenges for widespread application. [1] In this context, the construction of core-shell structures with precious metals on the surface will be important for cost reduction. For example, polymer electrolyte membrane (PEM) fuel cells will be more cost-competitive in automotive applications if the amount of Pt used in the cathode is lowered at least by a factor of two by a core shell structure design. [2]

Electrocatalytic processes are of growing importance in a variety of technological areas, including fuel cells, HCl electrolysis and others. Core-shell structure design is one of the most efficient approaches for catalysts preparation with regard to both cost reduction and activity enhancement. By using non noble metals such as Fe, [3] Ni, [4] Co [5] or other semiconductors including SnO₂, [6] iron oxide [7] as the core materials, the usage of precious metals can be lowered dramatically. Moreover, the influence induced by the core

materials in some cases can improve the catalytic capability. The most prominent case is Au@Pt catalyst. [8] Decoration of Pt on the surface of Au can cause a shift of the Pt d orbital, in turn decreasing the binding energy of the intermediates to Pt and thereby enhancing the activity.

4.1.2 Synthesis of M@Pt core-shell materials

There are various methods to fabricate M@Pt core-shell materials, namely, co-reduction, seed mediate growth, electrochemical deposition, electrochemical dealloying and galvanic replacement. Each approach is applicable to a certain condition with both advantages and shortcomings.

4.1.2.1 Co-reduction

Co-reduction is a facile method which involves a one-step process to prepared M@Pt catalysts. [9, 10] The redox potential of the respective metals plays a key role in the core-shell formation. In the case of Au@Pt, the reduction of Au core first takes place owing to the higher redox potential of $\text{AuCl}_4^{-1}/\text{Au}$ as compared to $\text{PtCl}_4^{2-}/\text{Pt}$. The resulting Au cores serve as the nuclear centre for the subsequently reduced PtCl_4^{2-} , thus resulting in a core-shell structure. Core-shell like Pd-Pt structure was also reported to be prepared by this method. The spontaneous separation of Pd interior and the dendritic Pt exterior was ascribed to the different reduction kinetics of the Pd and the Pt complexes with ascorbic acid. The thickness of the shell or the dendritic exterior Pt can be easily tuned via changing the original Pt source used. It is note worthy that the redox potential of the complexes can

be tuned by adding suitable coordinating agents, in turn leading to varying redox potential difference between the related metal complexes involved in the core-shell preparation. However, up to date, there is no particular rule reported for choosing which coordinating agent to adopt. As a result, there are limited literatures in this regard reporting the core-shell construction by this method.

4.1.2.2 Seed-mediate process

Seed-mediate process is a straightforward approach for core-shell material preparation. [11-21] It is the most commonly used method which is promising for large scale preparation. Compared to the above mentioned co-reduction approach, it involves two reduction steps in the seed-mediate process: firstly the reduction of the core material, followed by the reduction of related Pt salt which grow as a shell on to the nuclei formed by the reduced core. Theoretically, various materials can be employed as the core. Nevertheless, the synthetic conditions vary depending on the core materials chosen. For instance, Au@Pt core-shell structures are usually fabricated under aqueous medium since the Au surface is stable in an aqueous solution. [22, 23] On the other hand, preparation of core-shell materials involving transition metals [24], metal oxides [6, 7] and transition metal containing alloys [25, 26] as core is conducted in a non-aqueous system under the protection of N₂ to avoid surface oxidation of the cores. Similar to the co-reduction process, the thickness of the Pt shell can be controlled by varying the Pt source used in the growth process.

4.1.2.3 Galvanic replacement

Galvanic replacement is a practical method to prepare core-shell nanostructure. [27-30] It involves the synthesis of a template from non-noble metals which is subsequently replaced by precious metals ions such as PtCl_4^{2-} , PdCl_4^{2-} and AuCl_4^- . Similar to the seed mediate growth process, the galvanic replacement involving transition metal templates, such as Cu, Ni, are always carried out under the protection of N_2 to avoid surface oxidation. Generally, the shape of the core-shell nanostructure resembles that of the template. Therefore, materials of different morphologies can be readily fabricated including nanowire, nanorod and nanocubes by simply modifying the shape of the template used. Another advantage to this approach is that it is possible to prepare monolayer Pt structure by employing processes involving under potential deposit (UPD). [31-34] A single layer of copper is first deposited on a certain metal substrates (noble metals in most case) via UPD which is then displaced by Pt through redox exchange thus resulting in a monolayer Pt structure. Due to the involvement of UPD, it is not readily applicable to mass production for commercialization.

4.1.2.4 Electrochemical method

Electrochemical preparation of core shell structure can be classified into, namely, bottom-up or top-down construction. For the bottom up fabrication, the desired metals are electrodeposited on a certain substrate in a layer-by-layer fashion that forms the core-shell structure. As illustrated in Figure 4.1, Ni is deposited on to the ZnO nanorods first, and then Pt is decorated on the as formed ZnO@Ni, generating the ZnO@Ni@Pt composite. [35]

After the removal of ZnO, Ni@Pt core shell nanotubes are obtained. As for the top down construction, Pt containing alloys are first synthesized followed by the electrochemical dealloying to dissolve the less noble metals, thereby forming M@Pt nanostructure. [36-39]

Due to the redox potential difference between Pt and Ag, as shown in Figure 4.2, a suitable potential can be chosen to dissolve Ag without the dissolution of Pt. The electrochemical method construction of Pt core shell materials normally involves multiple steps, however, parameters such as shell thickness and morphology can be accurately controlled. Moreover, various core-shell nanostructures can be prepared by this method through precise experimental design.

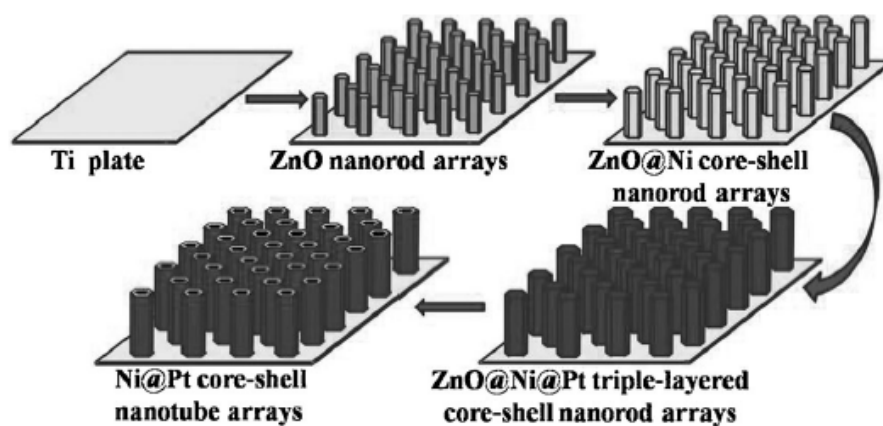


Figure 4.1 Schematic illustration of the Ni@Pt core-shell nanotube arrays. [35]

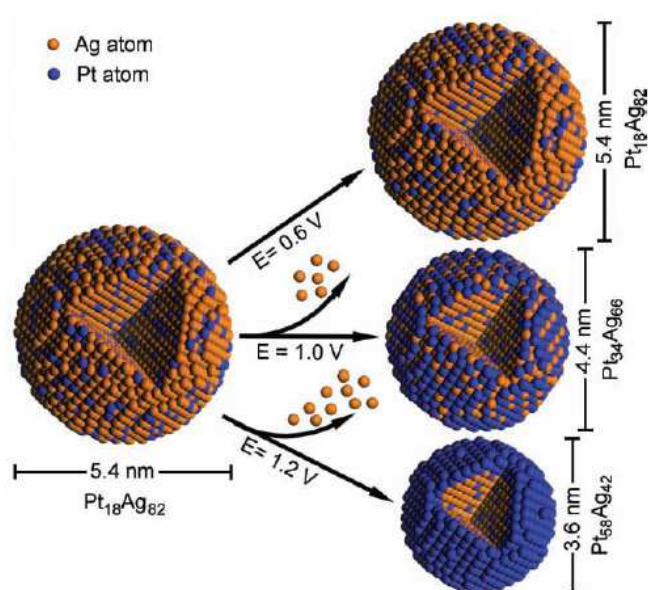


Figure 4.2 Electrochemical dealloying of PtAg nanoparticles. [37]

4.1.3 Recent development of Pt-Pd materials for electrocatalysis

Pd and Pt are two precious metals which play important role in electrocatalysis. In the past decades, there has been a large number of literatures related to Pt and Pd electrocatalysis, and great achievements have been made owing to the advancement of nanotechnologies and engineering. For the preparation of PtPd electrocatalyst, co-reduction is one of the most commonly used and convenient approach. [40-47] The electrocatalytic activity is enhanced which is proposedly due to the electronic effect caused by the interaction between Pd and Pt. The synergistic effect was reported to be correlated to the composition of PdPt electrocatalyst. [40, 41] Although there is no consensus as to what constitute the optimal molar ratio due to the variation in experimental condition. Another merit of the PdPt materials is the methanol tolerant ORR catalysis. [45, 46] By

incorporating of Pd into the Pt lattice, the resistance for methanol upon ORR is enhanced considerably. By adjusting the preparation condition, PtPd of multiple (111) twins with the exposure of high index facets can be obtained. [44] The surface with high index facets is vital for the activity improvement. Template assisted method is a versatile approach for the synthesis of PdPt materials with various morphologies since the final product normally inherit the same morphology as that of the templates. [48-50] Moreover, the morphology of the PtPd has been proven to have great influence on the activity of the catalysts, originating from increment of the surface area as well as the change in surface crystallinity. Pd@Pt core shell electrocatalysts have recently received considerable interest owing to its excellent electrochemical performance. These structures can be generated by electrodeposition [51], galvanic displacement [51-54], or physical process such as sputtering. [55] The coating of Pt on Pd surface would greatly increase the surface area of Pt, thus enhancing the Pt utilization. Interactions between the Pd core and the Pt shell give rise to the electrocatalytic activity enhancement as well as stability improvement. In term of further development of the core shell structure Pd@Pt, a layer-by-layer assembly of Pd and Pt was reported and resulted in an electrocatalyst with high efficiency. [56] The Pd/Pt bimetallic alternating multilayer mesoporous film exhibited good catalytic activity in methanol oxidation.

4.2 Preparation of Pd@PdPt/MWCNTs composite

4.2.1 Catalyst preparation

For the preparation of Pd/MWCNTs composite, 2mg of acid treated carbon nanotubes (MWCNTs, multi-wall) was dispersed in 50ml of deionised water by ultrasound for 30min. Then the black dispersion was heated to 60°C in an oil bath. After that, a desired amount of K_2PdCl_4 was added into the dispersion while stirring. The mixture was stirred for another 2 hour for the complete hydrolysis of $PdCl_4^{2-}$. The black solid was separated by centrifugation and washed twice with deionised water. For the reduction process, the as obtained black solid was re-dispersed in 50ml of deionised water in a round bottom flask and was bubbled with pure hydrogen for 10min. The round bottom flask was sealed and the mixture was heated to 60°C under the protection of hydrogen. After stirring for another 2 hour, the product was collected by centrifugation and washed twice with deionised water and dried at 60°C for further used. The preparation process for the Pt/MWCNTs is the same as that of the Pd/MWCNTs composite. As for the synthesis of Pd@Pt/MWCNTs, 1mg Pd/MWCNTs composite was dispersed into 5mL of deionised water in a vial by sonication for 5min. A desired amount of K_2PtCl_4 was then added into the dispersion. The vial was heated to 90°C and stirred for 1h. The product was collected by centrifuge and wash twice with deionised water. The catalysts were characterized by transmission electron microscopy (TEM), X-ray diffraction (XRD), and X-ray photoelectron spectroscopy. The mass loading of the carbon tube supporting samples was measured by induce coupled plasma mass spectrometry (ICP-MS).

4.2.2 Electrochemical measurements

All electrochemical characterizations were conducted on CHI 660D electrochemistry station under room temperature. A conventional three-electrode system was used with the saturated calomel electrode (SCE) and Pt foil as the reference and counter electrodes respectively. All the potentials reported are in reference to SCE unless stated otherwise. For the preparation of the working electrode, 1mg catalyst was dispersed into 800 μ L of deionised water and 200 μ L of isopropanol by ultrasonic for 30min. 2 μ L dispersion was casted on to the glass carbon electrode (GCE) with a micro-pipette. After drying in air, 2 μ L of 0.05% nafion solution was dropped on to the GCE to improve the attachment. Cyclic voltammetry and chronoamperometry were performed for diagnostic purpose and catalytic activity investigation. The working electrolyte was purged with pure N₂ for 15min before each measurement. For the accelerate durability test, the working electrode was swept for 1000 cycle in the respective electrolyte.

4.3 Results and discussion

4.3.1 Scheme of preparation of Pd@PdPt/MWCNTs

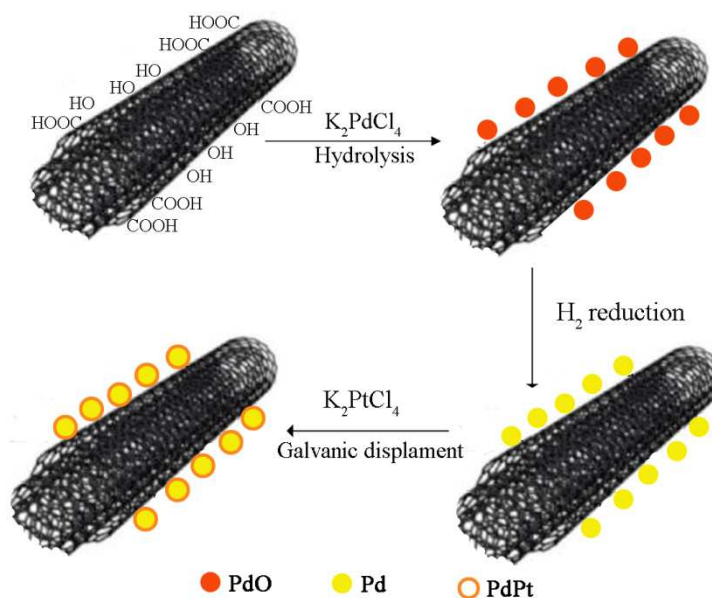


Figure 4.3 Preparation scheme of Pd@PdPt/MWCNTs composite.

The synthetic scheme of Pd@PdPt/MWCNTs was illustrated in Figure 4.3. PdO/MWCNTs was prepared by the hydrolysis of K_2PdCl_4 in the presence of MWCNTs. Due to the high affinity of Pd toward oxygen, $PdCl_4^{2-}$ will react with the oxygen containing functional groups on the side wall of MWCNTs, forming PdO on the surface of MWCNTs. The resulting PdO was then reduced by hydrogen under $60^\circ C$ to generate a surfactant free Pd surface for further modification. PdPt alloy coating of the Pd nanoparticles was achieved by the galvanic displacement between $PtCl_4^{2-}$ and Pd. The advantages of this synthetic method include that it is quite applicable for mass production which is in high demand for fuel cell catalysts production and it is environmentally benign since no surfactants and capping agents is needed which is commonly used to achieve better particle

size distribution.

4.3.2 Verification of the hydrolysis of PdCl_4^{2-}

To verify the formation of PdO, XRD analysis was carried out. Figure 4.4 shows the XRD pattern of the sample before and after hydrogen reduction. Clear transforming of crystal phase could be observed upon the reduction. The peak marked with star corresponds to the (002) faces of MWCNTs. The diffraction peaks at 2θ value of 34.1 degree for the sample before reduction corresponds to the (101) planes of PdO while other peaks were also compatible to that of palladium oxide. [57] After reduction, the XRD pattern showed a crystalline Pd face centre cubic (fcc) phase with diffraction peaks correspond to the (111), (200), (220), (311) planes of Pd. Provide further proofs for the occurrence of the hydrolysis of PdCl_4^{2-} , a control experiment was carried out in 0.1M H_2SO_4 instead of deionised water. Base on both TEM and EDS measurements, we could not observe the signals originating from Pd which suggested that no hydrolysis took place. This is in good agreement with the hypothesis since the hydrolysis of PdCl_4^{2-} would be hindered in an acidic medium and therefore PdO can not be formed. The pH values can also provide evidences for the hydrolysis of PdCl_4^{2-} . Table 4.1 lists the pH value at different stage of the reaction mixture. The pH value had dropped by 2 after the reaction between PdCl_4^{2-} and MWCNTs. Taking into accounts the influence of water since hydrolysis of PdCl_4^{2-} can occur in water, a decrease of only about 1 in pH value was observed. This implies that the addition of MWCNTs enhance the hydrolysis of PdCl_4^{2-} , which generates PdO on the surface of

MWCNTs owing to the oxygen containing group on the surface of MWCNTs. It is known that carbon nanotube is a superior supporting material for precious metals such as Pt and Pd which can enhance the utilization of the noble metals when used as electrocatalysts for PEMFCs. It has stimulated numerous research works in this aspect. [58-61] Very recently, it is reported that apart from being the supporting materials, MWCNTs can act as a reducing agent also for the fabrication of M/MWCNTs composites (M=Pt or Au). [62] Xie et. al. also demonstrated the successfully synthesis of Pd/graphene composite through the redox reaction between PdCl_4^{2-} and graphene. However, in our case PdO/MWCNTs composite was obtained before the reduction by hydrogen as is confirmed by XRD analyses presented in Figure 4.4. A strong diffraction peak appears with a 2 theta value of around 34 degree which corresponds to the (101) plane of PdO. [63] Photographs of the MWCNTs dispersion before and after reaction with K_2PdCl_4 clearly shows that aggregation of the MWCNTs was induced after the deposition of PdO on the surface. The discrepancy between our synthesis compared to that in the literatures might be due to the different synthetic condition. In our case a relatively high temperature (60°C) was employed whereas 0°C was chosen in Xie's preparation. Hydrolysis of PdCl_4^{2-} can take place readily in this temperature forming stable PdO, hindering the electron transfer from MWCNTs to Pd^{2+} . In addition, the redox potential of graphene and MWCNTs also played a critical role as it is highly dependent on the physical state of the graphene layer. [64, 65]

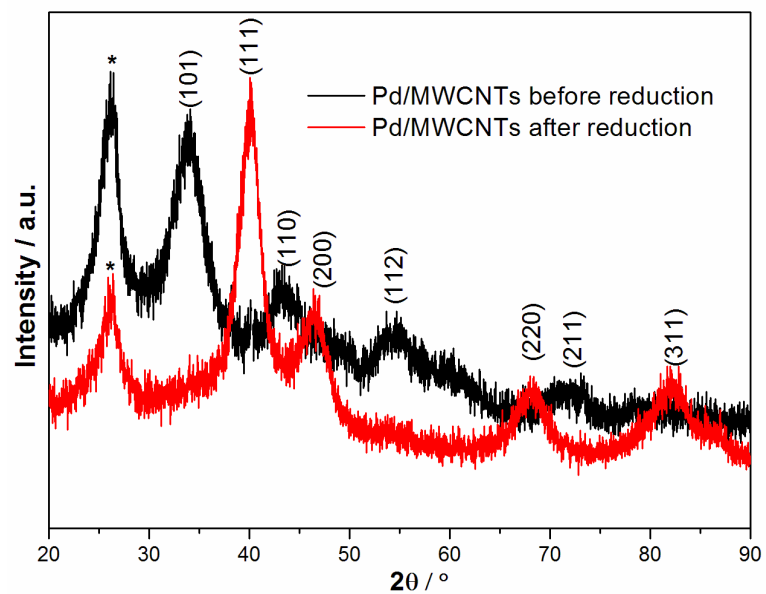


Figure 4.4 XRD patterns of Pd/MWCNTs before and after reduction, Peaks marked with * starts correlate to 002 plate of MWCNTs.

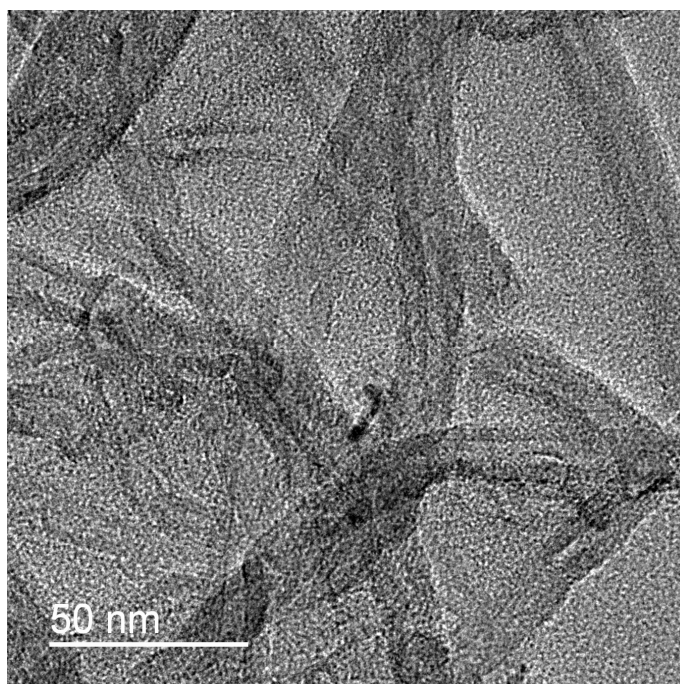


Figure 4.5 TEM image of Pd/MWCNTs prepared under 0.1M H₂SO₄.

Table 4.1 pH value of the respective solutions

Solution	pH
Deionised water	5.62
MWCNTs + deionised water	5.32
K_2PdCl_4	4.21
MWCNTs + K_2PdCl_4	3.45

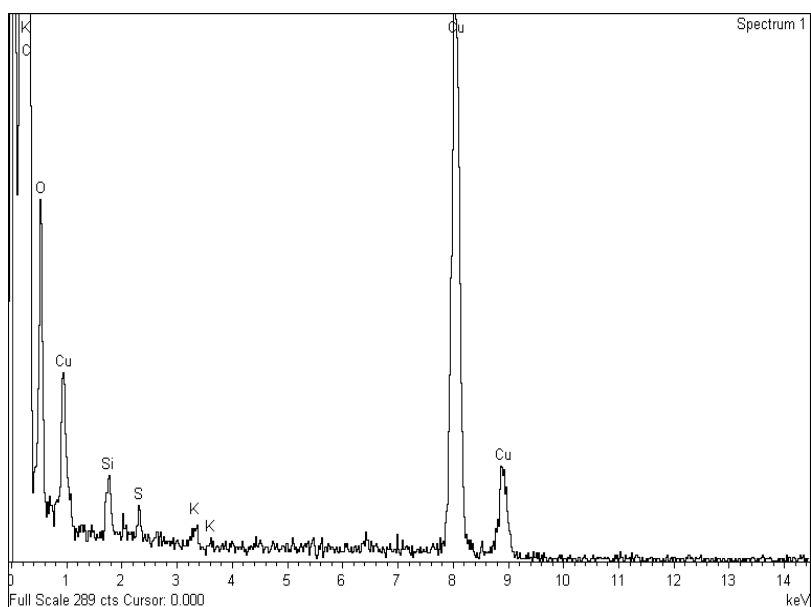


Figure 4.6 EDS pattern of the sample prepared under 0.1M H_2SO_4 .

4.3.3 EDS, XRD and XPS characterizations

The modification of Pd was achieved by galvanic displacement between Pd and $PtCl_4^{2-}$. Based on the above discussion, the as prepared Pd/MWCNTs composite was surfactant free which is quite applicable for the surface decoration through galvanic replacement. Energy

dispersive spectroscopy was used to study the composition of the Pd@PdPt/MWCNTs catalyst. The result is shown in Figure 4.7. A Pd : Pt atomic ratio of 2.6 : 1 was obtained, which is higher than that of the stoichiometric ratio of the precursors (1.5 : 1) in the preparation process. The lower content of Pt in the final product may be due to termination of the galvanic displacement once a complete layer of PdPt alloy is formed on the surface of Pd nanoparticles. Similar results were observed as we varied the amount of Pt precursor in the galvanic displacement process. The surface composition of the Pd@PdPt catalyst was further investigated by XPS. The atomic ratio between Pd and Pt was 1 : 1 as revealed by the XPS measurement. Compared to the EDS analysis which can be used to study the overall atomic ratio of the samples, XPS measurement is a surface characterization technique that cannot account for the core content of samples. Therefore, a relatively lower Pd content was obtained as compared to the EDS study. This result is a good evidence for the alloy nature of the PdPt shell of the synthesized catalyst as proposed in Figure 4.3. The formation of PdPt alloy was confirmed by the shift in the binding energy of palladium's 3d orbital. As shown in Figure 4.8, the binding energy of Pd_{5/2} and Pd_{3/2} for Pd/MWCNTs and Pd@PdPt/MWCNTs were 335.09eV, 340.39eV and 335.66eV, 340.93eV respectively. The lower binding energy for the Pd@PdPt/MWCNTs compared to that of the Pd/MWCNTs unambiguously indicates the modification of the electronic structure by the alloy formation. Considering the electronegativity of the two metals, electrons will be withdrawn by Pd from Pt in the PdPt alloy thus resulting in a lower binding energy of Pd compared to its monometallic counterpart. XRD was used to study the crystal structure of the as prepared catalyst. As shown in Figure 4.9, the diffractions of the Pd/MWCNTs and the

Pd@PdPt/MWCNTs composite both displays fcc crystalline structure. A slightly down shift of the diffraction peaks was observed for the Pd@PdPt/MWCNTs nanocatalyst compared to Pd/MWCNTs indicating the decrease of the d value upon the galvanic replacement.

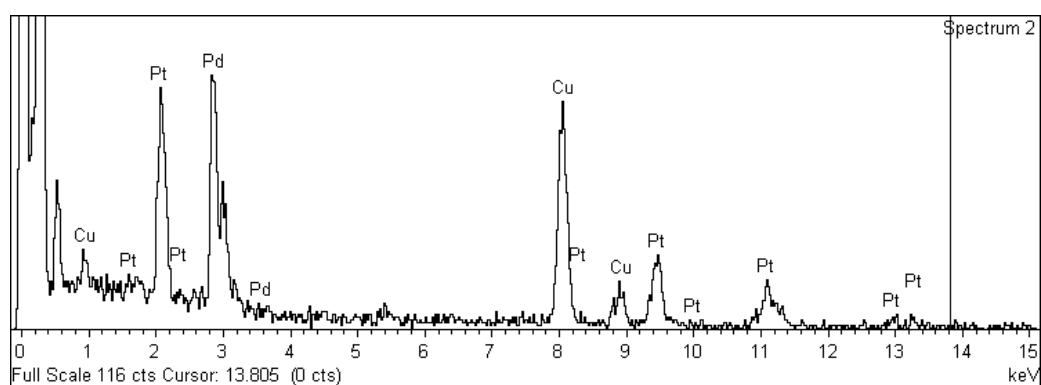


Figure 4.7 EDS pattern of Pd@PdPt/MWCNTs

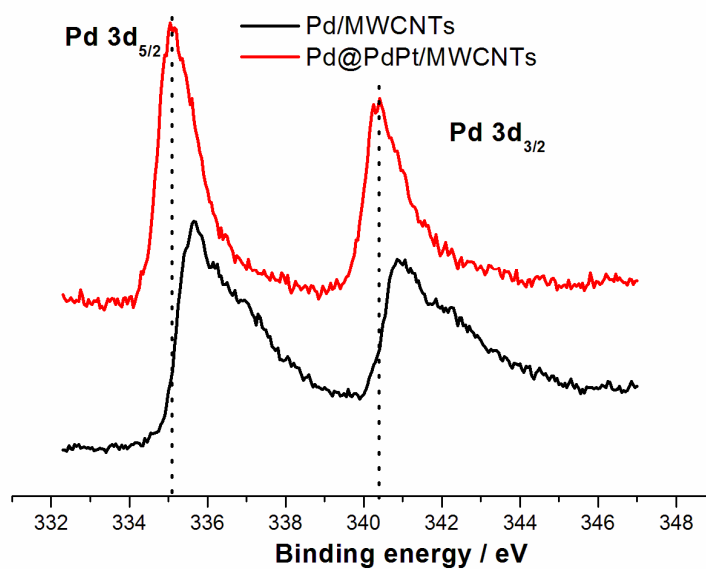


Figure 4.8 XPS spectra for the Pd 3d core levels of Pd/MWCNTs and Pd@PdPt/MWCNTs.

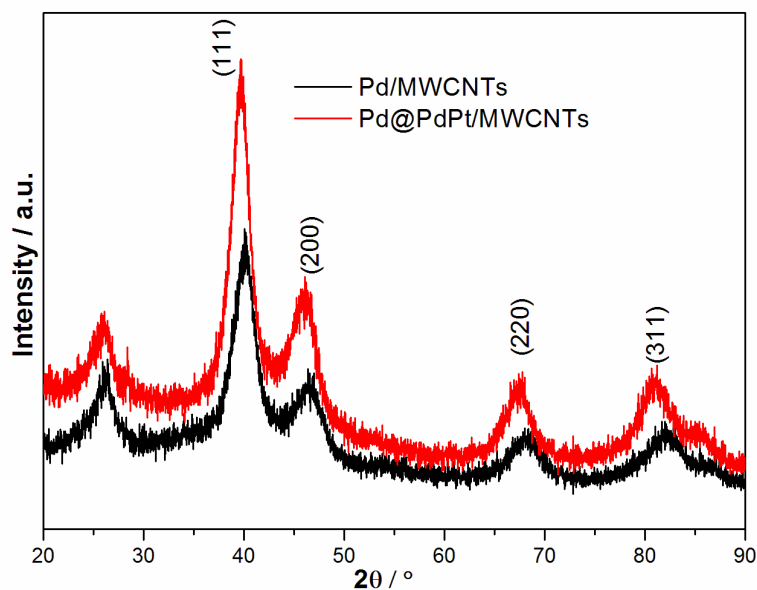


Figure 4.9 XRD patterns of Pd/MWCNTs and Pd@PdPt/MWCNTs

4.3.4 TEM characterization

Pd loading can be readily controlled in this synthetic protocol of Pd/MWCNTs. A different loading can be obtained by varying the ratio between the metal precursor and the MWCNTs. Figure 4.10 presents typical TEM image of Pd/MWCNTs composites. The Pd loading can be increased up to around 58% (w.t.). Further increase in the amount of Pd precursor could not result in a higher loading, implying that the surface had reached a saturated state. A closer observation revealed that a slight change in size of the nanoparticles occurs as the metal loading increases, from ca. 2.3 ± 0.1 nm at 6.1% loading to ca. 3.5 ± 0.1 nm at 33.8%, as shown in Table 4.2. Noticeably, no aggregation of nanoparticles can be seen at relatively high metal loading which demonstrated that the synthetic method is a highly efficient approach to prepare Pd/MWCNTs with better size distribution. To examine the morphology change after the coating of PdPt alloy through

galvanic displacement, TEM analysis was also performed. For the purpose of comparison, TEM images of Pd/MWCNTs before and after surface modification are shown in Figure 4.11. After the decoration by Pt, no obvious change in morphology was observed. However, a d value of 2.28Å correlating to the (111) face was obtained by the HRTEM of the sample Pd@PdPt/MWCNTs (inset of Figure 4.11(B)), indicating the formation of PdPt alloy. [10, 48] The small decrease in the d value agrees well with the result of XRD measurements which shows a slight down-shift for all the diffractions.

Table 4.2 Data summary derived from TEM studies

K ₂ PdCl ₄ applied/g	Loading/%	Particle size/nm
0.41	6.1	2.3 ± 0.1
0.82	11.5	2.3 ± 0.1
1.63	20.6	2.5 ± 0.1
3.27	33.8	3.6 ± 0.1
6.53	48.6	3.6 ± 0.1
13.06	58.0	3.6 ± 0.1

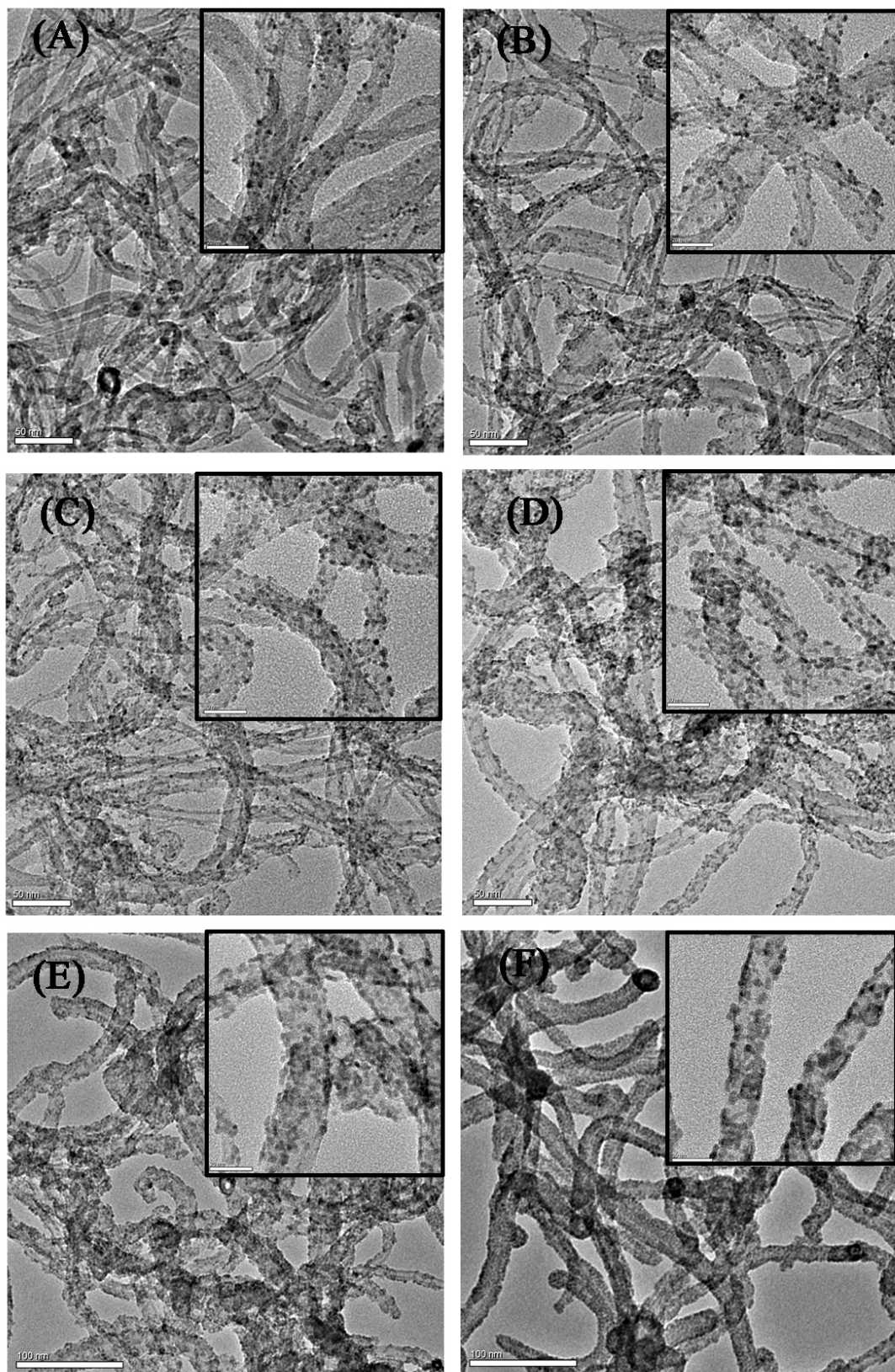


Figure 4.10 TEM images of Pd/MWCNTs composite with different metal loading: (A) 6.1%; (B) 11.5%;(C) 20.6%; (D) 33.8%; (E) 48.6%; (F) 58.0%.

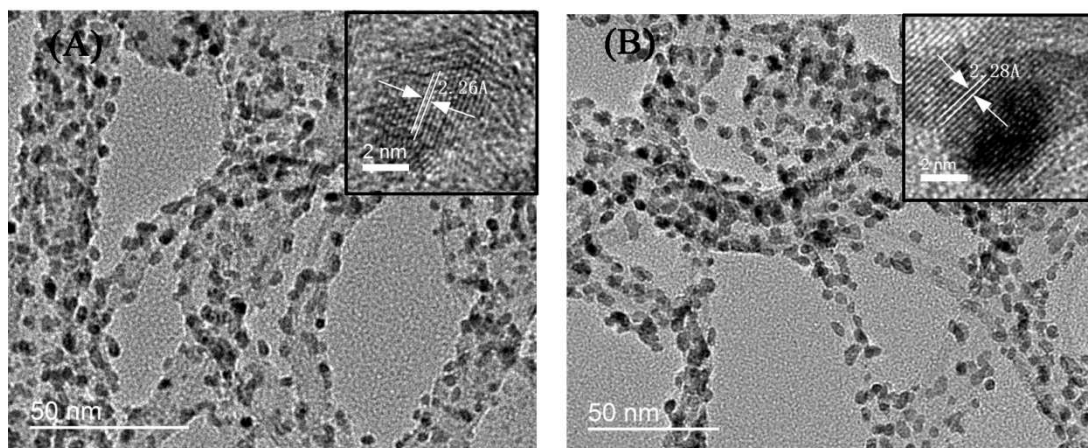


Figure 4.11 (A) TEM image of Pd/MWCNTs composite; (B) TEM image of Pd@PdPt/MWCNTs composite. Insets: HRTEM.

4.3.5 Electrochemical characterization

4.3.5.1 Cyclic voltammetry in sulfuric acid

Cyclic voltammetry (CV) is a commonly used method to study the precious metals-containing electrocatalysts for diagnostic purpose such as electrochemical active surface area and catalytic activity measurement. The CV curves for Pd/MWCNTs, Pt/MWCNTs and Pd@PdPt/MWCNTs are presented in Figure 4.12. Obvious change can be observed for the Pd/MWCNTs after modification by Pt. In the hydrogen characteristic region, namely between -0.24V and 0V (vs SCE), both the adsorption and desorption peaks shifted negatively, implying the formation of PdPt alloy. On the other hand, considering the metal oxide reduction region between 0.4V and 0.8V, the intensity of the metal oxide reduction peak decreased for Pd@PdPt/MWCNTs compared to that of Pd/MWCNTs accompanied by a positively-shifter the onset potential, which indicates the coating of PdPt

alloy on the surface of Pd nanoparticles. The result of CV analysis was in good agreement with the physical characterizations.

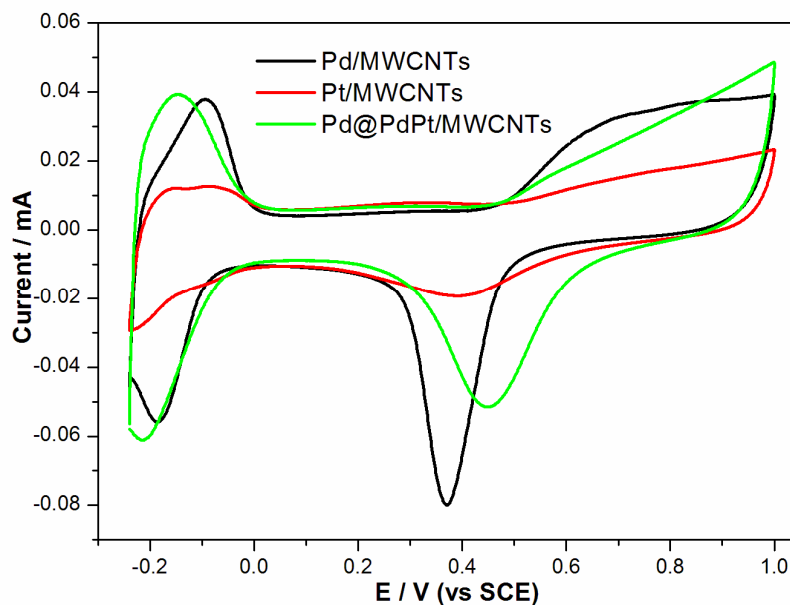


Figure 4.12 CVs in 0.1M N_2 saturated H_2SO_4 , 50mV/s. Loading for the catalysts: Pd/MWCNTs: 33.8%; Pt/MWCNTs: 29.9%; Pd@PdPt/MWCNTs: 38.7%.

4.3.5.2 Methanol and ethanol oxidation

The electrochemical activity of Pd@PdPt/MWCNTs for methanol was examined by linear sweep voltammetry (LSV) in 0.1M H_2SO_4 + 0.1M methanol. For comparison purposes, the LSV for Pt/MWCNTs and commercial Pt/C were also carried out under the same condition. The results were shown in Figure 4.13. The current are corrected with reference to the metal mass for easy comparison. It is well known that Pd is inert towards methanol oxidation. The inset of Figure 4.13 shows the CVs of Pd/MWCNTs in 0.1M H_2SO_4 + 0.1M methanol. No current signal corresponding to methanol oxidation appeared. However, the Pd@PdPt/MWCNTs displayed superior activity for methanol as proven by

the LSV in Figure 4.13. The activity at 0.55V for the Pd@PdPt/MWCNTs is 400mA/mg, whereas the values for Pt/C and Pt/MWCNTs were only 142.8 mA/mg and 164.1 mA/mg, respectively. An enhancement by a factor of 2.4 was achieved. Moreover, a close look at the onset potential for the methanol oxidation revealed that a negative shift of around 40mV for the Pd@PdPt/MWCNTs (ca. 0.117V) as compared to that of Pt/C and Pt/MWCNTs (ca. 0.153V).

The Pd@PdPt/MWCNTs catalyst displayed excellent electrochemical performance towards ethanol oxidation also. Figure 4.14 shows LSVs of ethanol oxidation using Pd/MWCNTs, Pt/MWCNTs and Pd@PdPt/MWCNTs in 0.1M NaOH solution containing 0.1 M ethanol. The current values were normalized to the total metal mass of the catalysts which was measured through ICP-MS. It is noteworthy that the current density of the Pd@PdPt/MWCNTs composite is the highest over the entire potential region as compared to the other catalysts. The peak current density of the Pd@PdPt/MWCNTs was calculated to be 335.8mA/mg, which is about 1.4 and 2.2 fold higher than those of the Pd/MWCNTs (240.3 mA/mg) and the Pt/MWCNTs (153.7 mA/mg) catalysts, respectively. Moreover, the Pd@PdPt/MWCNTs shows a more negative onset potential value (ca. 0.667V) as compared to those of Pd/MWCNTs (ca. 0.642V) and Pt/MWCNTs (ca. 0.613V). The enhanced electrocatalytic activity of the Pd@PdPt/MWCNTs can be ascribed to the synergetic effect caused by the formation of PdPt alloy. The PdPt alloy has a modified electronic structure as compared to its monometallic counterparts, and so improvement of electrocatalytic properties was resulted. [66-68]

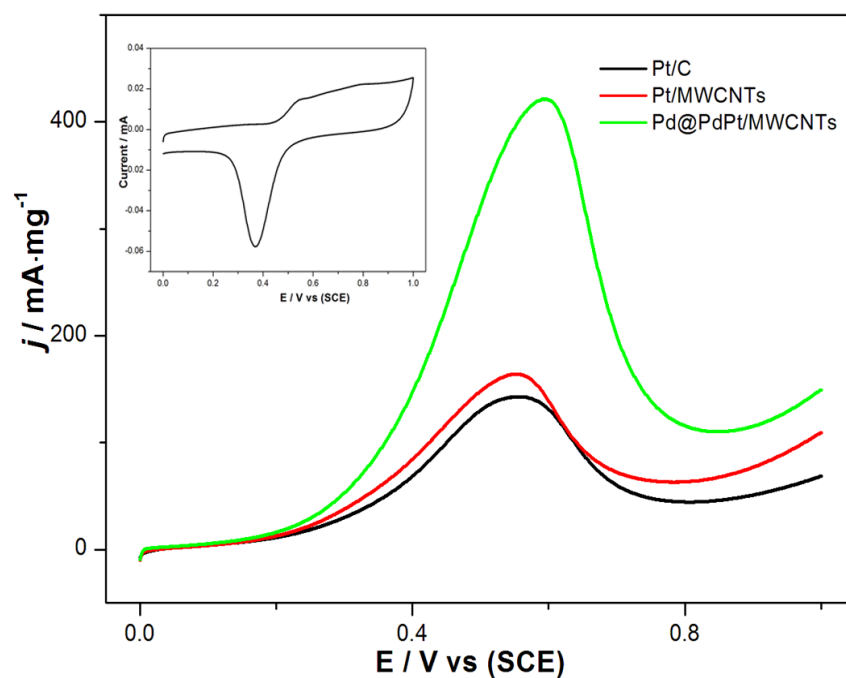


Figure 4.13 LSVs in 0.1M H₂SO₄ + 0.1M methanol of different electrocatalysts, inset: CV of Pd/MWCNTs in 0.1M H₂SO₄ + 0.1M methanol; Current was normalized to the mass of metals.

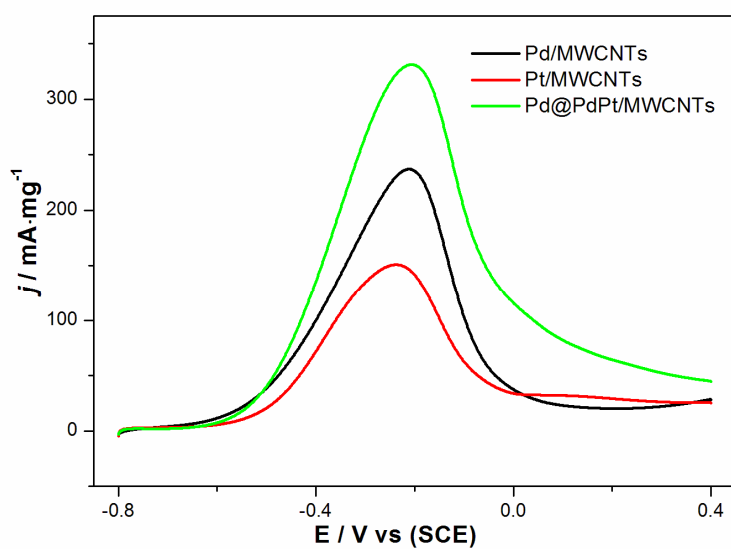


Figure 4.14 LSVs in 0.1M NaOH + 0.1M ethanol of different electrocatalysts; Current was normalized to the mass of metals.

4.3.5.3 Chronoamperometry characterization

Chronoamperometry is a practical approach for performance evaluation for electrocatalysts. In this measurement, potential of interest was chosen for polarization for a certain period of time. The current response was expected to decline over time due to two possible reasons. [69] The first is the accumulation of intermediates on the electrode surface which hinders any the further electrochemical reaction; the second is that the electrode material, particularly metal nanoparticles, usually undergoes coarsening and dissolution during the operation. Figure 4.15(A) presents the chronoamperometry results of Pt/C, Pt/MWCNTs and Pd@PdPt/MWCNTs in 0.1M H₂SO₄ + 0.1M methanol. The polarization potential was 0.45V and was held for 1000s. The Pd@PdPt/MWCNTs exhibited the highest current respond throughout the whole measurement. The retained current for Pd@PdPt/MWCNTs, Pt/C and Pt/MWCNTs were 33.4%, 28.3% and 21.2% respectively, demonstrating that the highest stability of Pd@PdPt/CNT among the three.

It is well known that Pd is an excellent electrocatalyst for ethanol oxidation. However, the low stability of Pd has limited its widespread application. The Pd@PdPt/MWCNTs possesses high electrochemical stability compared to Pd/MWCNTs and Pt/MWCNTs. Figure 4.15(B) shows the chronoamperometric experiments at -0.2V vs. SCE of different composites. Pd@PdPt/MWCNTs maintained a higher activity throughout the measurement revealing the better electrochemical stability compared to Pd/MWCNTs and Pt/MWCNTs. The retained activity for the Pd@PdPt/MWCNTs, Pd/MWCNTs and Pt/MWCNTs catalysts

were 56.7%, 10.8% and 37.5% respectively.

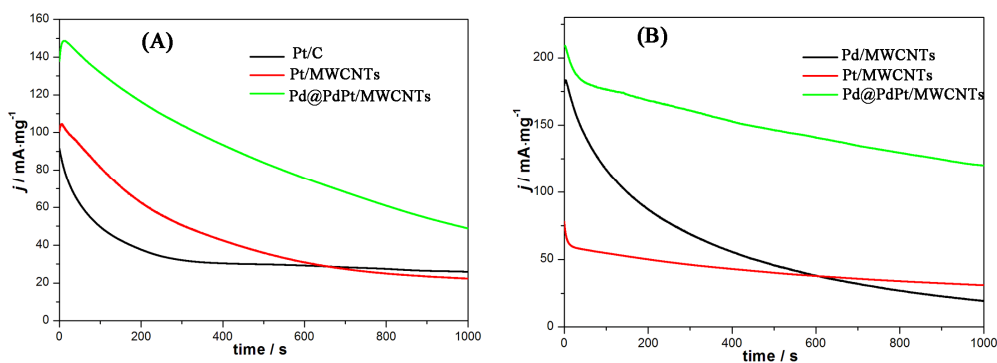


Figure 4.15 Chronoamperometric curves in (A) 0.1M H₂SO₄ + 0.1M methanol, 0.45V and (B) 0.1M NaOH + 0.1M ethanol, -0.2V.

4.4 Summary

To summarize, Pd@PdPt/MWCNTs core-shell nanocatalyst was prepared through galvanic replacement by using Pd/MWCNTs composite as the precursor.

- (1) Pd/MWCNTs composite was synthesized by a newly developed method which involved the hydrolysis of PdCl₄²⁻ in presence of MWCNTs, and the crude product was subsequently reduced by hydrogen. XRD analysis and pH value change measurement were used to prove the hydrolysis of PdCl₄²⁻. The synthetic method was environmentally benign since no surfactant was used. Moreover, it is applicable for mass production.
- (2) The Pd/MWCNTs composite exhibited better size distribution. The Pd loading can be readily controlled with this synthetic method without obvious change in the size of Pd nanoparticle. Aggregation of nanoparticles did not occur for a relatively high Pd loading

as confirmed by the TEM observation. The Pd/MWCNTs composite provides a surfactant free Pd surface for further modification. Pd coating by PdPt alloy was achieved by the galvanic displacement of Pd and PtCl_4^{2-} . The formation of PdPt alloy was confirmed by XPS, XRD, HRTEM as well as CVs analysis.

- (3) Electrochemical studies demonstrated that the Pd@PdPt/MWCNTs possess superior performance for methanol and ethanol oxidation. The improvement of electrochemical properties may be ascribed to the electronic effect induced by the alloy formation.

References

- [1] S. J. Guo, E. K. Wang, *Nano Today* **2011**, 6, 240.
- [2] H. A. Gasteiger, S. S. Kocha, B. Sompalli, F. T. Wagner, *Appl. Catal. B* **2005**, 56, 9.
- [3] X. B. Zhang, J. M. Yan, S. Han, H. Shioyama, Q. Xu, *J. Am. Chem. Soc.* **2009**, 131, 2778.
- [4] Y. Chen, F. Yang, Y. Dai, W. Wang, S. Chen, *J. Phys. Chem. C* **2008**, 112, 1645.
- [5] S. Mandal, K. M. Krishnan, *J. Mater. Chem.* **2007**, 17, 372.
- [6] J. C. M. Silva, R. F. B. De Souza, L. S. Parreira, E. Teixeira Neto, M. L. Calegari, M. C. Santos, *Appl. Catal. B-Environ.* **2010**, 99, 265.
- [7] V. M. Dhavale, S. Kurungot, *J. Phys. Chem. C* **2012**, 116, 7318.
- [8] L. Kuai, S. Wang, B. Geng, *Chem. Commun.* **2011**, 47, 6093.
- [9] H. A. Esfahani, L. Wang, Y. Nemoto, Y. Yamauchi, *Chem. Mater.* **2010**, 22, 6310.
- [10] L. Wang, Y. Nemoto, Y. Yamauchi, *J. Am. Chem. Soc.* **2011**, 133, 9674.
- [11] S. I. Sanchez, M. W. Small, J. M. Zuo, R. G. Nuzzo, *J. Am. Chem. Soc.* **2009**, 131, 8683.
- [12] D. Zhao, B. Q. Xu, *Angew. Chem, Int. Ed.* **2006**, 45, 4955.
- [13] S. Alayoglu, A. U. Nilekar, M. Mavrikakis, B. Eichhorn, *Nature Mater.* **2008**, 7, 333.
- [14] S. J. Guo, L. Wang, S. J. Dong, E. K. Wang, *J. Phys. Chem. C* **2008**, 112, 13510.
- [15] S. Alayoglu, B. Eichhorn, *J. Am. Chem. Soc.* **2008**, 130, 17479.
- [16] H. L. Gao, S. J. Liao, Z. X. Liang, H. G. Liang, F. Luo, *J. Power Sources* **2011**, 196, 6138.
- [17] S. J. Guo, J. Li, S. J. Dong, E. K. Wang, *J. Phys. Chem. C* **2010**, 114, 15337.

- [18] Y. Wang, N. Toshima, *J. Phys. Chem. B* **1997**, 101, 5301.
- [19] Y. Y. Feng, H. Ma J, G. R. Zhang, G. Liu, B. Q. Xu, *Electrochem. Commun.* **2010**, 12, 1191.
- [20] S. J. Guo, S. J. Dong, E. K. Wang, *J. Phys. Chem. C*, **2009**, 113, 5485.
- [21] H. L. Gao, S. J. Liao, J. H. Zeng, Y. C. Xie, D. Dang, *Electrochim. Acta* **2011**, 56, 2024.
- [22] N. Kristiana, Y. Yu, P. Gunawan, R. Xu, W. Deng, X. Liu, X. Wang, *Electrochim. Acta* **2009**, 54, 4916.
- [23] S. Yan, S. Zhang, *Int. J. Hydrogen Energ.* **2012**, 37, 9636.
- [24] Y. Chen, F. Yang, Y. Dai, W. Wang, S. Chen, *J. Phys. Chem. C* **2008**, 112, 1645.
- [25] W. Lia, P. Haldar, *Electrochem. Solid St.* **2010**, 13(5), B47.
- [26] Y. Kang, L. Qi, M. Li, R. E. Diaz, D. Su, R. R. Adzic, E. Stach, J. Li, C. B. Murray, *ACS Nano*, **2012**, 6(3), 2818.
- [27] Z. D. Wei, Y. C. Feng, L. Li, M. J. Liao, Y. Fu, C. X. Sun, Z. G. Shao, P. K. Shen, *J. Power Sources* **2008**, 180, 84.
- [28] C. Xu, Y. Liu, J. Wang, H. Geng, H. Qiu, *ACS Appl. Mater. Inter.* **2011**, 3, 4626.
- [29] C. H. Chen, L. S. Sarma, D. Y. Wang, F. J. Lai, C. C. A. Andra, S. H. Chang, D. G. Liu, C. C. Chen, J. F. Lee, B. J. Hwang, *Chem. Cat. Chem.* **2010**, 2, 159.
- [30] M. J. Liao, Z. D. Wei, S. G. Chen, L. Li, M. B. Ji, Y. Q. Wang, *Int. J. Hydrogen Energ.* **2010**, 35: 8071
- [31] H. I. Karan, K. Sasaki, K. Kuttiyiel, C. A. Farberow, M. Mavrikakis, R. R. Adzic, *ACS Catal.* **2012**, 2, 817.

- [32] Y. Yu, Y. Hu, X. Liu, W. Deng, X. Wang, *Electrochim. Acta* 2009, 54, 3092.
- [33] K. Sasaki, H. Naohara, Y. Cai, Y. M. Choi, P. Liu, M. B. Vukmirovic, J. X. Wang, R. R. Adzic, *Angew. Chem. Int. Ed.* **2010**, 49, 8602.
- [34] D. Wang, H. L. Xin, Y. Yu, H. Wang, E. Rus, D. A. Muller, H. D. Abrun, *J. Am. Chem. Soc.* **2010**, 132 (50), 17664.
- [35] L. X. Ding, G. R. Li, Z. L. Wang, Z. Q. Liu, H. Liu, Y. X. Tong, *Chem. Eur. J.* **2012**, 18, 8386.
- [36] Y. Y. Feng, J. H. Ma, G. R. Zhang, G. Liu, B. Q. Xu, *Electrochem. Comm.* **2010**, 12, 1191.
- [37] Z. Peng, H. You, H. Yang, *Adv. Funct. Mater.* **2010**, 20, 3734.
- [38] S. Koh, P. Strasser, *J. Am. Chem. Soc.* **2007**, 129, 12624.
- [39] C. Kulp, X. Chen, A. Puschhof, S. Schwamborn, C. Somsen, W. Schuhmann, M. Bron, *Chem. Phys. Chem.* **2010**, 11, 2854.
- [40] H. X. Zhang, C. Wang, J. Y. Wang, J. J. Zhai, W. B. Cai, *J. Phys. Chem. C* **2010**, 114, 6446.
- [41] S. Y. Huang, P. Ganesan, B. N. Popov, *ACS Catal.* **2012**, 2, 825.
- [42] H. Wu, H. Li, Y. Zhai, X. Xu, Y. D. Jin, *Adv. Mater.* **2012**, 24, 1594.
- [43] Y. Y. Chu, Z. B. Wang, Z. Z. Jiang, D. M. Gu, G. P. Yin, *J. Power Sources* **2012**, 203, 17.
- [44] A. X. Yin, X. Q. Min, W. Zhu, H. S. Wu, Y. W. Zhang, C. H. Yan, *Chem. Commun.* **2012**, 48, 543.
- [45] W. Wang, Q. Huang, J. Liu, Z. Zou, Z. Li, H. Yang, *Electrochem. Comm.* **2008**, 10,

1396.

- [46] W. He, M. Chen, Z. Zou, Z. Li, X. Zhang, S. A. Jin, D. J. You, Ch. Pak, H. Yang, *Appl. Catal. B-Environ.* **2010**, 97, 347.
- [47] F. Kadirgan, S. Beyhan, T. Atilan, *Int. J. Hydrogen Energ.* **2009**, 34, 4312.
- [48] J. W. Hong, S. W. Kang, B. S. Choi, D. Kim, S. B. Lee, S. W. Han, *ACS Nano*, **2012**, 6(3), 2410.
- [49] B. S. Choi, Y. W. Lee, S. W. Kang, J. W. Hong, J. Kim, I. Park, S. W. Han, *ACS Nano*, **2012**, 6(6), 5659.
- [50] C. Zhu , S. Guo , S. Dong, *Adv. Mater.* **2012**, 24, 2326.
- [51] C. S. Chen, F. M. Pan, *J. Power Sources* **2012**, 208, 9.
- [52] C. Koenigsmann, A. C. Santulli, K. Gong, M. B. Vukmirovic, W. Zhou, E. Sutter, S. S. Wong, R. R. Adzic, *J. Am. Chem. Soc.* **2011**, 133, 9783.
- [53] D. Wang, H. L. Xin, H. Wang, Y. Yu, E. Rus, D. A. Muller, F. J. DiSalvo, H. D. Abruna, *Chem. Mater.* **2012**, 24(12), 2274.
- [54] X. M. Wang, M. E. Wang, D. D. Zhou, Y. Y. Xia, *Phys. Chem. Chem. Phys.* **2011**, 13, 13594.
- [55] H. Wang, C. Xu, F. Cheng, M. Zhang, S. Wang, S. P. Jiang, *Electrochem. Comm.* **2008**, 10, 1575.
- [56] H. Wang, S. Ishihara, K. Ariga, Y. Yamauchi, *J. Am. Chem. Soc.* **2012**, 134(26), 10819.
- [57] K. Ding, G. Yang, S. Wei, P. Mavinakuli, Z. Guo, *Ind. Eng. Chem. Res.* **2010**, 49, 11415.

- [58] D. Long, W. Li, W. Qiao, J. Miyawaki, S. H. Yoon, I. Mochidab, L. Ling, *Chem. Commun.* **2011**, 47, 9429.
- [59] B. Fang, M. S. Kim, J. H. Kim, M. Y. Song, Y. J. Wang, H. Wang, D. P. Wilkinson, J. S. Yu, *J. Mater. Chem.* **2011**, 21, 8066.
- [60] S. Chen, Z. Wei, L. Guo, W. Ding, L. Dong, P. Shen, X. Qia, L. Li, *Chem. Commun.* **2011**, 47, 10984.
- [61] A. Orfanidi, M. K. Daletou, S. G. Neophytides, *Appl. Catal. B-Environ.* **2011**, 106, 379.
- [62] H. C. Choi, M. Shim, S. Bangsaruntip, H. Dai, *J. Am. Chem. Soc.* **2002**, 124, 9058.
- [63] K. Ding, G. Yang, S. Wei, P. Mavinakuli, Z. Guo, *Ind. Eng. Chem. Res.* **2010**, 49, 11415.
- [64] K. K. Kim, J. J. Bae, H. Ki Park, S. M. Kim, H. Z. Geng, K. A. Park, H. J. Shin, S. M. Yoon, A. Benayad, J. Y. Choi, Y. H. Lee, *J. Am. Chem. Soc.* **2008**, 130, 12757.
- [65] M. Zheng, B. A. Diner, *J. Am. Chem. Soc.* **2004**, 126, 15490.
- [66] B. Lim, M. Jiang, P. H. H. Camargo, E. C. Cho, J. Tao, X. Lu, Y. Zhu, Y. Xia, *Science* **2009**, 324, 1302.
- [67] Z. Peng, H. Yang, *J. Am. Chem. Soc.* **2009**, 131, 7542.
- [68] Q. Yuan, Z. Zhou, J. Zhuang, X. Wang, *Chem. Commun.* **2010**, 46, 1491.
- [69] A. M. Remona, K. L. N. Phani, *J. Fuel Cell Sci. Technol.* **2011**, 8, 11001.

Chapter 5

Conclusions

The high cost of Pt catalysts for direct liquid fuel cells limits their widespread applications. In this regard, three approaches were developed to enhance the utilization of Pt, namely, submonolayer Pt structure construction, hollow structure fabrication and core-shell nanostructure design.

Submonolayer Pt structure was successfully prepared on the surface of gold nanoparticles by a so-called ions adsorption and electrochemical reduction method. Au/MWCNTs composite was prepared via traditional chemical impregnation. Complete deposition of Au nanoparticles on MWCNTs was confirmed by UV-vis measurement. TEM analyses illustrated that the particle size is in the range between 4 to 9 nm. Au loading on Au/MWCNTs composite can be easily controlled by varying the amount of Au source, while some aggregations were observed at high loading. XRD studies demonstrated that Au nanoparticles exhibited a fcc structure. Au@Pt/MWCNTs composite was fabricated by ions adsorption and *in situ* electrochemical reduction. Linear sweep voltammetry and XPS were used to confirm the adsorption of PtCl_4^{2-} on to the surface of Au nanoparticles. The driving force for the Pt chloride ions on the Au surface is considered to be the strong interaction between Au and chlorine. The key role of chlorine atom in the ions adsorption process was proven by replacing the Pt chloride with Pd chloride based on their similar molecular structure. The sub-monolayer Pt structure on the surface of Au nanoparticles was verified for the first time by cyclic voltammetry. Electrochemical studies demonstrated that the Pt

coverage can be controlled by varying the concentration of the Pt ions in the adsorption process or repeated immersions. Direct oxidation of formic acid occurred on catalysts with lower Pt coverage, namely less than 40%, while both direct and indirect pathway took place on those with higher Pt coverage due to the ensemble effect. Moreover, the Au@Pt/MWCNTs possess higher stability as compared to commercial Pt/C which made it a promising electrocatalysts for direct formic acid fuel cells.

Catalysts with lower Pt coverage showed excellent performance for methanol tolerant ORR catalysis as they were inactive towards methanol. Both the CVs and chronoamperometric studies provided evidences for this conclusion. In addition, the specific area activity of ORR was also enhanced as compared to the commercial Pt/C catalyst.

PtAg hollow nanospheres were prepared via galvanic displacement by using silver nanoparticles as template. Ag nanoparticle seeds were obtained by chemical reduction with sodium borohydride as the reducing agent. The growth process was performed under a weak reducing agent, $\text{NH}_2\text{OH}\cdot\text{HCl}$ at room temperature. The galvanic displacement reaction was conducted at 60°C . The thickness of the hollow sphere can be easily controlled by simply changing the amount of Pt source used. EDS study revealed that the ratio of Pt and Ag was in a range of 4.2 to 7.2, but was difficult to tune either by varying the precursors ratio or reaction temperature. Both the XRD and XPS analyses confirmed the formation of alloyed of Pt and Ag. Electrochemical investigations revealed that the PtAg alloy displays higher activity and stability towards methanol and formic acid oxidation when compared to commercially available Pt black.

Pd@PdPt/MWCNTs core-shell nanocatalyst was obtained through galvanic displacement between Pd/MWCNTs and PtCl_4^{2-} . Pd/MWCNTs composite was synthesized by a newly developed method which involved the hydrolysis of PdCl_4^{2-} in presence of MWCNTs and subsequently reduced by hydrogen. XRD analysis and pH value change measurement were used to prove the hydrolysis of PdCl_4^{2-} . The synthetic method is environmentally benign since no surfactant was required. Moreover, it is suitable for mass production. The Pd/MWCNTs composite exhibited better size distribution. The synthetic method can easily control the Pd loading without obvious change in the size of Pd nanoparticle. Aggregation of nanoparticles did not occur for relatively high loading composites as confirmed by the TEM observations. The obtained Pd/MWCNTs composite can provide surfactant free Pd surface for further modification. Pd coating by PdPt alloy was achieved by means of galvanic displacement of Pd and PtCl_4^{2-} . The formation of PdPt alloy was confirmed by XPS analysis, XRD, HRTEM as well as CVs. Electrochemical studies demonstrated that Pd@PdPt/MWCNTs possess superior performance for methanol and ethanol oxidation. The improvement of electrochemical properties may be ascribed to the electronic effect induced by the alloy formation.

Chapter 6

Experimental Details

6.1 Materials

Auric chloride acid (HAuCl_4), potassium chloroplatinate(II) (K_2PtCl_4), potassium tetrachloropalladate(II) (K_2PdCl_4), platinum black, silver nitrate (AgNO_3), multi-wall carbon nanotubes (MWCNTs), sodium borohydride (NaBH_4), hydroxylamine hydrochloride ($\text{NH}_2\text{OH}\cdot\text{HCl}$), sodium citrate ($\text{Na}_3\text{C}_6\text{H}_5\text{O}_7$), ethylene glycol ($\text{C}_2\text{H}_6\text{O}_2$), methanol (CH_3OH), ethanol ($\text{C}_2\text{H}_5\text{OH}$), formic acid (HCOOH), sulfuric acid (H_2SO_4), ammonium hydroxide ($\text{NH}_3\cdot\text{H}_2\text{O}$), sodium hydroxide (NaOH), nitric acid (HNO_3), hydrochloric acid (HCl) were purchased from SIGMA-ALDRICH and used as received unless otherwise stated.

The industrial grade gaseous nitrogen, oxygen and hydrogen were purchased from Hong Kong Air Oxygen and stored in high pressure stainless steel cylinder and used as received.

6.2 Sample preparations

6.2.1 Au/MWCNTs composite

Au/MWCNTs were prepared through traditional chemical deposition. HAuCl_4 was used as the Au source and NaBH_4 as the reducing agent. Sodium citrate and ethylene glycol were used as stabilization agents. Experimental details were presented in chapter 2.

6.2.2 Au@Pt/MWCNTs composite

Pt deposition on the surface of Au nanoparticles was achieved by ion adsorption and *in situ* electrochemical reduction. Au/MWCNTs composite was loaded onto GCE and electrochemically cleaned through repeating CVs until a stable curve was obtained. After that, the GCE was immersed into a 0.1M H₂SO₄ solution containing K₂PtCl₄ of different concentration for the ion adsorption. Then the GCE was washed and electrochemically reduced at -0.1V (vs SCE) for 50s.

6.2.3 PtAg hollow nanospheres composite

Ag nanoparticles were used as the template for the construction for the hollow nanospheres. Ag colloid was prepared through chemical reduction of silver nitrate with NaBH₄ in the presence of sodium citrate. Galvanic displacement between the Ag colloid and K₂PtCl₄ was employed for the fabrication of PtAg hollow spheres.

6.2.4 Pd@PdPt/MWCNTs composite

Pd/MWCNTs was first prepared by the hydrolysis of PdCl₄²⁻ in the presence of MWCNTs and was followed by hydrogen reduction. Surface modification of Pd was realized by galvanic replacement of Pd and PtCl₄²⁻.

6.3 Instrumentation

6.3.1 Transmission Electron Microscope (TEM)

All morphological studies were carried by Transmission Electron Microscope (TEM,

FEI Tecnai G2 20) equipped with an energy dispersive X-ray spectroscopy (EDS, Oxford) for composition analyses. High resolution Transmission Electron Microscope (HRTEM) and selected area electron diffraction (SAED) were performed on field emission Transmission Electron Microscope (FETEM, JEOL JEM-2100F). For sample preparation, the solid were dispersed into ethanol by sonication for 10min and then dropped onto a carbon coating Formvar copper grid. The sample containing copper grid was finally dried in air before TEM measurements.

6.3.2 Powder X-Ray Diffraction (XRD)

Powder X-ray diffraction (XRD Rigaku SmartLab) with Cu K α ($\lambda=1.5406\text{\AA}$) was carried out at a scanning rate of $0.05^\circ/\text{s}$ with 2θ ranging between 20° and 90° . The samples were grinded and placed on a single crystal silicon substrate for measurements.

6.3.3 UV-visible Spectroscopy (UV-vis)

UV-vis spectroscopic study was conducted with a UV-vis spectrometer (HP 8453). 100 μL metal nanoparticle colloidal solution was transferred to a cell and diluted to 4mL with deionised water. The adsorption spectra were scanned between 200 to 800nm.

6.3.4 X-Ray Photoelectron Spectroscopy (XPS)

XPS patterns were recorded on X-ray photoelectron spectroscopy (XPS, ESCALAB 250).

6.4 Electrochemical Measurements

All electrochemical measurements were performed through a three-electrode system on the CHI 660D electrochemical station (Shanghai Chenhua). The working electrode was a catalyst modified glass carbon electrode (GCE). Saturated calomel electrode (SCE) and platinum plate were employed as reference electrode and counter electrode respectively. For the preparation of the working electrode, the catalysts were dispersed into a certain solvent (details were presented in the respective chapters) and casted onto the GCE. Before loading of catalyst, the GCE was polished with 0.3 and 0.05 μm alumina slurries, then washed with water and ethanol. The catalyst layer was then dried in air prior to electrochemical measurement. Before each measurement, the electrolyte was purged with nitrogen gas for 15min.